Calculation of Femoral Strain During Normal Activities

Using Efficient Computational Methods

by

HAMED ZIAEI POOR

Principle Supervisor: Prof. Mark Taylor

Associate Supervisor: Dr. Saulo Martelli

Flinders University, College of Science and Engineering
Medical Devices Research Institute

In partial fulfillment of the requirements for the degree of

Doctor of Philosophy (Ph.D.)

December 2019

ABSTRACT

FLINDERS UNIVERSITY, COLLEGE OF SCIENCE AND ENGINEERING
MEDICAL DEVICES RESEARCH INSTITUTE

<u>DOCTOR OF PHILOSOPHY</u>

CALCULATION OF FEMORAL STRAIN DURING NORMAL ACTIVITIES USING EFFICIENT
COMPUTATIONAL METHODS

HAMED ZIAEI POOR

Efficient calculation of femoral strain is important for various biomechanical applications, such as predicting femoral strains over multiple physical activities; improving the design of implantable devices; and assessing the risk of femoral fracture. The finite-element method has been used largely for the calculation of femoral strain. However, generating and solving the models using common image-based procedures make it practically impossible, particularly for large studies of bone which need to run the thousands of simulations to explore the interdependence between femur anatomy, bone quality, strain, and motor task using lots of point data, meaning that FE models are extensively large and computationally too expensive to run. Surrogate modelling techniques are used successfully for various applications in biomechanics however the characteristics of these methods need to be investigated further.

This thesis proposes a novel technique for the efficient calculation of femoral strain over multiple activities and individuals. This is achieved by taking three different steps: (I) assessing the ability of Multivariate Linear Regression (MLR) to predict the femoral strain field in a single participant while executing different normal activities; (II) developing a training-free method based on the Superposition Principle Method (SPM) and comparing its performance against that of three popular surrogate models; and (III) evaluating the feasibility of using Principle of superposition for prediction of femoral strain within a cohort of patients. To achieve this, Superposition Principle Method needs to be integrated with an Active Shape and Appearance Model, allowing to predict femoral strain by capturing the variation in femur geometry, bone distribution, and thereby enabling population-based studies into multiple subjects and motor tasks.

The MLR model provided a viable solution for the rapid calculation of full femoral strain fields by estimating femoral strain for a full activity cycle in 13 seconds compared with 55 minutes for FEM, enabling large statistical analyses. The SPM method provided the lowest error (RMSE = 40 me), the fastest model construction time (3.2 h) and the second-fastest prediction time per activity (36 s) after the MLR method. Finally, the integration of SPM combined with statistical shape and appearance models enabled efficacy in the prediction of femoral strain for an arbitrarily selected instance within the population and motor task. The peak error was 1.4 – 4.9%, in agreement with the error (i.e., 4.2 – 8.3% of peak strain) in current FE technologies based on CT images for predicting femoral strain. When the performance of the model was examined for three randomly selected participants which were not used previously for building the model, a good correlation was observed between the FE and SPM2 strain calculations (RMSE < 10% of peak strain, R^2 > 0.86). This was in agreement with previous studies (RMSE 11 – 15 % of peak strain, R^2 > 0.88). The major source of error was related to the reconstruction of three independent femurs from the Active Appearance Model (RMSE = 488$\mu\varepsilon$, R^2 = 0.95) compared with the error originated from Active Shape Model (RMSE = 261$\mu\varepsilon$, R^2 = 0.97). In conclusion, the combination of the Superposition principle and Principal component analysis is an effective solution for a running population-based simulation of femoral mechanics during activity. However, active appearance models need further improvement to be used for large biomechanical analysis of intact or implanted bone.

DECLARATION

I certify that this thesis does not incorporate without acknowledgment any material previously submitted for a degree or diploma in any university; and that to the best of my knowledge and belief it does not contain any material previously published or written by another person except where due reference is made in the text.

HAMED ZIAEI POOR

ACKNOWLEDGEMENTS

CONTENTS

TABLES

FIGURES

Chapter 1 : INTRODUCTION

Introduction

Efficient calculation of femoral strain is important for various biomechanical applications, such as estimation of femoral strain for multiple activities (Martelli et al., 2014b), where muscle and joint forces are assumed to be stochastic, rather than deterministic variables (Martelli et al., 2015a; Martelli et al., 2015b), or in large biomechanical analyses of bone. The Finite Element (FE) method has been used extensively for decades as a powerful computational tool for calculation of femoral strain (Taylor and Prendergast, 2015). While the computational costs of the FE method for single-subject conditions (Polgar et al., 2003), or single-subject studies of bone (Noda et al., 2018; Taylor and Prendergast, 2015) is not a major computational issue. However, the adoption of the FE method into clinical practice, and also for solving large-scale studies of bone (e.g. population-based studies) is still a computational barrier. For example, to generate FE models for multiple-subject studies, a level technical competences, and a lengthy process is needed: obtaining patient anatomic geometries of bone from CT or MRI images via segmentation process (Rathnayaka et al., 2011); obtaining the material properties of bone via calibration and mapping the density distribution (Taddei et al., 2004); defining the loading and boundary conditions in FE models (Keyak et al., 2001), and then solving the FE models using FE solvers. This process may take varying lengths of time, between minutes and several days, depending on the scale and the complexity of the model (e.g. contact modelling, or linear-elastic models). Therefore, there is a growing interest to decrease the current computational costs needed for generating and solving FE models.

Several different research groups have attempted to reduce the computational costs associated with building FE models by taking various approaches, such as partially or fully automating the image segmentation to eliminate manual intervention and its laborious

processes (Almeida et al., 2016; Carballido-Gamio et al., 2015; Pauchard et al., 2016), or by building statistical shape and appearance models of bone as a resource for running large scale FE studies; such as assessing the risk of fracture in a population with 1000s of femur samples (Bryan et al., 2010; Grassi et al., 2017; Taghizadeh et al., 2015; Vaananen et al., 2012). However, there are still some limitations. For example, to calculate femoral strain in large statistical models, the FE model needs to be generated for each patient individually, and by changing the loading condition, the FE models needs to be solved, requiring a time-consuming and labour-intensive process. This computational barrier could prohibit the application of bone biomechanical analysis becoming commonplace in clinics (Martelli et al., 2015a; Martelli et al., 2015b). In fact, if the strain could be calculated in a fraction of the time – a few seconds or minutes, rather than hours or days – then it would be feasible to calculate femoral strain for different clinical applications (Pizzolato et al., 2017b), such as providing biofeedback to patients and clinicians during exercise (Pizzolato et al., 2017b), and assessing the performance of implantable devices by considering various surgical and patient variabilities (Bieger et al., 2012; Helwig et al., 2009).

Surrogate modelling techniques are used as a viable solution to reduce the computational costs needed for solving expensive FE models. The basis of the technique lies in fitting a function into a set of training data sets consisting of inputs (e.g. forces) and outputs (e.g. strain/stress) to represent the response of the system by finding the causal relationship between inputs and outputs (Taylor et al., 2017). Although there is an upfront computational cost for training the surrogate model, once constructed, the model can be used for rapid prediction of femoral strain. The capability of surrogate modelling techniques has been explored for various orthopaedic biomechanics applications, such as assessing the effect of implant positioning on the primary stability of a total hip replacement (Bah et al.,

2011), or the estimation of micromotion between bone and implant during a complete gait cycle (Fitzpatrick et al., 2014). Although these surrogate models are able to improve the speed of computation for biomechanical applications significantly, there are still some limitations with these approaches. For example, the performance of a surrogate model depends on the type of application. For instance, while a linear-based surrogate model could be suitable for linear-elastic FE models (Fitzpatrick et al., 2014), it may be unsuitable for highly non-linear systems, such as modelling the pattern of wear on an implantable knee (Lin et al., 2009). Further to this, the way that the surrogate model is trained can affect its performance. For example, a surrogate model developed based on a set of training data obtained from normal walking may not be capable of predicting other types of activities, such as jumping, with a higher degree of accuracy. In addition, a surrogate model developed for a single patient is only usable for that specific patient, because of differences in terms of shape, material properties, and physiological loading conditions. Therefore, more generalised techniques need to be explored, so that strain predictions can be performed for multiple subjects and activities, without these limitations.

Objectives and outline

The overall aim of this PhD thesis is focused on developing and testing the performance of potential computational methods for rapid prediction of femoral strain. While there are studies that used maximum principal stress and strain criteria for various clinically-relevant scenarios, like bone failure mechanism (Keyak and Rossi, 2000; Kheirollahi and Luo, 2015), the current research uses equivalent von Mises strain as a compact indicator of both compressive and tensile strain states. In the first stage, this research will explore the performance of Multi-Linear Regression (MLR) for predicting femoral strain fields during a series of daily activities. To build the model, the original training datasets, consisting of

muscle, joint reaction forces and femoral strain fields for 1000 frames of motion will be computed using a previously developed musculoskeletal and finite-element model (Martelli et al., 2015b). This work will provide an insight into the efficacy and accuracy of such a linear-based surrogate model when strain calculation was compared with FE results. In the second stage, by leveraging the linearity of elastic FE models of bone, the superposition of principle method (SPM) will be used to calculate full femoral strain during normal physical activites. The outcome of SPM method would be a tensor of strain, allowing to examin to examine any strain metric without having to train a new model, a limitation of other surrogate modelling techniques.

The performance of this method will then be compared with three popular surrogate models: Multi-Linear Regression (MLR), Multivariate Adaptive Regression Splines (MARS), and Gaussian Process (GP). The training datasets required for building the surrogate models will be created using Latin Hypercube (LH) sampling and Design of experiments (DOE). The performance of the investigated methods will be examined by measuring the strain error observed between the calculated strain fields and FE results, and the CPU time needed for both construction and solution phases.

The ultimate aim of this work is to test the applicability of Superposition principle method for estimating femoral strain in a population-based study by incorporating both geometry and the material property distribution of bones using a PCA-based statistical model. To fit the PCA model into training datasets, all femurs will be registered via an established procedure (Bryan et al., 2010) to make a point-to-point correspondence between each member of the training dataset. To make sure that the developed statistical model is able to reproduce the femurs accurately, a leave-one-out approach will be used and the reconstructed error associated with shape and modulus of femurs will be analysed. The

9

accuracy of the Superposition principle method then will be examined for synthetic population derived from a statistical model, and unseen femurs during a replicated random frame of motions. The obtained results will be compared with the corresponding FE calculations as the reference.

Structure of thesis

The literature review is split into three chapters. *Chapter* 2 provides an introduction to the musculoskeletal system of the lower limb with the main focus on the anatomy and biomechanics of the femur during motion. *Chapter* 3 discusses the relevant literature about the development of musculoskeletal-FE models and population-based studies of bone. *Chapter* 4 reviews the application of popular surrogate modelling techniques in orthopaedic biomechanics and provides an overview of the characteristics of each technique. *Chapter* 5 explores the capability of Multi-Linear Regression (MLR) for rapid prediction of femoral strain. *Chapter* 6 explains the development process of Superposition of principles and compares its performance with three popular surrogate models by measuring the time and strain error. *Chapter* 7 evaluates the applicability of Superposition of principles integrated with a PCA-based statistical model for rapid prediction of femoral strain during locomotion in the population. Finally, *Chapter* 8 discusses the significant findings of this thesis, as well as its limitations, applications and potential future improvements.

Publications

The work described in this thesis has led to the following conference abstracts and journal publications:

- ***Chapter 5***

  H. Ziaeipoor, S. Martelli, M. Pandy, M. Taylor, 2019 'Efficacy and efficiency of multivariate linear regression for the rapid prediction of the femoral strain field during activity', Medical Engineering & Physics, Vol. 63, PP. 88-92.

  H. Ziaeipoor, S. Martelli, R. Al-Dirini, D. O'Rourke, M. Taylor, 'An efficient computational model for predicting the strain distribution during common physical activities: Surrogate modelling vs FE simulations', XXVI Congress of the International Society of Biomechanics, Brisbane, Australia, ***podium***, 2018.

- ***Chapter 6***

  H. Ziaeipoor, M. Taylor, M. Pandy, S. Martelli, 2018 'A novel training-free method for real-time prediction of femoral strain', Journal of Biomechanics, Vol. 76, PP. 100-116.

  H. Ziaeipoor, S. Martelli, M. Taylor, 'Comparison of computational methods for the calculation of femoral strain during normal activity', 8th World Congress of Biomechanics, Dublin, Ireland, ***podium***, 2018.

  H. Ziaeipoor, S. Martelli, M. Taylor, 'Rapid prediction of femoral strain using a novel computational model' 24th Annual Scientific Meeting ANZORS, in Perth, Australia ***podium***, 2018.

- ***Chapter 7***

  H. Ziaeipoor, S. Martelli, M. Taylor, (2019), "Time-effective population-based modelling of femoral mechanics during physical activity", The European Society of Biomechanics, ESBiomech2019, Vienna, Austria, ***podium***, 2018.

  H. Ziaeipoor, S. Martelli, M. Taylor, "A novel computational method for rapid prediction of femoral strain in the population" 25th Annual Scientific Meeting ANZORS, in Canberra, Australia ***podium***, 2019.

Chapter 2 : MUSCULOSKELETAL SYSTEM OF LOWER LIMB

Structure, function and mechanical properties of bone

Bone is a living, growing and rigid tissue with a complex structure that performs both mechanical and metabolic functions. The primary mechanical role of bone is to provide support, structure, and locomotion through interaction with muscles and ligaments. The second mechanical role of bone is to provide protection for other organs and maintain the shape of the body. The main metabolic function of bone is to store nutrients, minerals, and lipids and produce blood cells that nourish the body and protect the body against infection.

The skeletal system is approximately composed of 260 bones and the shape of each influences its function. For example, flat bones (e.g. skull and sternum) can mainly play a protecting role, while long bones (e.g. femur and humerus) primarily enables the body to have different ranges of locomotion. A typical long bone can be divided into three main regions, consisting of the central cylindrical shaft, known as the diaphysis, and two rounded and broader ends, known as the epiphyses (Figure 2.1). The metaphysis with a conical shape connects the diaphysis with each epiphysis. The epiphyseal and metaphyseal regions are wider, resulting in the provision of greater support to articular cartilage (Cowin, 2001).
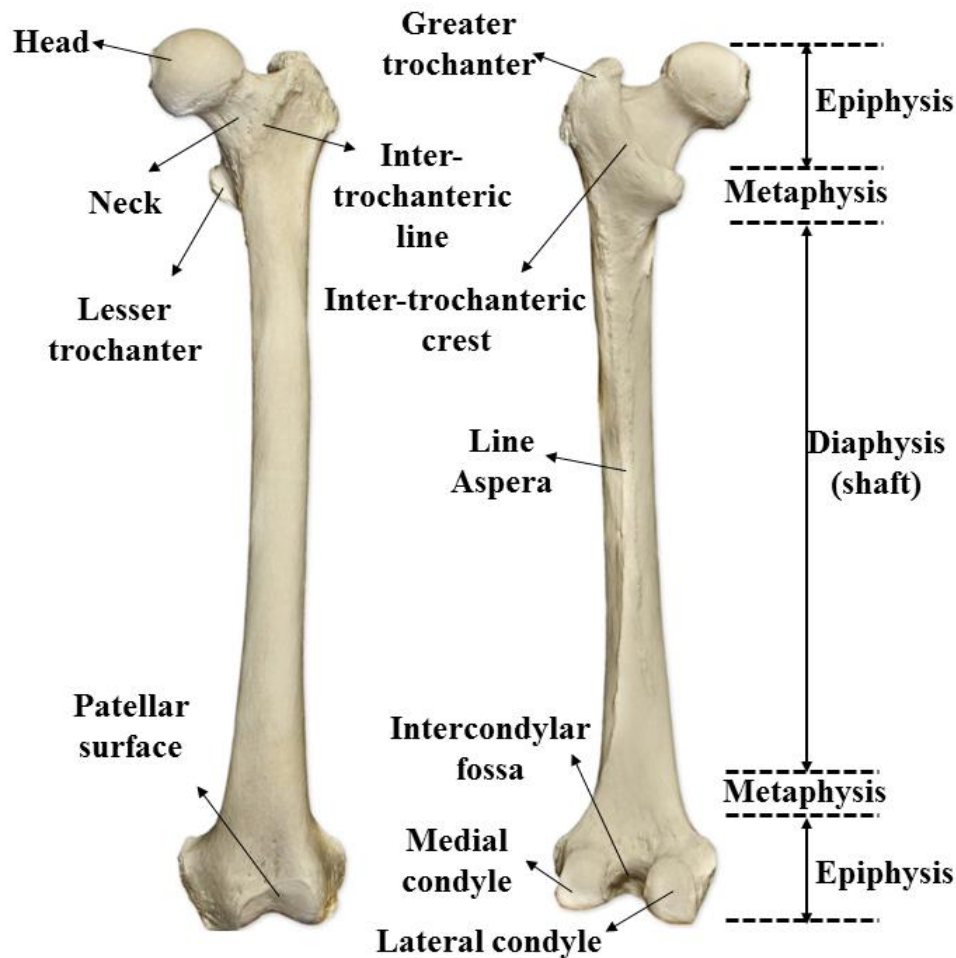
Figure 2.1: Anterior (left) and posterior (right) views of left femur, "The figure was reproduced with permission from https://www.skullsunlimited.com".

A bone structure comprises two parts, (i) the inner volume which is made up of cancellous bone and bone marrow, and (ii) the outer later which is composed of cortical bone. The cortical bone primarily forms the diaphysis area, while cancellous bone forms the inner metaphysis and epiphysis (Cowin, 2001). Cortical bone is a dense structure, which provides greater strength compared to cancellous bone, a suitable load bearing capability during motion, and provides the required attachment site for the surrounding muscles and ligaments (Cowin, 2001). At the microscopic level, the diaphyseal cortical bone consists of two distinct types of bone: haversian bone, which forms the bulk of the diaphyseal volume,

and laminar bone, which covers the endosteum and periosteal surfaces (Cowin, 2001). At the microscopic level, both haversian and laminar bones can be considered as composite structures (Figure 2.2). The laminar bone is composed of concentrically arranged lamellae, with a typical thickness of 200 μm, and a network of blood vessels to supply nutrients to the surrounding bone. Each lamella comprises of five sublayers (Weiner et al., 1999), and each sublayer is an array of aligned mineralised collagen fibrils of different orientations. The osteon is approximately 200 μm in diameter and 20 μm in length (Figure 2.2). The haversian canals enable blood vessels and nerves through the Osteon.
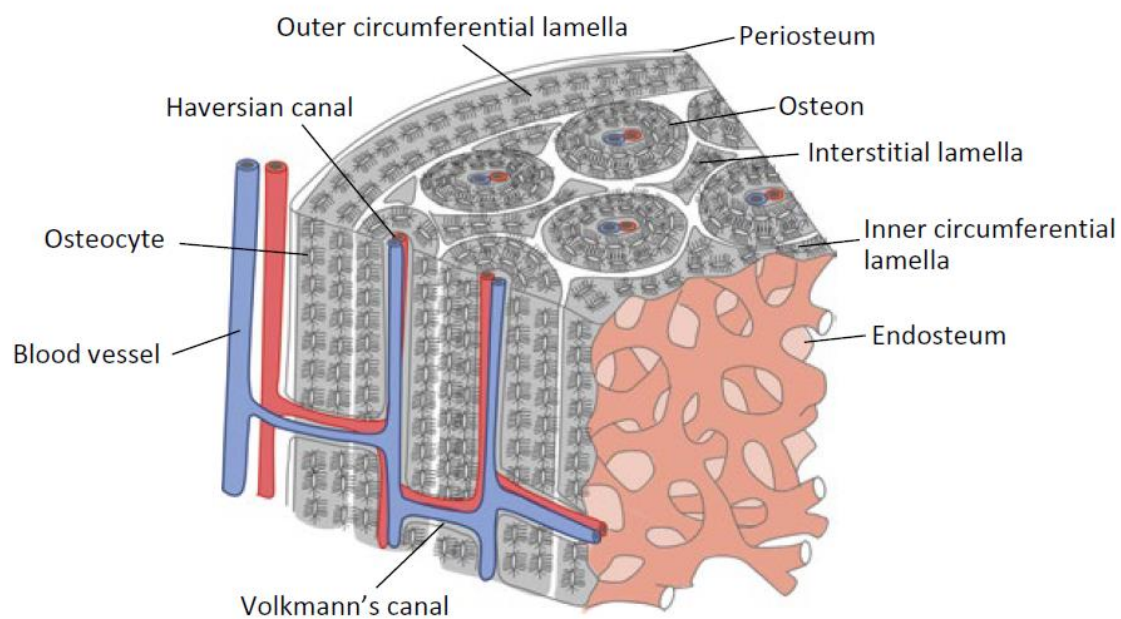
Figure 2.2: Microscopic structure of compact bone (Nakano, 2015), "Reprinted by permission from Springer Series in Biomaterials Science and Engineering: Advances in Metallic Biomaterials, Springer-Verlag GmbH Berlin Heidelberg, by Takayoshi Nakano, Copyright (2015)".

Cancellous bone, also known as spongy or trabecular bone, is a complex three-dimensional porous structure which forms approximately 20% of the human skeleton, and the surface area per unit volume is approximately eight times bigger than that in the cortical bone. Cancellous bone is made of plates and bars (trabeculae bone) adjacent to small,

irregular cavities that contain most of the body's red bone marrow, which produces blood cells (Cowin, 2001). In addition to providing structural stability, cancellous bones also contain many stem cells which are precursors of osteoblast and osteoclast responsible for bone regeneration. Furthermore, while apparent density, which is defined as the mass of the sample divided by the total sample volume, including porosity (Oftadeh et al., 2015) is an important parameter in the determination of the mechanical properties of bone, bone response to loads is not just dependent on apparent density. The apparent density itself is reported primarily in two different forms: apparent wet density which refers to the wet tissue mas divided by the total specimen volume, and apparent ash density which is the ash mass divided by the total specimen volume (Oftadeh et al., 2015). It has been discussed that both cancellous and cortical bones are made of similar composition, and the difference in their mechanical properties is primarily due to their difference in apparent density (Carter and Spengler, 1978). Cortical bone has an apparent density ranging from 1.5 to 2.0 g/cm^{-3}, while cancellous bone has a lower density changing from 0.05 to 1.1 g/cm^{-3}(Carter and Spengler, 1978; Martin, 1991).

Bone composition

From a material science point of view, bone is a composite material with a complex cellular architecture, which changes throughout the life of an individual (Webster and Ahn, 2007). As a dynamic tissue, bone continually remodels itself with the addition or removal of material in response to its mechanical environment and loading condition. Within a bone, osteoblasts are mainly involved in the formation and mineralisation of bone. Osteocytes play a crucial, central role in regulating the dynamic nature of bone by sensing the mechanical loading of bone and regulating the onset of both bone formation and resorption (Schaffler and Kennedy, 2012); Osteocytes regulate local mineral deposition and chemistry at the bone

matrix level, and they also function as endocrine cells producing factors that target distant organs such as the kidney to regulate phosphate transport. Osteocytes appear to be the major local orchestrator of many bone functions.

The mineralised organic matrix of bone is primarily collagen (35%), which provides its toughness; the mineral phase is carbonated hydroxyapatite (65%) for structural stiffness and active proteins to regulate cellular functions (Henkel et al., 2013; Martin, 1991; Martin, 1998). The entire volume of trabecular bone is replaced every 3 – 4 years, and around 5 – 7% of cortical bone changes weekly (Marieb, 2004). The rate of bone modelling is higher during the bone growth and this drops when the skeletal system becomes more mature (Frost, 1990).

Mechanical properties of cortical bone

Young's modulus and the ultimate strength of bone are most commonly used for reporting the material properties of bone by using two techniques, including mechanical tests (Choi and Goldstein, 1992; Rho et al., 1999), ultrasonic measurements (Grant et al., 2014; Rho et al., 1993) and nanoindentation tests (Wang et al., 2006b). The advantage of the ultrasonic method over mechanical tests is that this non-destructive method allows testing of specimens with more complex geometries from macro to microstructure levels (Oftadeh et al., 2015).

Measurement of the mechanical properties of bone using the above mechanical tests showed that cortical bone is transversally isotropic and is 1.5 – 2 times stronger in the longitudinal direction compared with radial and circumferential directions (Ashman et al., 1984; Wang et al., 2006b). Young's Modulus of bovine cortical measured by a nanoindentation test was shown to be 24.7 ± 2.5 GPa for osteons and 30.1∓2.4 GPa for

interstitial lamellae longitudinally. The average elastic modulus of bovine cortical was reported to be 19.8 $\mp$ 1.6 GPa in the transversal direction (Wang et al., 2006b), which was in agreement with the values of previous studies reported for osteons (22.5 GPa) and interstitial lamellae (25.8 GPa) by Rho et al. 1997. The ultrasound assessment of elastic moduli of cortical bone was shown to be between 20 – 22 GPa longitudinally, and 12 – 14 GPa transversally (Ashman et al., 1984). These findings were comparable with previous studies obtained from the mechanical tests ranging from 14-20 GPa (Reilly and Burstein, 1974). The differences in these studies was likely due to the viscoelastic nature of bones and the rate of the applied loads, since the mechanical loading demonstrates a quasi-static load case whereas the acoustic analysis represents a higher load rate, and hence can create higher strain rates (Oftadeh et al., 2015).

Mechanical properties of cancellous bone

Cancellous bone has a highly anisotropic behaviour, and its strength and density depends upon the direction of the applied loads, and can be largely effective for particular bones and regions. For example, in the femoral head, the main trabecular structure aligns with the direction of the hip force to provide greater strength. However, for bones under largely uniaxial loads (e.g. vertebrae), trabecular bone often has a columnar structure with cylindrical symmetry, to provide a greater strength in the direction of load, while having a lower strength in the transversal direction (Gibson, 1985).

The mechanical testing of Young's Modulus of cancellous bone has been shown to range as low as 12 MPa (Martens et al., 1983) to as high as 3350 MPa (Kaneko et al., 2004) as a function of its density, and varies marginally from compression to tension and is also dependent on the anatomical site (Morgan et al., 2003). As can be seen from Table 2-1, the

highest elastic modulus was observed for the femoral neck with approximately 3 GPa (Morgan and Keaveny, 2001). Furthermore, it has been shown that yield strains vary between sites by at most 20%, depending on various parameters such as, hard tissue material properties, trabecular architecture, or a combination of these two factors. This finding was also observed in an earlier (Hildebrand et al., 1999; Kopperdahl and Keaveny, 1998) by presenting a ''rod-like'' structure for trabecular bone from the human vertebra, which is more susceptible to large deformations (e.g. bending and rotation), compared with ''plate-like'' structure from femoral head and neck.

Table 2-1: Mechanical properties of cancellous bone classified based on anatomic sites and modes of loading.

Anatomic site–Loading mode		Apparent density (g/cm3)	Modulus (MPa)	Yield Strain (%)	Yield Stress (MPa)
Vertebra	Compression	0.18 ± 0.05	344 ± 148	0.77 ± 0.06	2.02 ± 0.92
	Tension	0.19 ± 0.004	349 ± 133	0.70 ± 0.05	1.72 ± 0.64
Proximal Tibia	Compression	0.23 ± 0.06	1091±634	0.73 ± 0.06	5.83 ± 3.42
	Tension	0.23 ± 0.10	1068± 840	0.65 ± 0.05	4.50 ± 3.14
Greater Trochanter	Compression	0.22 ± 0.05	622 ± 302	0.70 ± 0.05	3.21 ± 1.83
	Tension	0.22 ± 0.04	597 ± 330	0.61 ± 0.05	2.44 ± 1.26
Femoral Neck	Compression	0.58 ± 0.11	3230± 936	0.85 ± 0.10	17.45 ± 6.15
	Tension	0.54 ± 0.12	2700± 772	0.61 ± 0.03	10.93 ± 3.08

Keaveny and Morgan (2001) evaluated the relationship between the trabecular bone strength and the anatomic site. They discovered that the yield strain/stress was dependent on the anatomical sites both for compressive and tensile loading (Table 2-1). The yield strain was higher in compression than tension, regardless of the anatomical sites. The average tensile yield strain ranged from 0.61 ± 0.03% for the femoral neck and the trochanter to 0.70 ± 0.05% for the vertebra. The average compressive yield strains ranged from 0.70 ± 0.05% strain for the trochanter to 0.85 ± 0.10% strain for the femoral neck (Table 2-1). A similar behaviour was noted when the relationship between stress and the apparent density was analysed. For example, for an apparent density of 0.30 g/cm^3, the yield stress (in compression) between vertebra to proximal tibia was differed by 31%.

Mathematical relationships between density, Young's modulus and strength

The mechanical properties of bones can be estimated from Computed tomography (CT) scans. Computed tomography is a non-invasive diagnostic imaging procedure that uses computer and a rotating x-ray beam to produce images of the body. The CT scans of bones can define the density of each point using pixel greyscale values. Image segmentation, which is the process of partitioning a digital image into multiple segments, provides the material properties and geometry of bone. An accurate segmentation of bone is of importance for the 3D reconstruction of bone and can be effective on the accuracy of the geometry and material of bone used for developing the computer-based models (Mouloodi et al., 2019a). It has been shown that through a segmentation process that Young's Modulus of a single femur varies from 77 – 1,835 MPa within the trabecular bone, and changes from 1,850 – 16,737 MPa for cortical bone (Wagner et al., 2010).

Different approaches were used for generating the segments from CT scan images, such as manual, semi-automatic and automatic segmentations. Each procedure has its pros and cons. Users can take a manual segmentation approach, but this can be a time-consuming process, particularly when a high number of slices of CT images are required. Semi-automatic segmentation requires user interaction as they need to provide a small amount of input data to improve the accuracy of segmentation. Automatic segmentation is the fastest procedure which does not need user involvement, but the accuracy can be compromised. However, for segmentation of a large number of CT images, automatic segmentation is the only feasible approach and several commercially computer packages are available for this.

The correlation between Young's modulus and apparent density has been determined by defining different forms of equations, including linear, power or exponential ones. However, the modulus-density relationship is well-reported generally in the form of a power law, in which *A* and *B* are constants:

$$E = A\,\rho^{B}$$

Morgan et al. (2003) evaluated the relationship between elastic modulus and density for trabecular bone by collecting 142 specimens from 61 donors for different anatomical locations and under different loading conditions (Morgan et al., 2003). They found a large variability across different anatomical sites, which was mainly due to the health status and ethnicity of the studied population. According to their research, values for constant of *A* varied from 3000 – 30000, and ranged from 1.14 to 3.2 for constant of *B*. This study highlighted the importance of defining an ideal representation of the Young's modulus

(Table 2-2). The below table shows other equations relating the Young's modulus and density of bone at different anatomical sites and range of ages.

Table 2-2: Modulus – density relationships for different bone anatomical sites and range of ages

Study (reference)	Cadavers (No.)	Type of Bone	Young's modulus (E, GPa) Strength (σ, MPa)	Age (years)
(Lotz et al., 1991b)	123	Femoral metaphysis (Cortical)	$E = -13.43 + 14.261\rho$	23 – 90
(Keller, 1994)	5	Femur (Cortical and Trabecular)	$E = 10.5\rho^{2.29}$	46 – 84
(Morgan et al., 2003)	61	Femur (Trabecular)	$E = 6.850\rho^{1.49}$	67 ±15
(Kaneko et al., 2004)	10	Femur (Trabecular)	$E = 10.88\rho^{1.61}$	45 – 67
(Lotz et al., 1990)	4	Femur (Trabecular)	$\sigma = 25.0\,\rho^{1.80}$	25 – 82
(Mosekilde et al., 1987)	42	Lumbar spine (Trabecular)	$\sigma = 24.9\,\rho^{1.8}$	15 – 87
(Kopperdahl and Keaveny, 1998)	11	Lumbar spine (Trabecular)	$\sigma = 33.2\,\rho^{1.53}$	32 – 65

The anatomy and function of the femur

The femur is one of the most prominent bones in the human body. The main component of a femur is the femoral head, femoral neck, the greater trochanter and lesser trochanter. The hip is a unique load-bearing joint surrounded by powerful and well-balanced muscles, enabling a series of different motions while providing suitable stability. The hip joint can be represented by a ball (femoral head) and socket joint (acetabulum) which has translation stability and rotational mobility. Therefore, a healthy hip can perform a diverse range of

movements, including flexion – extension, medial rotation and lateral rotation – externally rotate, and abduction – adduction.

Articular cartilage covers approximately 60 to 70% of the hip joint (Byrne et al., 2010). The hip joint also has a synovial membrane, which generates and contains synovial fluid to lubricate the joint and to decrease the frictional forces between surfaces within the joint. Cartilage is an avascular material and hence relies on the synovial fluid to provide nutrients as well as remove waste products. The femoral head is connected to the femoral shaft by the femoral neck. The femoral neck has a cylindrical shape and has an angle of 120-135 degrees with the femoral shaft, known as the neck-shaft angle. The femoral neck anteversion (FNA) is the angle between the longitudinal axis of the neck and the axis passing horisontally through femoral condyle and can be varied depending on foetal development, heredity, mechanical forces, and intrauterine position (Guidera et al., 1994). For example, the FNA angle at birth is about 40 degrees and decreases gradually to approximately 8 – 15 degrees in adulthood (Fabeck et al., 2002). The FNA angle higher than 20 degrees is considered excessive, whereas an angle of less than 10 degrees is considered femoral retroversion (Tonnis and Heinecke, 1999; Tonnis and Skamel, 2003). The femur is often described as being slightly curved in the sagittal plane (Harper and Carson, 1987) and may vary by ethnicity.

Muscles around the hip joint

The hip is a load bearing joint which is surrounded by large muscles and ligaments. The 21 muscles that cross the hip provide both triplanar movement and stability between the femur and acetabulum (Neumann, 2010; Schache et al., 1999). The principal muscles driving the different movements of the hip joint are listed below (Figure 2.3):

- **Flexion**: rectus femoris, iliopsoas, sartorius, and pectineus.

- **Extension:** gluteus maximus and hamstring muscles, including semimembranosus, semitendinosus and biceps femoris.

- **Abduction:** gluteus minimus, gluteus medius, piriformis and tensor fascia latae.

- **Adduction:** adductors longus, brevis and magnus, pectineus and gracilis.

- **Lateral rotation:** biceps femoris, gluteus maximus, piriformis, assisted by the obturators, gemelli and quadratus femoris.

- **Medial rotation:** anterior fibres of gluteus medius and minimus, and tensor fascia latae.

The primary hip flexor and hip extensor muscles are iliopsoas and gluteus maximus respectively, however there are other muscles which are also involved with this movements, such as psoas, iliacus, rectus femoris, tensor fasciae latae, biceps femoris, and semitendinosus. The tensor fascia latae and gluteus medius and minimus are known as primary hip abductor muscles, while adductor longus, adductor brevis, and adductor magnus are more involved with hip abduction. Finally, the gluteus medius, gluteus minimus, and the tensor fascia latae are the main internal rotators of the hip joint.
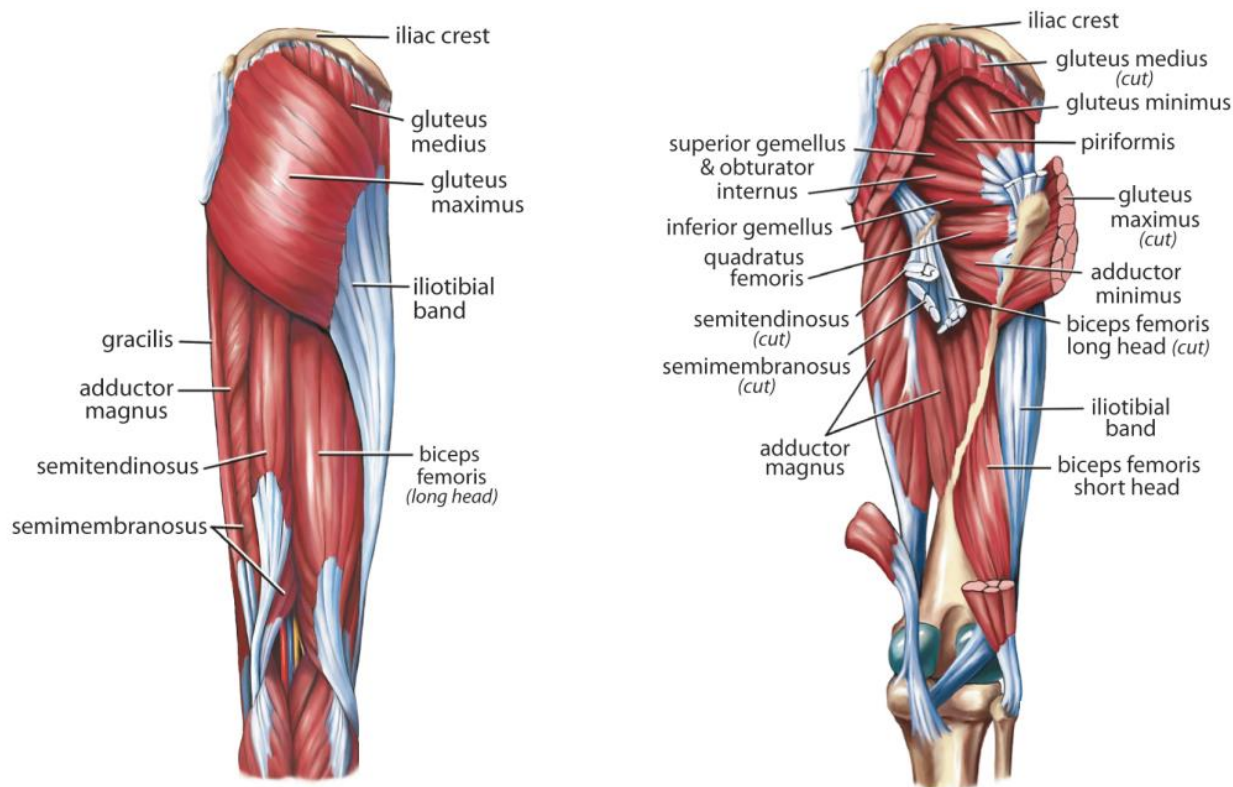
Figure 2.3: Deep (right) and superficial (left) muscles around the hip (Retchford et al., 2013), "with permission from http://www.ismni.org/jmni/ ".

Each of the above motions has some limitations during locomotion; for example, the maximum degree of rotation for the flexion is about 120, and this rotation is restricted by the contact between the abdominal wall and the thigh. The extension of the hip is variable between individuals, but it is around 20 degrees. The maximum value of hip rotation in the case of combining lateral rotation and medial rotation is about 90°. The abduction and adduction have a rotational degree of 45.

Muscles can only contract and apply tensional loading at their insertion. Besides, some muscle is wrapped around the femur, resulting in a contribution to bending, torsion and also shear loading of the bone. Another point to note is that the attachment sites of different muscles can also be important in terms of their functional tasks. For example, the rectus

femoris originates on the anterior inferior iliac spine, passes across the hip joint, down the shaft of the femur superficially, and lastly attaches to the tendons around the knee. This muscle has some actions on the flexion as it crosses two major joints in the lower extremity, hence it has some actions on the flexion and extension of hips and knees, and it is also an active muscle during walking.

Ligaments around the hip

Hip ligaments have two different functions (Figure 2.4). The first function of ligaments is to guide the motion of the joint by providing the required flexibility and stability for the femoral head to move within the acetabulum during motion. The second task is providing a supportive role for the surrounding muscles to prevent excessive motion and injury (O'Donnell et al., 2018). The most notable ligaments in the hip joint and their specific tasks are listed as below (Bowman Jr, 2010; Ranawat et al., 2009):

Iliofemoral is one of the strongest ligaments with a 'Y' shaped appearance, which helps to provide stability of the body during the standing position. This ligament also keeps the femoral head pressed into the acetabulum to provide a safe constraint, limiting the risk of joint dislocation.

Ischiofemoral is the longest ligament in the body, which twists around the femoral head and extends into the femoral neck. This ligament has different tasks, such as limiting hip's extension, adduction and abduction while allowing the maintenance of the upright posture by reducing the need for muscle contractions.

Pubofemoral is a ligament on the inferior side of the hip joint which attaches the most forward part of the pelvis to the femur. This ligament, which has a triangular shape, prevents excessive extension and abduction of the hip.
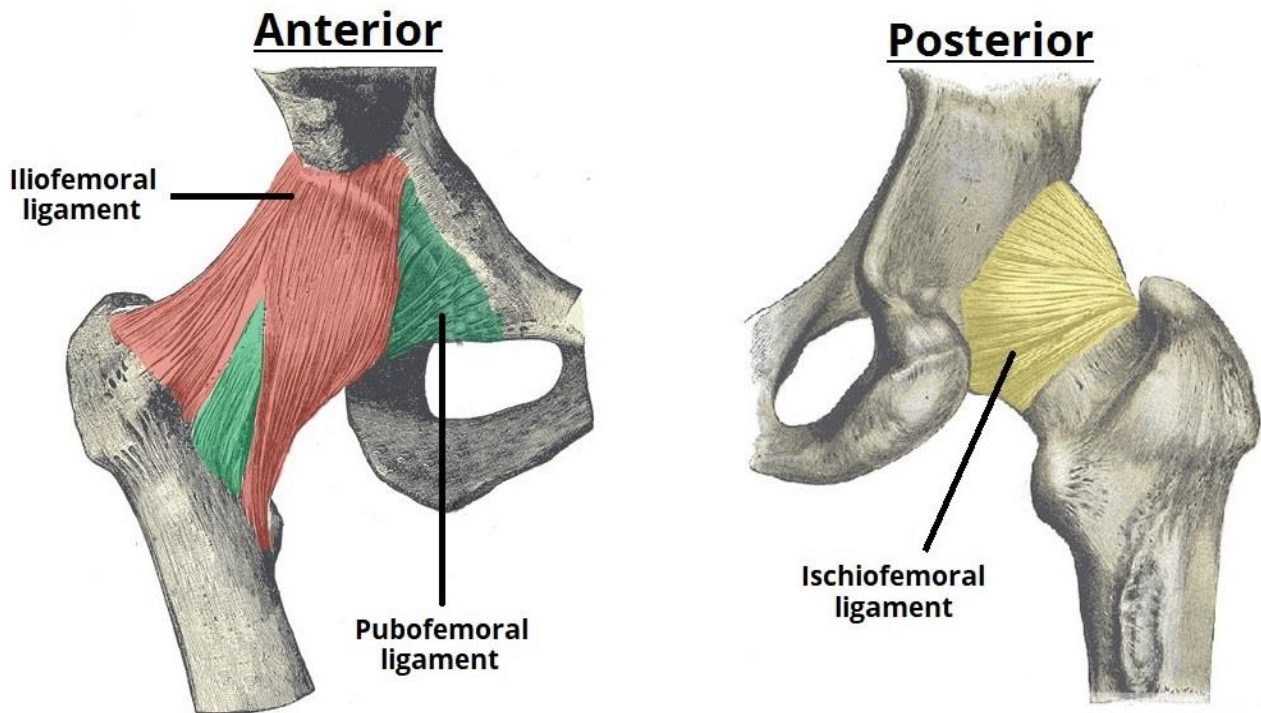
Figure 2.4: The extracapsular ligaments of the hip joint; pubofemoral, ischiofemoral and ileofemoral ligaments, "with permission from https://teachmeanatomy.info".

Kinematics and kinetics of the hip

Lower-limb motions are very important for investigating various daily activities, such as walking, sitting down, ascending and descending stairs, sit to stand to sit, and deep knee bends. Among daily activities, walking in the most common daily and physical activity which has been investigated, by largely using motion analysis of the lower limb. Walking is a complex movement which requires a body to be in perfect harmony inside.

Studying the static and dynamic behaviours of the body during motion requires some information about the position of the body during motion and finding the force applied on the hip. To gain such an understanding, gait cycle has been suggested as a standard loading condition (Figure 2.5). Gait is a sequence of movements occurring between two consecutive heel strikes of the same foot and contains two main phases: stance and swing. In other words, a gait is a sequence of motions from the initial heel strike to the next heel strike of the same leg. The stance phase makes up 60% of the gait cycle, while the swing phase forms the other 40%. The main phases are sub-divided into separate sub-phases. The body has double limb support at the initial contact and the terminal swing. During normal gait cycle, the hip rotates approximately 40° in the sagittal plane with a maximum hip flexion of 30-35 degrees occurring in the late swing phase, and 10 degrees of hip extension near toe-off. In the frontal plane, the hip has 10 degrees' adduction at initial contact and has 5-10 degrees of hip abduction in the early swing phase. The total of internal/external rotation along the pelvic is approximately 15 degrees. It has been reported that the maximum internal rotation occurs near mid-stance and the hip externally rotates during the swing phase (Krebs et al., 1998).
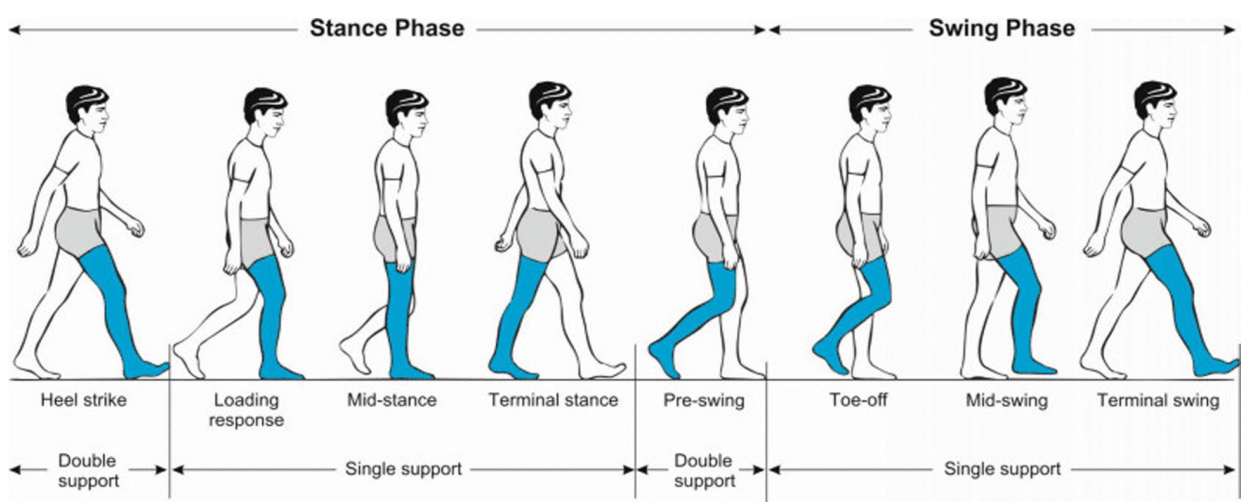
Figure 2.5: Different phases of a gait cycle (Moltedo et al., 2018), "with permission from https://jneuroengrehab.biomedcentral.com".

While most muscles are active in the beginning and end of the swing and stance phase (Gate et al., 2009), some muscles are active in particular phases to perform a specific tasks. The hamstrings and gluteus maximus are active to aid hip extension at the initial contact phase. The abductors provide stability of the pelvis during the mid-stance phase. Gluteus medius and minimus remain active in terminal stance to provide a stability for lateral pelvic. The adductor longus is the most persistent hip flexor. In terminal swing, the hamstrings and gluteus maximus are strongly active to decelerate knee extension and hip flexion (Krebs et al., 1998).

In order to understand the mechanical behaviour of the femur, it is essential to gain an understanding about the forces that act upon it. During motion two types of forces are generated, which are muscle forces and joint reaction force. Research shows that no one has measured the muscle forces which work together to generate hip joint contact force. A possible solution is to use the musculoskeletal to estimate muscle forces and this will be discussed later in the next chapter.

Forces acting on implanted femoral components were measured directly for the first time in 1966 for a relatively few patients and time points shortly after implantation (Rydell, 1966). While the implants were permanent, the sensors and wires were used temporary and were designed to be removed after early postoperative data collection. In the mid to late 70s, passive telemetry (wireless) systems were used to measure metalon-cartilage pressures in a hemiarthroplasty (Carlson et al., 1974a; Carlson et al., 1974b). Battery-powered telemetry has also been used to measure forces in a total hip arthroplasty femoral component (English and Kilvington, 1979).

Advances in electronics has enabled the measurement of activity-dependent magnitudes and directions of hip contact forces with multiple instrumented total hip implants with multiple patients and activities monitored over several years after surgery (Bergmann et al., 2001; Graichen and Bergmann, 1991). Investigating the instrumented prostheses implanted in seven patients showed the highest joint reaction forces for 'uncontrolled' stumbling that exceeded by far those measured for any other activity. In this case, the maximum resultant force was reported to be approximately 400% of body weight (BW) during normal walking, and rose to 870% of BW during stumbling (Bergmann et al., 2004). A list of routine activities and the range of the joint reaction forces on the hip joint are collected and compared in Table 2-3.

Another important feature was generated joint reaction force varied between different patients, activities and even among various trials. Considering the joint reaction force for two patients while performing stair climbing (Bergmann et al., 1995) revealed that the peak hip contact force reached to 3.5 body weight (BW) for one patient, and in another patient was 5.5 body weight (BW), thus it can be concluded that this value may vary between different patients.

Table 2-3: Joint reaction force for daily activities.

Activity	Joint reaction force (BW%)	Reference
Walking	280–480	(Bergmann et al., 1993)
Walking	238–427	(Heller et al., 2005)
Walking	200–400	(Stansfield et al., 2003)
Walking	300-360	(Li et al., 2014)
Jogging	550	(Bergmann et al., 1993)
Stair climbing	251–556	(Heller et al., 2005)
Stair climbing	350–550	(Bergmann et al., 1995)
Standing up	181–220	(Bergmann et al., 2001)
Sitting down	149–176	
Knee bend	117–177	
2-1-2 stance	223–253	
2-1-2 stance	250–350	(Stansfield et al., 2003)
2-1-2 stance	250–300	(Li et al., 2014)
Sit to stand	200	(Stansfield et al., 2003)

Chapter 3 : MODELLING FEMORAL MECHANICS DURING NORMAL PHYSICAL ACTIVITY

Introduction

Computing femoral strain distribution during normal physical activity is important for simulating bone tissue adaptation (Adams et al., 1997; Geraldes and Phillips, 2014), for diagnosing individuals most at risk of femoral fracture (Bessho et al., 2009; Lotz et al., 1991a), and for optimising biomechanical behaviour of implantable devices (Chanda et al., 2015; Helwig et al., 2009). To gain an understanding about the generated femoral strain during locomotion, the forces that are applied to the femur need to be identified, namely the joint contact and the muscle forces. Since the direct measurement of muscle forces *in vivo* is not possible, ground reaction force and joint kinematic data obtained through motion analysis are often used in conjunction with musculoskeletal and finite-element modelling to estimate muscle and joint forces and the respective elastic response of the femur.

Human motion analysis based on stereophotogrammetry

The aim of human motion analysis is to provide a 3D realistic representation of the movement of the musculoskeletal system during motor task performance. This can be achieved by collecting informative data about the mechanics of the musculoskeletal system of the whole body during the execution of a physical activity. This collected information can include various parameters such as the relative movement of adjacent bones; kinematics of joints; centre of mass; forces exchanged with the environment, and the loads transmitted between body segments and tissue, such as muscles, tendons, ligaments. This information can be provided during motion. The 3D model of the musculoskeletal system requires following information to be collected:

- Positions of skin-mounted markers (e.g. marker trajectories) using stereophotogrammetry (motion capture).

- External forces typically measured by dynamometers, such as force plate.

- Electrical activity of muscles using Electromyography.

The Stereophotogrammetry system determines the location of the markers using multiple video cameras installed at different sides of a room. The position of markers in 2D coordinates are used to determine the 3D coordinates of markers by matching views captured by different cameras from their locations. Stereophotogrammetry systems are typically two types, which are marker-based and marker-less systems. Marker-based systems either use passive markers, typically coated by a reflective paint to reflect the light, or active light-emitting markers (Davis et al., 1991; Dorn et al., 2012). Marker-less systems use a pattern of near-infrared light to determine the location of markers. Marker-less motion capture systems can provide a reduction in preparation time of the subjects for motion data recording, and the absence of markers that can modify the naturalness of a subject's movement. However, setting up the cameras and tools in a marker-less motion capture system is technically challenging, especially for systems (e.g. optical systems) which are sensitive to lighting. In contrast, marker-based motion capture systems suffer from disadvantages; for example, it can cause some artefacts due to moving the markers on a person's skin or clothing. However, marker-based approaches have been used widely as the preferred method for collecting motion data (Ceseracciu et al., 2014; Georgios et al., 2015; Martelli et al., 2015c; Yunardi and Winarno, 2017), since this method is easier to use and cheaper compared to marker-less systems.

Measurements of force magnitude and centre of pressure (COP) location during human locomotion is an important step during motion analysis. This data can be collected by placing force plate on the ground of laboratories. Typical force plates are equipped with

sensors to measure the magnitude of the force components (F_x, F_y, F_z) in the form of an electrical output, which is proportional to the force applied on the plate. Other approaches use strain gauge technology (AMTI, Advanced Medical Technology Inc.), or piezoelectric technology (Kistler, Zurich Switzerland) to improve the accuracy and capability of methods by capturing a wide range of forces.

A small change in the origin and magnitude of the ground reaction force can lead to a considerable change in calculated joint moments. Hence, the error which occurs during collection of the motion data needs to be evaluated. The error committed during quantification of centre of pressure (COP) can be determined by comparing the data obtained from force platforms and those obtained from a motion capture system (Holden et al., 2003; Rabuffetti et al., 2001). Furthermore, a pole that is instrumented with a load cell has been used for testing the measurements of forces plates by taking two approaches: full calibrations (Gill and O'Connor, 1997; Hall et al., 1996) and spot checks (Holden et al., 2003; Lewis et al., 2007). Full calibration is a thorough testing regime, performing a more controlled and systematic testing for a large volume of the surface of the force plate. However, this is generally time consuming, and henceforth not suitable for daily use. Spot checks can be performed using a pole with a simple design and with using a minimal number of markers attached to it. This method affects the accuracy of measurement by performing the tests for some spots on the surface of the force plate, but is quicker and suitable for frequent routine use. It has been shown that a typical force plate can predict the centre of pressure (COP) with an average RMSE of 2.4 to 6.6 cm (Karatsidis et al., 2016), and the ground reaction forces with a normalised average RMSE, ranging from 14.6% (Karatsidis et al., 2016) to 17.7% (Fluit et al., 2014) of body weight.

Another important part of motion analysis is related to assessing muscle activation. Electromyography (EMG) is a method which provides information about muscle electrical activity and activation time (onset and offset). EMG is frequently measured by electrodes placed on the skin (known as surface EMG), according to previous placement guidelines (Forman et al., 2019; Holmes et al., 2015). During recording of the data, EMG produces a real-time analogue signal in millivolts (mV), so that a greater level of voltage shows a higher level of muscle contraction.

Musculoskeletal modelling

Musculoskeletal modelling is a computational technique that provides a non-invasive estimate of the internal joint loads and muscle forces used for activities in daily living (Correa et al., 2010; Schellenberg et al., 2015). The first musculoskeletal models of the hip were generated by John Paul (1967) who investigated the effect of 21 muscles on the hip joint contact force, which were represented by grouping muscle forces into different functional groups. Since then, musculoskeletal models have become more sophisticated by adding more muscle forces, and modelling the whole leg from the hip to ankle; in addition, extension to the forefoot has been considered with all fifty muscles in each leg which perform various functions. The main challenge for simulating such a complex model is that, for example, there are twenty-one muscles at the hip with three force components in (X, Y, and Z), leading to the formation of a multi-body system with a complex mechanical linkage along the chains. Thus, as each joint is spanned by several muscles, a net joint moment can be defined by an infinite number of muscle recruitment solutions.

Two main approaches can be used to compute muscle and joint forces during motion: Inverse dynamics and Forward dynamics. Inverse dynamics relies on the collected motion

data (e.g. ground reaction force and the experimental joint kinematics) and uses them to estimate forces and the moments about each joint that are necessary to produce motion. Static optimisation can then be used to solve the muscle-moment redundancy problem each time instantly by minimising a given performance criterion, such as the sum of squares of muscle activations (Anderson and Pandy, 2001b). In contrast, Forward dynamics computes joint torques/forces to estimate the resultant motions by imitating the function of the human body. In this case, the equations representing muscle contraction dynamics, body-segmental dynamics, and muscle activation dynamics are combined simultaneously to estimate the resulting joint motion. Forward dynamics is a more computationally demanding process as it must solve an entire trial at once unlike the inverse dynamics which solve the equations for each frame individually (Lin et al., 2012; Pandy, 2001). Other approaches such as Neuro Musculoskeletal Tracking (NMT) (Seth and Pandy, 2007) and Computed Muscle Control (CMC) (Thelen et al., 2003) have been developed to use forward dynamics methods much more efficiently. These algorithms use feedback control theory to produce forward dynamics simulations including muscle activation dynamics, adopting two different approaches to solve the muscle load sharing problem: NMT, which uses a time-dependent performance criterion over the entire task period, and CMC which uses static optimisation at each time step. However, it has been shown (Lin et al., 2012) that static optimisation, NMT and CMC techniques do not produce significant different muscle force. The patterns of muscle loading predicted by the three methods were similar for both walking and running with a coefficient of correlation between any two sets of muscle-force solutions ranging from 0.46 to 0.99 ($\rho < 0.001$) for all muscles. This means the robustness and efficiency of static optimisation make it the most attractive method for estimating muscle forces in human locomotion, and suggesting that more time-consuming dynamic optimisation approach is less justifiable.

Recent numerical advances in dynamics and kinematic studies of human locomotion have been implemented in numerous software packages. LifeMod, AnyBody, and Opensim are example of packages created for a wide variety of biomechanical and clinical purposes. In this thesis, OpenSim has been used to compute the muscle forces and joint reaction force. Therefore, the focus of the following section is on OpenSim familiarise the reader with the main characteristics of this helpful biomechanical tool.

Musculoskeletal modelling: OpenSim

OpenSim is a popular biomechanical system which has been established based on a multibody dynamics engine known as 'Simbody' (Delp et al., 2007). OpenSim can create a dynamic simulation using its available library of models, which consist of a variety of musculoskeletal structures, such as joints, bones, contact components and ligaments (Sherman et al., 2011). A Hill-type model is used in OpenSim to reproduce muscle behaviour by describing the relationship between muscle force, length, activation and contraction velocity (Delp et al., 2007). OpenSim uses inverse kinematics to match the experimental marker trajectories collected from the motion capture system and the virtual markers available in Opensim library, by providing the joint angles, or generalised coordinates (Setha et al., 2011), for each frame of motion. Inverse dynamics tool determines the generalised forces (i.e., net joint forces and torques) that cause particular motions. To determine the internal moments and forces, OpenSim solves the equations of motion by using the input of joint angles and external forces (e.g., ground reactions forces) to the model, and calculating the output of the net joint moments/forces. OpenSim uses an optimisation approach to process the motion data (e.g. muscle forces, muscle length) as input, and provide an output of interest (e.g., joint torques) via minimising an objective function, such as the sum of

squared muscle forces (Delp et al., 2007), or energy consumption (Anderson and Pandy, 2001a).

Adjustment of a musculoskeletal model directly from the MRI of a given subject is difficult. Musculoskeletal models need to be constructed based on a template (cadaver-based) dataset, which are scaled to adjust a specific subject using relatively simplistic linear scaling laws that do not change joint parameters (e.g. orientations). Scaling is an important step in building a musculoskeletal model, since it can be effective in solving inverse dynamics and inverse kinematics problems. This is because these methods are sensitive to the accuracy of the scaling step. By scaling a model, OpenSim can adjust both the mass properties (mass and inertia tensor), and the dimensions of the body segments (e.g. bone geometry) in a patient. Patient-specific scaling uses medical images such as computed-tomography (CT) or magnetic-resonance images (MR) for scaling the generic model. The MRI method provides accurate information about muscle–tendon attachment sites and paths, joint centre positions, and the orientations of joint rotation axes; however, this method is not suitable to extract the bone mineral density (BMI) as the input data for assigning elastic properties of bone. In contrast, despite extracting detailed anthropometric information (e.g. muscle–tendon attachment sites) from CT images can be complicated due to the low contrast in CT images. However, this method can provide more accurate data about material properties and geometry of bones. Hence, CT images are used as the preferred technique to develop musculoskeletal models (Martelli et al., 2015b; Martelli et al., 2015c; Valente et al., 2014).

Modelling human movement is a complex, multistep process. Different simplifications can be used for building a musculoskeletal model. For example, the full-body musculoskeletal model can be modelled using 12-segment with 31 independent degrees-

of-freedom actuated by 92 Hill-type muscle–tendon units (Martelli et al., 2015b). The muscles can be defined based on their line of actions (Hoy et al., 1990) via points, wrapping surfaces or 3D geometries (Arnold et al., 2000; Arnold et al., 2010; Modenese et al., 2013). The tendons are modeled as linear elastic (Hoy et al., 1990), or non-deformable elements (Carbone et al., 2015). The foot is modeled as a single segment, ingoring the motion of intrinsic joints (Damsgaard et al., 2006). The hip, shoulder and, lumbar joints are represented as perfectly spherical joints with three degrees of freedom via ball-and-socket joint, while the knee joint are assumed to be a translating hinge joint with a single degree of freedom (Martelli et al., 2014b). These simplifications and assumptions could generate some errors in musculoskeletal models, for example, the specification of the join centre during scaling can lead to an error in the subsequent kinematics and kinetics analysis of hip and knee joint (Kadaba et al., 1990). These errors could be reduced by taking some actions, for example by modelling the muscles as a complex structure, however wrapping and bending the muscles around other organs (e.g. joints, bones) is a challenging task. A possible solution to model each muscle by the use of a series of line segments (Cleather and Bull, 2012; Valente et al., 2012). However, even for such a simple model, a number of considerations are required to be included such as the number of paths, the location of paths, and the line of action of each muscle using either 'via points', or 'wrapping surfaces', so that the models accurately represent the anatomy (Valente et al., 2012).

The assumptions and simplifications used for building the musculoskeletal model lead to errors in the model's output (e.g. muscle forces). To understand the level of uncertainty, the error needs to be reported. It has been shown that the inertial parameters derived from simple anatomical measurements using regression equation can lead to an error lower than 21.3% (Durkin and Dowling, 2006). Estimation of a hip joint centre using the functional

method can generate an average error of 13 mm, while the error can reach as high as 30 mm using regression equations (Leardini et al., 1999). Clinical images can be used for estimation of the joint centres and axes, with a peak error up to 11 degrees calculated for the hip rotation angle, while the error due to grouping muscle and joint forces together has never exceeded 0.33 BW, a value that represents the 8–10% of the peak joint forces (Martelli et al., 2015c). The muscle attachment sites extracted from MRI images can present an error lower than 6.1 mm (Scheys et al., 2009), which the geometry of bones could be extracted from clinical images with an error of roughly two pixels (Testi et al., 2001). The sensitivity of calculated skeletal forces to changes of the model parameters has been investigated by several authors. Valente et al. (2015) showed that specifying different anatomy-based knee and ankle joints presented a difference in peak loading up to 2.40 BW at the knee and 1.54 BW at the ankle. Furthermore, changes of the muscle physiological cross section area within the physiological range can lead to variation up to 11% and 100% respectively for the calculated hip and muscle forces (Brand et al., 1986). The sensitivity analysis of individual muscle forces to perturbations in muscle parameters (e.g. the number of muscle lines of action, maximum isometric force, optimal lengths for fibre and tendon slack) with changing factors within the range of a ±10%, presented a variation in the calculated muscle forces up to 12.8 times the magnitude of the imposed parameter perturbations (Xiao and Higginson, 2010). Scaling a general pelvis model on personalised anthropometric information created a variation up to 30 mm for hip joint centre (HJC) location, and generated an error in the computed hip force in the order of 0.5 BW (Lenaerts et al., 2009).

Validity of a musculoskeletal model

The accuracy of musculoskeletal models for estimating joint contact forces and muscle has been validated by comparison with the experimental *in vivo* data of the same subject. The

validation of joint reaction forces can be performed *in vivo* by fitting an instrumented joint replacement into the patient's body (Lund et al., 2012). Fischer et al., (2018) compared the simulation results of a musculoskeletal model of the lower limb for patients undergoing the Total hip arthroplasty (THA) with the corresponding *in vivo* measurements from the OrthoLoad database (Bergmann et al., 2016) during activity for 10 subjects . The mean error during peak loads ranged from 8% for level walking to 12% for one-leg stance, which was in consistent with the earlier studies with 10% and 13% error, respectively during level walking and one-leg stance phase (Stansfield et al., 2003). Furthermore, the computed muscle forces can be validated using EMG measurements by comparing the timing of the onset and offset of muscle activations. However, in this case, there is inconsistency between different studies. A better correlation was noticed for some muscles, such as gluteus maximus and gluteus medius, and a lower correlation for deep muscles, such as biceps femoris, caput longum and semitendinosus (Modenese et al., 2011), which could be related to the approach taken during EMG measurements, such as defining the location of EMG electrode over the muscles and the neuromuscular junction or innervation zone. Therefore, in order to validate the results of joint contact loads and muscle forces computed by models and compare them to real life conditions, accurate experimental measurements are needed.

Musculoskeletal models and their simulation protocols offers a unique tool which can not only be used clinically but can also help researchers in their respective investigations to study a wide range of scenarios (e.g. muscle function and various loading conditions). As a powerful tool, the musculoskeletal model can manipulate various parameters to determine how outputs differ and with what magnitude, without the need to recruit specific populations that fit into the study.

Femoral strain assessment

In order to quantify femoral strain, different approaches and tools have been used by the biomechanics community. Experimental studies have used different tools such as extensometers (Boyd et al., 2001), strain gauges (Cristofolini et al., 2009), and, more recently, Digital Image and Volume Correlation (Acciaioli et al., 2018; Bettamer et al., 2017). However, the loads transferred to the bone through the joints and the very complex muscle structure are difficult to replicate experimentally (Acciaioli et al., 2018; Cristofolini et al., 2009). Furthermore, strain gauges provide measurements limited to only a few superficial locations (Cristofolini et al., 2009; D'Lima et al., 2013), while more advanced methods such as Digital Image Correlation is restricted to the entire surface. Digital Volume Correlation is able to compute the femoral strain for the entire volume, however, the acquisition time required to analyse the structure of bone is expensive (Acciaioli et al., 2018; Bettamer et al., 2017). Numerical methods can potentially provide the strain field over the entire volume and arbitrary complex loading condition. Early FE models were applied in computational biomechanics in the 1970s for the development of an idealised two dimensional model of skeletal parts (Brekelmans et al., 1972). Over time, more complex linear and non-linear models were developed and used in different engineering fields from mechanical engineering (Ghorbani Menghari et al., 2014; Ziaeipoor et al., 2014; 2010; 2013) to orthopaedic biomechanics (Taylor and Prendergast, 2015).

One of the applications of the FE method in orthopaedic biomechanics is to compute bone stress-strain fields under defined loading conditions. The FE results then can be compared with experimental measurements to compute the difference. In the case of human femurs under the loading case of single leg stance, studies have reported a strain prediction accuracy with a coefficient of determination ranging from 0.95 – 0.97 (Schileo et

al., 2008; Yosibash et al., 2007), whereas other studies performing femoral fracture assessment reported a coefficient of determination between 0.75 (Munckhof and Zadpoor, 2014) and 0.96 (Imai et al., 2006). Furthermore, a good correlation ($R^2 = 0.95$) was observed when the computed femoral strain was compared with the experimental measurements of a publicly available *in vivo* study (www.OrthoLoad.com, (Bergmann et al., 2016). This evidence presented a unique consistency of models in either topological or geometrical terms and showed that the available models can be used to study the typical patterns of physiological strain in elderly people ranging from 51-76 years of age.

The next step toward the determination of femoral strain *in vivo* is to couple models of femoral mechanics with models of muscle and joint forces (Martelli et al., 2014b), which can be archived by integration of musculoskeletal-FE pipelines (Figure 3.1) at two different levels: single and multiple subject studies. The single-subject studies provide information about the biomechanical response of a single femur under various physiological loading conditions (e.g. motor tasks), like assessing the femoral strain which may between the articular cartilage (Abrahamsen et al., 2009) and the femur shaft (Martelli et al., 2014b). However, the application of these single- studies requires the construct of a model for each patient and the entire model construction procedure needs to be repeated. Multiple-subject studies have the advantage of providing wider insight into the variation of femoral strain (Martelli et al., 2014b) and the risk of femoral fracture across a population (Qasim et al., 2016). Furthermore, larger studies can be used to determine how anatomical and functional variations across individuals affect femoral strains (Martelli et al., 2015b).
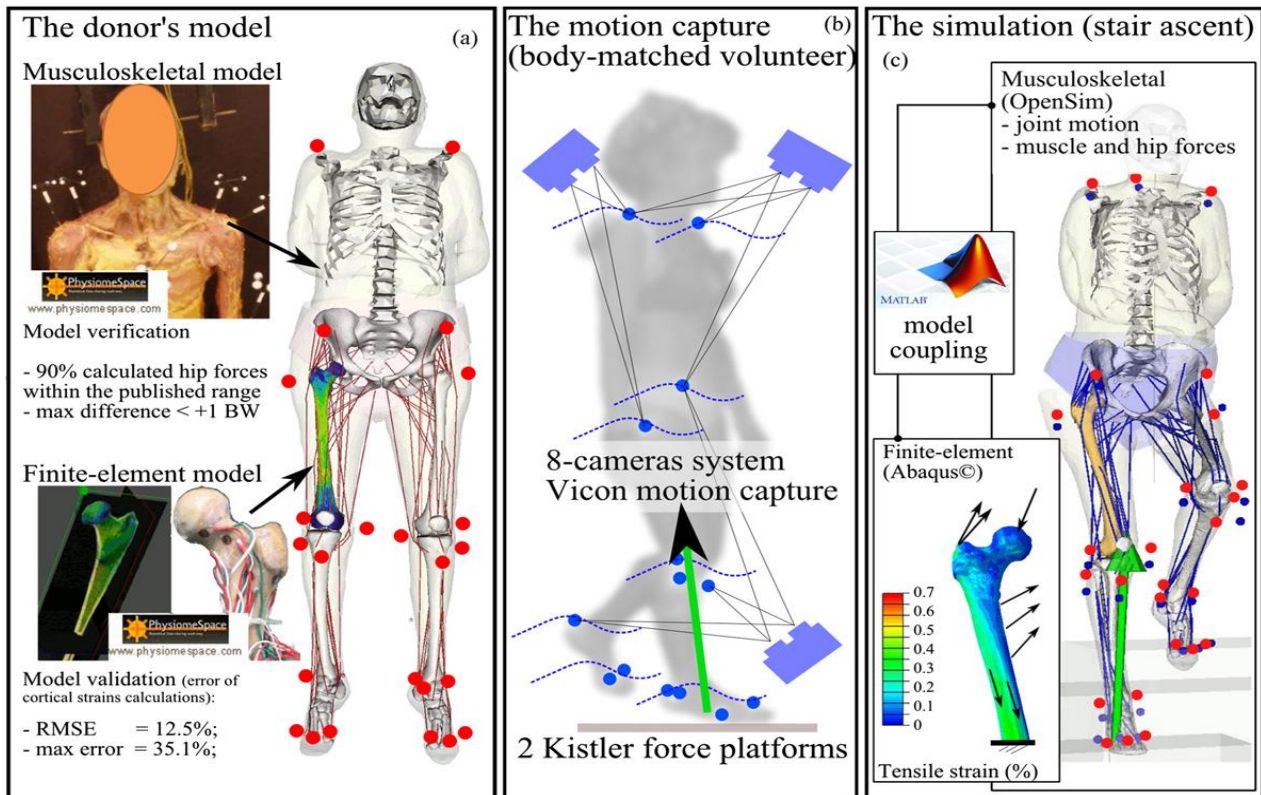
Figure 3.1: A pipeline to compute the femoral strain during an intermediate frame of simulated stair ascent (c), which were developed by collecting the motion data (b), and coupling the musculoskeletal-FE models (Martelli et al., 2014b). "Reprinted from 'Clinical Biomechanics', 29(8), Saulo Martelli, Peter Pivonka, Peter R. Ebeling; Femoral shaft strains during daily activities: Implications for atypical femoral fractures, 869 – 876, Copyright (2014), with permission from Elsevier".

Validity of FE models of bone

The prediction of femoral strain using FE models depends on several factors such as geometry, the material property of bone derived from CT scans, mesh generation procedure as well as the applied loading and boundary conditions (Taylor and Prendergast, 2015; Wagner et al., 2010). Therefore, reviewing these parameters would be helpful to gain an understanding about the critical aspects of building FE models of a femur.

The geometry and material properties of bone are key parameters for development of FE models and can be obtained from computed tomography (CT). Due to the presence of calcium in bone structure, a higher x-ray energy is absorbed by bone compared with the

surrounding tissue, resulting in well-contrasted edges (Winder and Bibb, 2005). The 3D bone geometry can be retrieved from the CT medical images via a process called bone segmentation, which requires labelling the region of interest (ROI) corresponding to bone in each CT slice using a partial or fully automatic process (Messmer et al., 2007). As a result of this process, the femur geometry is collected and converted into CAD format, and a 3D mesh can be generated using the available software (e.g. Simpleware) to subdivide the domain into a set of finite elements (Figure 3.2).

The material properties of bone need to be extracted and mapped into the generated volumetric mesh (Figure 3.2). To extract the bone density, the CT images need to be calibrated via determining the relationship between the grayscale intensity values in the images and corresponding bone mineral density values. To achieve this, Hounsfield units, which are a standard unit of x-ray CT density can be related with a wide range of known phantom densities to form a linear calibration curve (Ciarelli et al., 1991; Rho et al., 1995). The density of the bone can then be converted into Young's Modulus via the empirical relationships which are established experimentally (Keller, 1994; Morgan et al., 2003). To map the material properties of bone into the generated volumetric mesh two main approaches are used. First, assigning the density of each element directly from the CT sampling grid is done by finding the nearest point (Charras and Guldberg, 2000). Although this method is very simple to use, the accuracy of the mapped data can be affected when the element size is significantly larger that the CT grid (Charras and Guldberg, 2000; Weinans et al., 2000). The second approach uses all CT sampling points as a scalar field that fall inside the element volume, and assigns the average values to the elements, leading to grouping elements into groups of similar properties. However, this technique may not give satisfactory results when, the dimension of elements are of comparable measurement, or

smaller than the voxel size (Keyak, 2001; Ota et al., 1999; Taddei et al., 2004). As a result of calibration and material mapping, bone can be described as an isotropic (Geraldes and Phillips, 2014), anisotropic (Stolk et al., 2004), or orthotropic material (Geraldes and Phillips, 2014). However, most FE studies assume that bone is a linear-elastic, isotropic, inhomogeneous material, enabling consistency in the prediction of cortical bone with a good correlation greater than 0.9 (Fitzpatrick et al., 2014; Martelli et al., 2015b; Taylor et al., 2017).
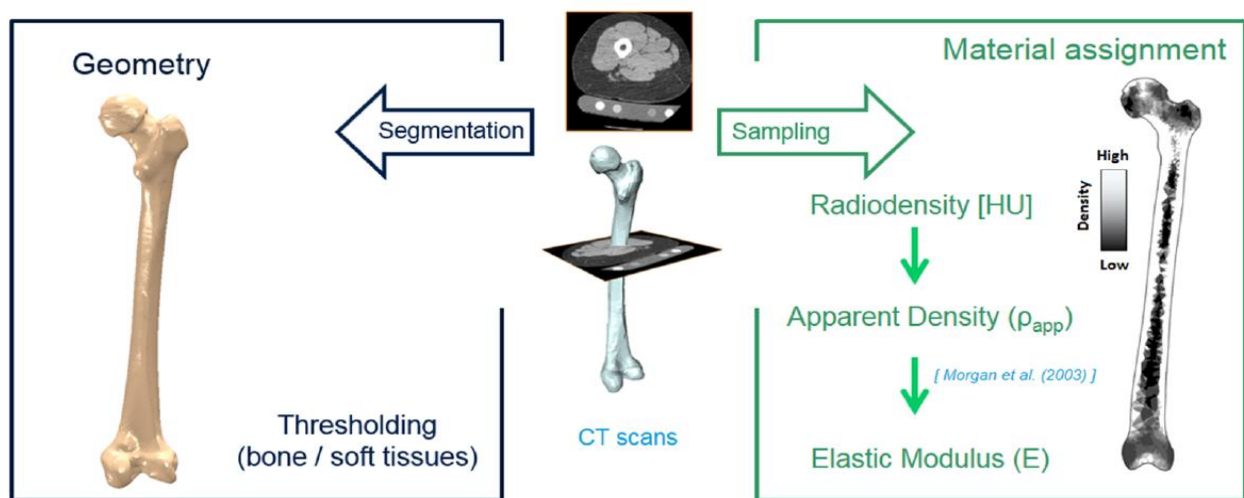
Figure 3.2: Constructing the 3D model of a femur by assigning the material properties and geometry (Cilla et al., 2017), "With permission from PLOS ONE as an open access article with no changes, available from: https://doi.org/10.1371/journal.pone.0183755".

The segmentation of bone has been characterised as a challenging part of developing a finite element model (Wang et al., 2006a). Manual segmentation of bone requires an extensive manual interaction, hence numerous approaches are used to speed up the bone reconstruction process such as contour extraction, thresholding (with morphological operations), the active shape based method (Pauchard et al., 2016; Wang et al., 2006a), and more recently, the active shape modelling technique (Yokota et al., 2013). For example, Pauchard et al. (2016) used an interactive graph cut segmentation method for rapid creation of FE femur models from clinical CT data for a population of bones, and compared the

obtained results to corresponding manual segmentation of the bone, and satisfactory agreement was observed with the average surface-to-surface differences of 0.22 mm and a high correlation for bone stiffness ($R2 = 0.95$), while reducing the user interaction time from 20 to 35 min (manual) to 2–5 min. Furthermore, it has been accepted that more accurate geometry can be obtained using semi-automatic segmentation, supported by manual correction of the threshold provided by the operator, which employs sensitive edge detection filters to distinguish the apparent tissue types (Rathnayaka et al., 2011). However, the result of a threshold-based segmentation may vary depending on the threshold chosen (Testi et al., 2001). In addition, the accuracy of 3D bone geometry can be influenced by the resolution of CT scans and has been improved over time from a slice thickness of 5mm to clinical scans at 0.6mm voxel size (Taddei et al., 2006b).

Another critical aspect is related to generating a volumetric mesh with a sufficient number of elements. Typically, three approaches have been used for mesh generation: structured, non-structured and voxel-based mesh. Structured mesh can generate more complex mesh (typically large hexahedral mesh) with accurate mapping of the material properties of different bone tissues, due to its advantage in defining the facets of the elements, and identification of the boundaries of bone tissues. When the mesh is non-structured, the mesh and the density distribution are perfectly registered in space, but the facets of the elements are not aligned with the CT axes nor with the boundaries between bone tissues, making the manual mapping of the material properties onto the finite elements complicated. In the voxel-based mesh generation technique, a pre-defined voxel from the CT scanning constitutes the elements, and there are no surface or solid bodies, and the mesh is directly defined from the CT voxel. Thus, the voxel-based mesh technique makes the process of mesh generation easier, since there is no need to process the images, but it

needs a mask for labelling the voxel. As well as this, generating the bone mesh using the voxel-based mesh technique is likely to introduce errors in the FE results as all surfaces present sharp edges (discontinuities) in stress concentration regions (Marks and Gardner, 1993). Furthermore, to evaluate the effect of mesh density on the corresponding FE results, Keyak and Skinner (1992) segmented the bone CT scans with the size of 1.38 mm and slices of 3 mm, and the FE model was meshed using the cubic elements with constant sizes of 4.8, 3.8 and 3.1 mm. They concluded that a consistency in the FE results was achieved when the minimum element size was in the order of 3mm. In contrast, a poor convergence in the material property distribution was obtained when the element size was significantly larger than the pixel size of the source CT data (Perillo-Marcone et al., 2003). Furthermore, in order to have a convergence in the FE results, the bone was meshed typically using approximately 100,000's first, or second order tetrahedral elements. While fine mesh is needed for the bone's region with a thin cortex (e.g. femoral neck), the mesh size can be larger in the diaphysis with the cortex in the range of 2-3 mm (Martelli et al., 2014b; Taylor et al., 2017).

Loading and boundary conditions

Femoral loads are determined by a complex muscle activity driven by the sensorimotor control system, which determines muscle synergies in response to a variable motor demand. The early FE models applied simplified loading cases, for example, using joint reaction force along with a few muscle forces, to explore the distribution of stress-strain within the femur (Rohlmann et al., 1983; Taylor et al., 1998). This idealised model provided good consistency in the stress-strain values in the proximal neck compared to distal diaphysis, but errors increased to 100% distally (Polgar et al., 2003). Later, the models became physiologically more realistic by adding more muscle forces, leading to a reduction on the overall bending

movement, and consequently reduced the generated stress-strain values in the diaphysis femur (Munih et al., 1992; Simoes et al., 2000). However, there was still considerable uncertainty in selection and simplification of a loading configuration that ensured realistic predictions from pre-clinical tests. An illustration of this is when the neglect of certain muscle forces happens, such as glutei, which can significantly change the internal forces within the femur (Duda et al., 1997), and correspondingly, the stress and strain distributions of the femur (Duda et al., 1998; Polgar et al., 2003). Furthermore, while some studies only considered a reduced set of loading conditions typically associated with particular loading such as stance phase of gait (Taylor et al., 2012; Taylor and Prendergast, 2015; Van et al., 2011), others investigated the biomechanical response of bone under various loading forces during multiple activities and multiple trials, such as normal walking, fast-walking, stair ascent/descent and chair rise (Martelli et al., 2014b). Other studies investigated the biomechanical response of a bone under the load conditions taken from other individuals, leading to uncertainty in the computed strain field due to the variation in the applied forces, such as joint reaction force which can differ by 2-4 BW.

Despite the great advancement in fidelity of the bone FE models, the models were still not used for a large scale studies of bone, with the majority of studies using either a single (Martelli et al., 2014b; Simoes et al., 2000; Taddei et al., 2006a) or small set of bone models (Martelli et al., 2015b), and extrapolating the results for the population as a whole. Furthermore, current models are not able to incorporate the large geometric and material quality variation that exists between individuals influenced by gender, age, ethnicity, underlying pathologies and their type of daily activities (Peacock et al., 1998; Theobald et al., 1998). Hence, it is essential to increase the size of FE models from single subjects to at least large cohorts to populations.

Population-based studies

Several FE studies have been conducted to quantify the femoral strain during motion for multiple subjects. At early stages, larger FE models was started by looking at 10's of bone models. For example, Lengsfeld et al. (2005) compared the strain values between implanted and intact contralateral hips by performing FE models for 11 subjects. Radcliffe and Taylor (2007) used an FE model consisting of 16 proximal femurs to investigate the effect of cement mantle thickness in femoral resurfacing. Martelli et al. (2015) applied a coupled musculoskeletal-FE model for 10 participants under six weight-bearing tasks to understand how scaling a scaled-generic musculoskeletal model to a participant's anatomy propagate to participant-specific (intra participant) femoral strains, and average (inter-participant) femoral strains within a cohort. Kersh et al. (2018) quantified the strains at the proximal femur for 20 postmenopausal women to identify specific muscle loading during jumping and stair usage to exploring the parameters affecting fracture risk, such as bone loss and bone formation (Kersh et al., 2018). These population-based studies were limited to about 20 subjects, but from a clinical point of view, studies with a large number of subjects are needed to provide a better understanding of biomechanical variation across individuals for particular clinical applications (Bryan et al., 2009). A major barrier in running multi-subject studies of bone as a commonplace practice is associated with the task of creating and running models from CT scans which will be time-consuming and labour-intensive tasks unless automated generation techniques are available. A viable solution is to use the statistical models of bone as a source for FE models.

The two main types of statistical models are the active shape model (ASM) and the active appearance model (AAM) which respectively describe the average shape and density distribution together with the main modes of variation within a population (Sarkalkan et al.,

2014b). SSMs and SAMs are built using a set of training datasets which provides a-priori information about existing variation in the shape and density of population (Bryan et al., 2010). To build a statistical model the training datasets need to be registered to establish a correspondence between two shapes, so that the registered training data is provided in the same coordinate axis (x, y, and z) with an equal number of points, which are relatively located in a close area of the model. To perform such a registration, two techniques can be used: Rigid or non-rigid registration. Rigid registration assumes the objects being transformed and matched are rigid, allowing them to be translated and rotated with 6 degrees of freedom. The Iterative Closest Point (ICP) algorithm is a common registration technique which has been used for rigid registration of objects (Vos et al., 2004). ICP uses a cloud of points for matching the surfaces of objects with the advantage of not requiring a predefined relationship between points. However, rigid registration techniques do not account for deformation/shape changes. In these cases, non-rigid registration techniques such as elastic registration can be used as a deformable mesh registration tool for alignment of a pair of surface meshes (Bryan et al., 2010 and 2012). This non-rigid surface registration technique uses an elastic matching algorithm iteratively to deform the baseline surface vertices, as the reference, to capture the geometry of the target bones by matching the given surfaces. The outcome of the surface registration technique is a three-dimensional correspondence between the baseline femur and target femurs. In a subsequent step, a volumetric meshing approach is applied to use the baseline mesh as the template for all the target mesh while tracking the moving/perturbed surfaces of the target femurs, which results in generating a unique mesh with the same number of nodes and elements for the entire bones (Bryan et al., 2012). Such a non-rigid registration scheme was successfully applied earlier by Bryan et al., (2010 and 2012) for building a statistical model based on principal component analysis (PCA). Bryan et al. (2010) developed a combined active shape and

appearance based on the PCA method using a training set of 46 femurs. The model performed well when 35 or more modes of variation of shape and density were used. The developed model was able to produce 400 synthetic femurs which were required for building FE simulations. It was highlighted that the registration scheme must be able to accurately capture the complex variable shape and material distribution of the femur.

The performance of PCA can be effected by the quality of image segmentation (Sarkalkan et al., 2014b) and by the number of samples (e.g. bones) chosen to represent the population (Grassi et al., 2014). In terms of errors associated with image segmentation, the reported mean segmentation errors of normal vertebrae varied from 0.47 mm (Iglesias and de Bruijne, 2007) to 0.82 mm (Roberts et al., 2012) and for semi-automatic segmentation errors ranged from 0.73mm (Mysling et al., 2013) to 0.93 mm (Roberts et al., 2009) and for automatic segmentation increased to 2.27 mm (Roberts et al., 2009) for the automatic segmentation of fractured vertebrae. Moreover, the number of bones which were used to represent the variation in density and geometry could affect the performance of PCA models (Zheng et al., 2009). According to one of the biggest active shape models developed from 115 femurs, the mean geometrical error can be as low as 0.5 mm, while the peak error can reach 5 mm in the condyles region (Grassi et al., 2014). It was concluded that the main source of error was due to the insufficient number of specimens to fully reproduce the anatomical and deterministic variability of the reference population (Grassi et al., 2014). Hence, the main challenge during building a statistical model of bone using PCA models can be associated with the number of bones used for generating the training datasets. Keyak et al. (2001) explored the application of PCA models for computational-experimental work using a relatively small number of femurs, 18, and noted that a good agreement can be achieved between the experiments and results of statistical models if the statistical models

can replicate the experiments accurately using a sufficient number of femurs representing different bone morphologies (Keyak et al., 2001; Sarkalkan et al., 2014b). Furthermore, PCA methods have been used successfully for various applications in bone-related research, such as assessing the risk of femoral neck fracture (Bryan et al., 2009) and investigating the effect of femoral head resurfacing on the bone-prosthesis load transfer (Bryan et al., 2012). Therefore, statistical models provide a potential source for large scale studies of FE models of bone (Bryan et al., 2009) with thousands of simulations. This could potentially, in the long term, provide an efficient computational tool for particular clinical applications such as designing implantable devices for a specific patient (Low et al., 2000).

Conclusion

In conclusion, FE models have the potential to be of clinical benefit, although building the models, generating a solution, and interpreting the results are time and labour-intensive. There are several bottlenecks in the process, including generating the model from clinical images through to the solution phase. Various groups are exploring methods to rapidly segment and generate the finite element models from CT scans. The next major issue is the solution phase, which needs to be faster so that it can be used for clinical applications which require quick diagnosis and treatment planning. If predictions could be made in seconds or minutes this could promote the development of clinical applications and large-scale studies of femoral strain.

Chapter 4 : SURROGATE MODELING METHODS

Rapid prediction of femoral strain

Computing the femoral strain in real or near real-time is important for various biomechanical applications, such as predicting femoral strains at different regions of interests (e.g. neck and shaft) during multiple activities and trials, allowing to examine the risk of femoral fracture (Martelli et al., 2014a; Martelli et al., 2014b), and studying large scale statistical models of femur mechanics with 100's (Martelli et al., 2015c) to 1000's (Martelli et al., 2015a) of loading cases during activity (Martelli et al., 2015a). Rapid estimation of femoral strain can also be applied for implanted femurs, either to study the influence of surgical variability in implant positioning on the primary stability of them (Al-Dirini et al., 2019), or to improve the design of implants by computing the level of micro-strain between bone and implants (Bieger et al., 2012). Furthermore, quantifying femoral strain efficiently can be useful for specific clinical applications, such as providing biofeedback to patients and clinicians during rehabilitation (Pizzolato et al., 2017b).

As mentioned in the previous chapter, The Finite Element method has been used for decades extensively as a powerful and invasive computational tool (Taylor and Prendergast, 2015). However, the current workflow for building and solving an FE model is a time consuming, labour intensive, and a lengthy process, requiring different steps: obtaining patient anatomic geometries using images (e.g. CT scans and MRI images) segmentation (Rathnayaka et al., 2011), extracting the material properties of bone via calibration and mapping the density distribution (Taddei et al., 2004) specifying the loading and boundary condition in the FE model (Keyak et al., 2001), and submitting the FE model to an FE solver (e.g. explicit or implicitly) to obtain the FE results. The entire process may take anywhere from hours to days depending on the complexity of the model and the power of the computer in terms of the number of CPUs and RAM capacity. Therefore, the adoption of the FE

method in clinical applications has been hampered by its complex workflow, which requires intensive computational costs and clinicians with high technical competency. Various groups have begun to speed up the process of building FE models, for example by automating the image segmentation process and creating FE models from CT scans (Carballido-Gamio et al., 2015; Pauchard et al., 2016). Therefore, difficulty remains in increasing the speed of the solution phase. If the solution phase can be reduced to seconds or minutes, it means that predictions could be conducted in clinics and can be used for rapidly estimating the femoral strain field in large-scale studies with 100s to 1000s of simulations (Martelli et al., 2015a).

A viable alternative approach is to approximate and replace the expensive finite element model with cheaper-to-run surrogate models, which can be trained using finite-element calculations of femoral strain for a limited number of training sets and then used to rapidly provide femoral strain estimates for an arbitrary frame of motion or an entire activity. The performance of such a surrogate model can be evaluated by assessing efficiency and efficacy (Wang et al., 2014). Efficiency refers to the time required for performing a prediction, and efficacy refers to the errors which happen in predicting a set of target measurements. Constructing a surrogate model is comprised of three key steps: generating the samples from the original data by implementing suitable sampling methods; training the surrogate models by fitting an analytical equation to determine the relationship between variables, and predicting the outcome for unseen data (Taylor et al., 2017).

Generation of the training dataset

The performance of a surrogate model depends on the training datasets used (Fitzpatrick et al., 2014; Taylor et al., 2017). A suitable training dataset needs to be representative of the entire data with a minimum level of clustering, which is a problem in terms of generating

the same or similar samples from the data (Han and Zhang, 2012). Popular sampling methods used are: Monte Carlo (MC) sampling; Latin hypercube (LH) sampling and Design of Experiment (DOE) sampling. Monte Carlo (MC) sampling uses random sampling from the original data. However, MC sampling often requires a large number of samples due to clustering, to ensure that the surrogate model represents the original simulation model well, leading to an unnecessarily increase in the size of training datasets, and training computational costs (Han and Zhang, 2012; Laz and Browne, 2010). Latin hypercube sampling which was first described by McKay in 1979, is a modified form of MC sampling and can cover the entire data by generating fewer number of samples compared to MC sampling. Latin hypercube sampling uses a random basis approach to generate samples by partitioning the data into sub-regions to ensue that all the probability regions are covered (Han and Zhang, 2012). The design of the experiment generates samples which are randomly similar to LH sampling, but tries to avoid the problem of clustering by removing the samples which are generated from the same or close regions, to ensure that the samples are the representative of the region of the data. Hence, the DOE method can capture the charactersitics of the entire data by generating fewer numbers of samples (Anthony Giunta et al., 2001).

Surrogate modelling techniques

A variety of surrogate models have been used by the biomechanics community including Multivariate Linear Regression (Fitzpatrick et al., 2014; Taylor et al., 2017), Bayesian modelling (Bah et al., 2011), Artificial Neural Networks (Eskinazi and Fregly, 2015; Liang et al., 2018; Taylor et al., 2017), Random Forest (Donaldson et al., 2015) and Kriging (Lin et al., 2009; O'Rourke et al., 2016; Walter and Pandy, 2017). This is either for linear problems such as assessment of femoral neck fracture (Taylor et al., 2017), or for non-linear problems,

such as modelling the contact between bone and implants (Fitzpatrick et al., 2014). The majority of studies applied the surrogate models for predicting a single scalar outcome, such as joint moments and muscle forces (Favre et al., 2012), contact forces and contact pressure (Eskinazi and Fregly, 2015; Halloran et al., 2009; Lin et al., 2009, 2010a; Pizzolato et al., 2017b; Walter and Pandy, 2017), fracture load (Taylor et al., 2017) implant micromotion (Bah et al., 2011), and stress shielding (Cilla et al., 2017). Other studies used surrogate modelling to estimate the full filed of outcome variables like the micromotion between bone and implants (Fitzpatrick et al., 2014). A brief overview of the characteristics of the most popular surrogate modelling techniques is provided in the following sections.

Artificial neural network

The artificial neural network (ANN) method is a computational method which was inspired by neural networks to process information in the human brain. This method consists of some basic units known as neurons. Each neuron is responsible for receiving the input data from other neurons or other external sources while communicating with other neurons via hidden layers using a system of weighted 'connections' (Figure 4.1). Once a training dataset including a set of inputs and the resultant outputs is fed to the network, the network 'learns' the interaction between inputs and outputs and stores the learned parameters in the form of numeric weights (Mouloodi et al., 2019b). The obtained set of weights enable the model to estimate the output of interests for a 'new' set of input that have not been seen by the network before.
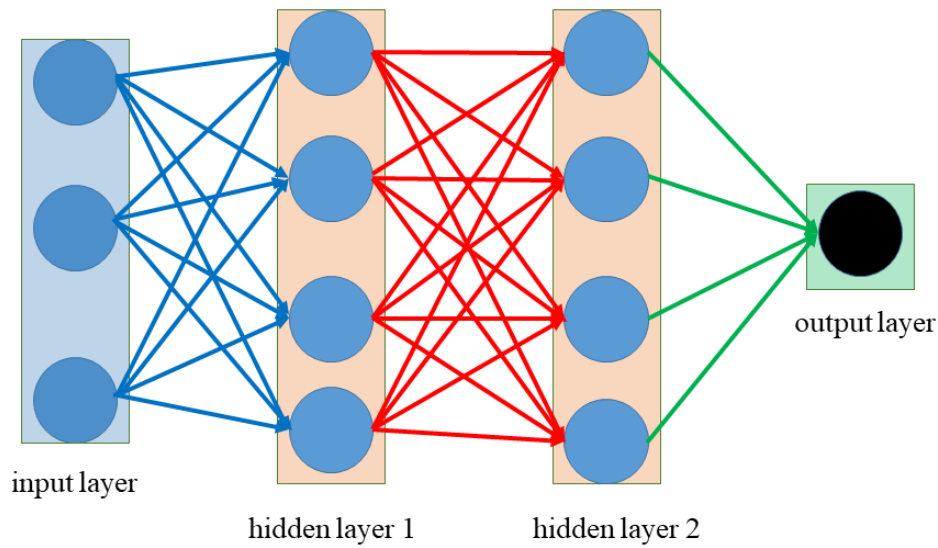
Figure 4.1: Different elements of a multi-layer artificial neural network.

The ANN method has been used in the orthopedic biomechanics community for reducing the computation cost of simulation-based studies, with application in contact mechanics (Ardestani et al., 2015; Eskinazi and Fregly, 2015), and non-contact mechanics (Taylor et al., 2017). The contact based models were used, for example, for assessing the primary fixation of joint replacement (Bah et al., 2011), and optimising the geometry of commercial short stem hip prosthesis in order to reduce stress shielding effects and improve the performance of short-stemmed implant performance (Cilla et al., 2017), while the non-contact based models were used for particular applications, such as estimating femur load fracture (Taylor et al., 2017).

Eskinazi and Fregly (2015) used feed-forward ANNs to develop a surrogate contact model using the elastic foundation (EF) contact model of an artificial tibiofemoral joint during activity. The artificial netural networks were constructed using four hidden layers of 30

neurons each and a single linear output neuron. The joint contact condition was divided into seven different domains and a portion of the samples were extacted from each domain to generate the training datasets (100 – 300 samples). Using this model it was feasible to estimate the forces and torques about 1000 times faster than EF contact model. They used 10 percent of the sample points as unseen data to evaluate the performance of the surrogate model and relativey low errors were observed with RMS errors fewer than 1% of the peak contact force reported for walking. Furthermore, the authors noted that the performance of the model was bound to the quality of the distribution of samples and the number of samples chosen from each domain.

Taylor et al. (2017) developed an ANN based surrogate model with a two-layer feed-forward network using 10 hidden neurons and one linear output neuron to predict femoral neck strains and corresponding fracture loads. The training sets of of 50, 100, 200, 500, and 1000 femurs were used to train the surrogate models and 100 femurs (10% of the data) were used as unseen data for testing. The performance of the surrogate models was shown to be a function of the size of training datasets by reducing the RMSE error in mean equivalent strain from 0.019 to 0.013% when the sample size increased from 50 to 500. A good corelation was nocticed between the predictions of FE-based and ANN surrogate models ($R^2 = 0.92 – 0.98$); the greatest variation tended to occur at higher fracture loads (e.g. , above 10,000 N for the level gait). Although the ANN method is shown to be a potential technique for estimating the full field of femoral strain (Taylor et al., 2017), this technique provides an effective solution when the optimum number of artificial neurons are known, otherwise the model may show poor performance during prediction (Cilla et al., 2017). Furthermore, determination of the optimum number of neurons and layers demands an

iterative try-and-error approach, henceforth identifying and training an optimal form of ANN can be a laborious process.

Multivariate linear regression

The Multivariate linear regression (MLR) method is an extention to linear regression, but instead of relating one outcome variable to one independent variable, it relates multiple independent variables to the dependent outcome. The MLR model has been applied in orthopedic biomechanics for different purposes. Taylor et al. (2017) used the MLR method to identify the key variables between different variables (e.g. femur length, femoral head diameter, femoral neck bone mass, etc.) that made a significant contribution to the output metrics. The identified variables with a p-value lower than 0.05 (significance level) were then included to build an ANN based surrogate model. Fitzpatrick et al. (2014) sucessfully applied the MLR method for estimating the full field of outcome in a linear elastic model. They trained a MLR based surrogate model to predict the micromotion field over the entire bone-implant interface for six patients during motion, while the training datasets were generated using the Latin Hypercube (LH) sampling method. A better correlation between the predictions of MLR and FE simulations was observed when 200 or more samples were used for training the model. The RMSE error was reduced from 8.3 ± 5.5 micromotion for 50 samples to 6.4 ± 4.2 micromotion for 200 samples, followed by a small improvement for 1000 samples reaching 6.2 ± 3.8 in micromotion. In terms of efficacy, FE analysis time for a complete gait cycle discretised into 51 increments using four computational processing units (CPUs) which was 15 h compared to 30s for the MLR model, revealing the capability of the MLR method for rapid prediction of full field of outcomes under a set of loading conditions. Although the applicability of the MLR model has been used for weak non-linear systems to model the full field of micromotion between bone and implants (Fitzpatrick et al., 2014), its

validity for predicting the outcome of interest in non-linear simulations has to be proven (Bevill et al., 2005; Cosmi et al., 2006).

Multivariate adaptive regression splines

Multivariate adaptive regression splines (MARS) are a flexible statistical method which has not been used in computational biomechanics, but has shown to be effective in large computational studies in earth science (Wang et al., 2014). This technique uses an automatic algorithm which involves a divide-and-conquer strategy to partition the training datasets into separate linear-cubic equations known as 'basis functions' (Kyra E. Stull, 2014). Such a partitioning algorithm allows for improved description of the linearity of the model by fitting a separate function for each portion of data (Zhang and Goh, 2016). While MARS showed capability for use in linear and non-linear models (Friedman and Roosen, 1995) unlike other methods such as the ANN method, MARS does not need *prior* information for building surrogate models. However, MARS needs to go through a forward and backward iteration process during fitting the model over each partition of the data, which may lead to increased compuational costs required for building the model over traditional MLR models (Friedman and Roosen, 1995).

Bayesian network

The Bayesian network is a statistical method aimed at determining the probability distributions of observed variables. A Bayesian network is essentially graphical modelling, in which dependencies among variables are depicted in a graph, with the nodes representing variables, and the arrows representing statistical dependencies between variables (Figure 4.2). So, as an arrow from A to C indicates that by knowing the A point, it is feasible to predict C.
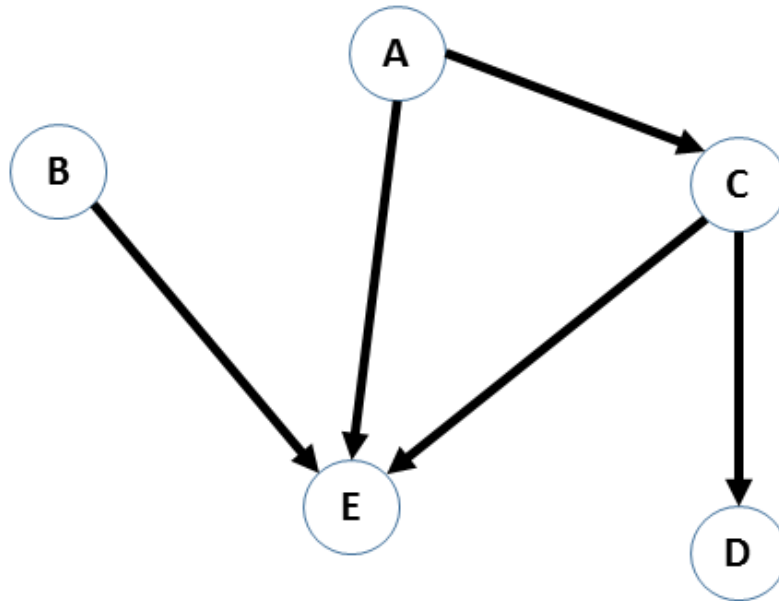
Figure 4.2: A graph representing the Bayesian network, including variables (circles), and statistical dependency between variables (black arrows).

The Bayesian network has been used as a replacement for non-linear FE models to assess the effects of implant positioning on the initial stability of a cementless total hip replacement (Bah et al., 2011). It was observed that RMSE errorrs (micromotion) for the region of interest reached to 3.6% (Bah et al., 2011). Therfore, the bayesian network has shown great potential in accounting for all the probabilities of a design and can be useful for improving the design of implantable devices. However, the Bayesian network can be computationally expensive for large scale studies, such as statistical models of femurs with thousands of loading cases (Martelli et al., 2015a), since it needs to determine the probability of the observed variables.

Gaussian process

The idea of the Gaussian Process (GP) was initially proposed as a classical statistical method by O'Hagan in 1978, and was used later in the 1990s as a common regression (and classification) technique for improving computational power for large data sets. The Gaussian process (GP) is a capable method to model both linear and non-linear systems. The main characteristic of the Gaussian process is it provides a trade-off between fitting the data and smoothing it out, and it can handle noisy training datasets while capturing the precise trend of the data (Wang and Shan, 2006). Furthermore, as the GP method is designed based on a probabilistic algorithm, it is feasible to use it for computing the empirical confidence intervals by refitting or adaptation over the given training datasets (Ackermann et al., 2011).

During building a Gaussian process the user can provide a-priori knowledge and specifications about the shape of the model by selecting different kernel functions. The flexibility of the Gaussian process is that by building models using an appropriate function helps to model the non-linearity of the training datsets and is an advantage compared with other models, such as neural networks. The Gaussian process has been used successfuly in various engineering fields such as mechanical engineering (Xia et al., 2011) and earth science (Jin, 2011). The Gaussian process has shown that it is capable of estimating the pattern of gait kinematics by computing the joint and motion trajectory with error in the order of 0.1 to 7 degrees (Yun et al., 2014). It was shown that Gaussian process can be used as a nonlinear regression algorithm which is suitable for databases whose input (e.g. body parameters) has high dimension and the input paramters are highly correlated (Yun et al., 2014).

Kriging method

The Kriging method predicts the value of a function at a given point as the weighted average of known values in the neighborhood points. The Kriging method has been used in orthopaedic biomechanics for reducing computational costs in repeated FE analysis, such as stochastic analysis of strain in the human pelvis (O'Rourke et al., 2016), sensitivity analysis of total knee replacements (Lin et al., 2009), or optimisation approaches (Lin et al., 2010b). The stochastic analysis of wear in knee replacements showed that computation time can be reduced from 284 h per analysis for simulations to 1.4 h for the surrogate contact models (Lin et al., 2009). Furthermore, the Kriging method can be used for sensitivity analysis when all the influential input parameters and interactions are identified and used in developing surrogate models for predicting acetabulum micromotion (O'Rourke et al., 2016). Kriging-based models have been used in multi-body contact problems (Lin et al., 2009; Walter and Pandy, 2017) for predicting tibiofemoral contact forces, patellofemoral contact forces and muscle forces occurring simultaneously in the knee during walking. This technique was shown to be efficient for modeling dynamic contact and wear simulations of total knee replacements by reducing the computational costs of simulations by 50 times (Lin et al., 2009). While the Kriging method has been used sucessfully for various biomechanical applications, Kriging-based models suffer from two disadvantages: firstly, as this model is able to interpolate a relatively low number of sample points at a time, thus training the model would be very computationally expensive and needs a considerable amount of memory, particularly when the sample points increases. Secondly, the most common implementation of Kriging interpolates the data, which affects the performance of the surrogate model in relation to the noise in the data. Specifically, this can be problematic for element based surrogate models whenever a proportionately small number of elements with a coarse mesh are loaded during low loading conditions (Fitzpatrick et al., 2014).

Table 4-1: Summary of the popular surrogate modeling in orthopaedic biomechanic.

Surrogae model/ Feature	Application	Sampling Information	Computational costs	Performance assessment	Computer Information
Artificial Neural Network	Estimating forces and torques via contact modeling of an artificial tibiofemoral joint **(Eskinazi and Fregly, 2015)**	100-300 samples were generated for each domain	The average prediction time improved by 17, 000 times.	RMS error was less than 1% of the peak contact force reported for walking	PC, Intel® Xeon® Quad Core 3.1 GHz processor
	Computing contact pressure at the medial tibiofemoral interface of a knee implant during **(Ardestani et al., 2015)**	214 gait cycles for training, and 74 gait cycles) for validation and testing	The average prediction time improved by 80 times.	Normalised RMSE error ranged from 5.7 – 10.4% across different subjects	CPU (Dual-Core CPU 2.93 GHz, 4 GB RAM)
	Prediction of femoral neck strains and corresponding fracture loads **(Taylor et al., 2017)**	Training datasets of 50, 100, 200, 500 and 1000 generated by LH sampling.	Training time = 1 sec; prediction time for one single load case = 0.002 sec.	R^2 = 0.92-0.98; Average RMSE,% strain 0.012-0.022 (500 samples is needed)	PC, 8 GB RAM
	Prior information is required for building the networks (e.g. numer of neurons), but can be applied for linear and non-linear systems.				
Multivariate Linear Regression	To predict micromotion over the entire bone–implant interface. **(Fitzpatrick et al., 2014)**	Generating cohorts of 10, 50, 100, 200 and 1000 samples using LH sampling.	The prediction time improved by 1800 times.	RMSE Error 6.4 ± 4.2 micromotion; R^2 = 0.83 (200 samples is needed)	Four processing units (CPUs)
	Can be applied for linear or weakly non-linear systems, not suitbale for highly non-linear models (e.g. wear modeling).				
Multivariate adaptive regression splines	**No prior information is required and is able to be applied for linear or highly non-linear systems, and the outcome can be presented in simpler, easier-to-interpret models. This method has never been used in biomechanics.**				

Bayesian network	To study the effect of implant positioning on the initial stability of a cementless total hip replacement **(Bah et al., 2011)**	Latin hypercube sampling technique was used to pre-define 58 implant positions	The computational costs reduced by approximately 2000 times.	Average and peak RMSE for the region of interest (bone-implant interface) with greater than 50 micromotion were 0.5% and 3.6%, respectively	A cluster of seven dual-core processors each with 8 GB of RAM
	Can be used for contact modeling (weakly non-linear models), however, as it computes an extensive probability analysis betveen variables, it can be computationally very expensive for large scale studies (e.g. multiple subjects with different load cases).				
Gaussian process	**Can be used for non-linear systems, and provides a trade-off between fitting the data and smoothing out, allowing to handle noisy training datasets. This technique has been used for estimating the pattern of gait kinematics (Yun et al., 2014), which was not fit with the contents of this table.**				
Kriging	To predict the contact and wear in total knee replacements **(Lin et al., 2009)**	300 samples were used to train the model	The prediction time improved by 60 times	Surrogate models produced wear volumes within 0.5% error, compared to simulations	3.4 GHz Pentium IV PC
	Sensitivity analysis of the FE model of intact hemipelvis to determine the most influential input parameters and their interactions on equivalent strains **(O'Rourke et al., 2016)**	Training sets were consist of 10, 20, 30, 40, 50, 100, and 200 sample points.	The computational costs reduced by approximately 24 times.	The median RMSE error ranged from 2.7–178.9; and the peak error ranged from 134.5– 5383.2 microstrain	Eight CPUs (Intel Xeon 2.4 GHz processor, 32 GB RAM)
	Can be used for non-linear simulations (e.g. wear modeling), but can be computationally very expensive for large datasets, and is very sensetive to noisy data.				

Conclusion

A variety of surrogate models have been used by the biomechanics community to reduce the computational costs required by FE models, including artificial neural networks (Cilla et al., 2017; Eskinazi and Fregly, 2015; Taylor et al., 2017), multivariate linear regression (Fitzpatrick et al., 2014), multivariate adaptive regression splines (Friedman and Roosen, 1995; Wang et al., 2014), the Kriging method (Walter and Pandy, 2017) and the Gaussian process (Seeger, 2004). However, the performance of each surrogate model is bound by the scope of training data (Forrester and Keane, 2009; Jin et al., 2001) meaning that, for example, a surrogate model trained on level gait is unlikely to be as effective in predicting musculoskeletal loading patterns for activities with a higher degree of variability such as stumbling and jumping. Furthermore, the performance of surrogate modelling techniques is dependent on the application type. For example, while the multivariate linear regression is a suitable technique for linear or weakly non-linear models (Fitzpatrick et al., 2014), it is likely to be less effective for non-linear systems, such as modelling the wear mechanism between bones and implants (Bevill et al., 2005; Cosmi et al., 2006).

Chapter 5 : EFFICACY AND EFFICIENCY OF MULTIVARIATE LINEAR REGRESSION FOR RAPID PREDICTION OF FEMORAL STRAIN FIELDS DURING ACTIVITY

Introduction [1]

Among the surrogate modelling techniques, multivariate linear regression (MLR) has been demonstrated to be one of the most efficient methods (Fitzpatrick et al., 2014) which was applied previously for different biomechanical applications, such as predicting femoral neck strain (Kersh et al., 2018), sensitivity analysis of fracture load (Taylor et al., 2017) and estimation of micro-movement at the bone implant interface (Fitzpatrick et al., 2014). However, the error and the computational advantage of MLR over finite-element models remains unclear for the calculation of strain over the femoral volume and across normal activities of daily living. This chapter aimed to explore the efficacy and efficiency of MLR method as the simplest surrogate modelling technique for rapid prediction of femoral strain fields during normal activities, including normal-walking, fast walking, stair ascent, stair descent and chair sitting, with different repetitions for each task, here referring to 'trials'.

Materials and methods

A coupled musculoskeletal and finite-element was taken from the previous work (Martelli et al., 2015b) to calculate muscle and joint forces and femoral von Mises strain for a single healthy participant (female, 68-year-old, 53 kg weight, 157 cm height). All experimental and computational methods are described in detail by Martelli et al. (2015) and Dorn et al. (2012), respectively and described briefly below.

Data collection

---

[1] The work presented in this chapter has been published in *Medical Engineering and Physics*.

The CT images of pelvic and thigh region was provided for the participant was taken from the previous work (Martelli et al., 2015b), where more details about data collection, experiments and tools could be found. However, for the sake of completeness, the details of this work are summarized here. The images were provided using two different scanners from both whole body and axial sides, while a sample calibration phantom was placed below the participant's dominant leg during scanning, providing images with the slice thickness of 0.5 mm and, the spacing of 0.5 mm. Gait analysis was recorded at the Biomotion Laboratory in University of Melbourne which was equipped with a 10-camera motion capture system (VICON, Oxford Metrics Group, Oxford) and sampling at 120 Hz. Forty-six reflective markers were attached to the skin at different anatomical landmarks described by Dorn et al. (2012), comprising the pelvis (3), thigh (6), shank (5) and foot (6), while the rest of markers were used for upper extremities and torso. The Ground reaction forces and moments were recorded using a force platform equipped with three strain-gauged (AMTI, Watertown, MA) sampling at 2000 Hz. Marker trajectories and ground reaction forces were recorded for five trials of each of the following five tasks: walking at the self-selected speed (normal walking), fast walking, stair ascent, stair descent, and rising from and sitting down on a chair (chair rise). Trials with incomplete marker trajectories were discarded, resulting in five repetitions for normal walking, fast walking and stair descent; four trials for stair ascent; and one trials for chair rise (Figure 5.1). The marker trajectories were labelled using a VICON motion capture system (Vicon, Oxford, UK), saved as c3d files, and then converted into OpenSim format using MOtoNMS (Mantoan et al., 2015).
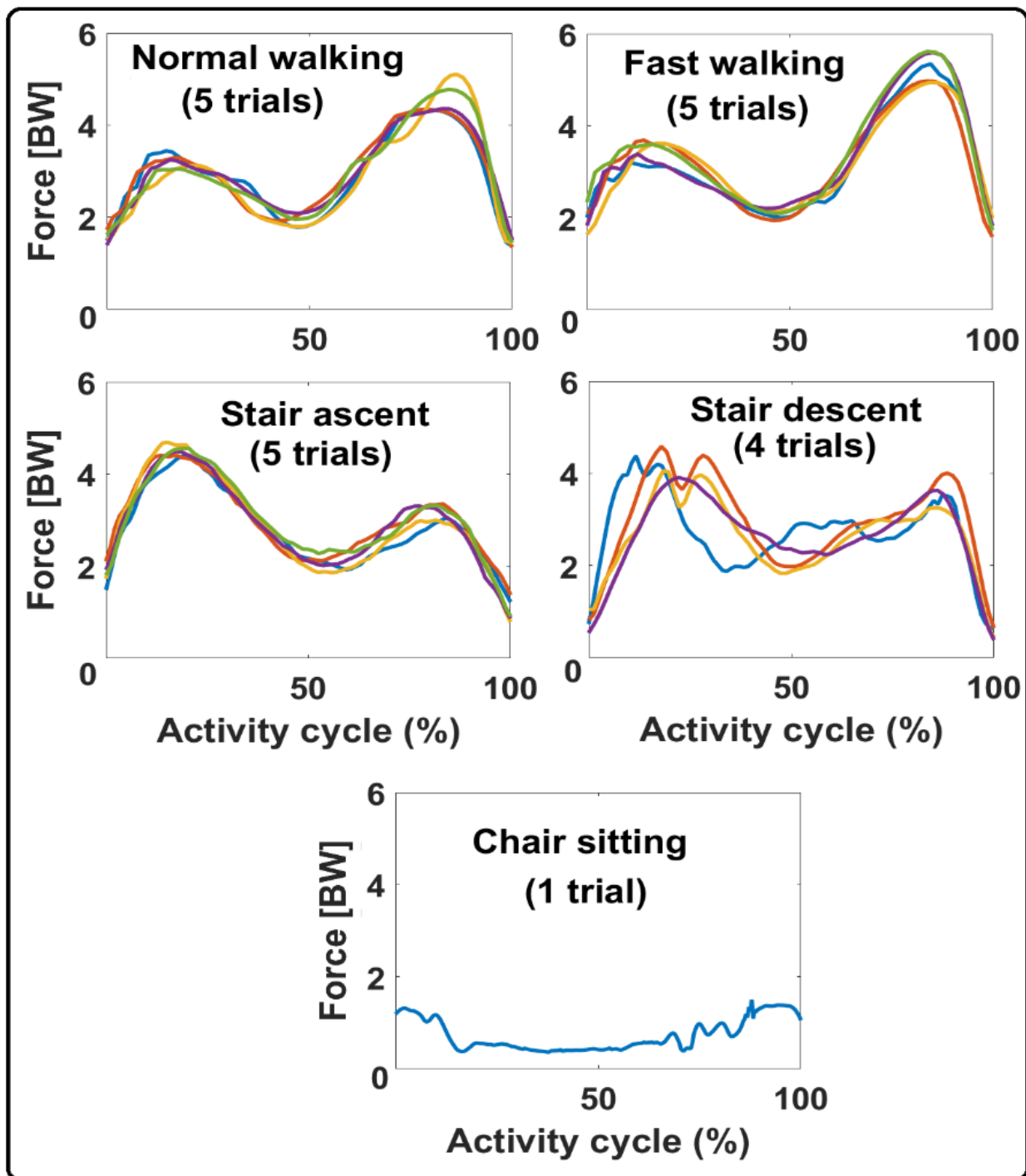
Figure 5.1: The magnitude of hip joint reaction force expressed in Body Weight (BW) for the investigated normal activities.

A previously developed musculoskeletal model (Martelli et al., 2015b) with 12-segment and 92 Hill-type muscle–tendon units proposed by Delp et al. (2007) was scaled to the

participant mass and anthropometry using measurements of body weight and segment lengths acquired during a static trial (Figure 5.2). The mass of the generic model was scaled to match that of each participant by computing the mass ratio between segments in the generic model. The distance between markers recorded during a stance trial was used for scaling different parameters, including joint centres, bone geometries, joint rotation axes, fibre lengths, muscle paths and tendon slack. A ball-and-socket joint was used to represent each shoulder, lumbar joint, and each hip; each knee joint was represented as a translating hinge joint; a universal joint was used for representing each ankle. While, the elbow and shoulder joints were actuated by 10 ideal torque motors, all other joints were simulated using Hill-type muscle–tendon units. The centre of hip joint was determined as the centre of the sphere used to best-fit the femoral head surface. The knee axis was assumed to be placed on the axis which connects the femoral epicondyles. Muscle paths was also registered on the skeletal surfaces by placing the muscle lines-of-action onto the CT data. The optimum length for muscles and tendon slack was determined by scaling the values reported by Delp et al. (1990), so that each muscle develop its peak isometric force at the same joint angle. Finally, joint angles, muscle forces, and joint reaction forces were calculated using, respectively, inverse kinematics, static optimization and joint reaction analysis tools available in OpenSim (Delp et al., 2007).
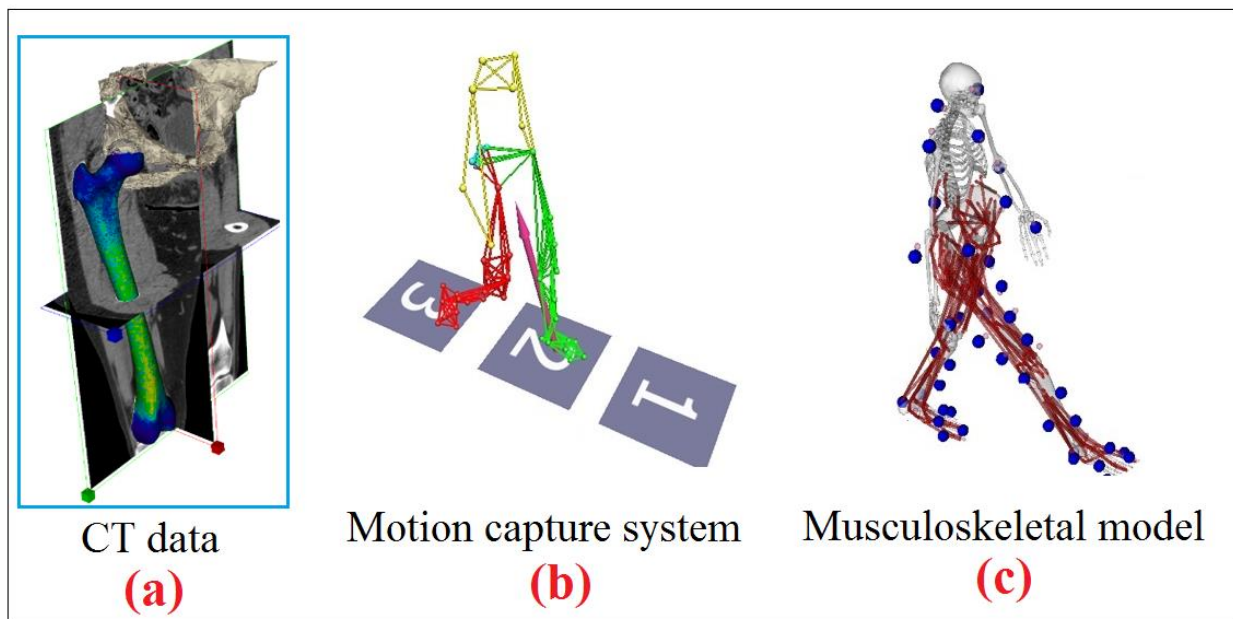
Figure 5.2: (a): CT data used to define the material properties and geometry; (b): The motion capture system in Vicon Nexus used to generate marker trajectories and ground reaction force; (c): A musculoskeletal model used for computing muscle and joint reaction forces.

The muscle and joint reaction forces calculated at each time frame then were applied to a finite-element model of a femur using an automatic pipeline developed in an earlier study (Martelli et al., 2015b). The finite-element model of the femur was a locally isotropic, unstructured mesh comprised of 213,559 nodes and 143,534 elements (C3D10: Ten-node tetrahedral element) that was fully constrained distally (Figure 5.3). The femur model was fully constrained distally to satisfy equilibrium according to earlier studies (Behrens et al., 2009; Zhou et al., 2017). The finite-element model was loaded by applying muscle forces and the hip joint reaction force for 50 frames uniformly distributed over each activity. The unit force vectors describing the line-of-action of each muscle force was assumed to originate at the muscle's attachment point on the femur and was oriented along the line-of-action of the muscle force. The muscle force components was then computed by multiplication of the muscle force calculated from static optimization and the unit force vector, and then were applied at the node closest to the muscle attachment point in the FE

model. The hip joint reaction force was applied on a node places on the surface of femoral head and was oriented toward the centre of femoral head (centre of pressure) determined by the musculoskeletal model for each frame of motion. Five layers of elements around the muscle attachment points were excluded to avoid boundary condition artefacts. The anatomical coordinate systems for pelvic, femoral and tibial was defined based on International Society of Biomechanics standards (Wu et al., 2002). The musculoskeletal and finite-element models were coupled using custom code developed in Matlab (MathWorks Inc., Natick, MA). The equivalent strain at the element centroid was computed using the linear-elastic solver implemented in Abaqus (Dassault Systems, USA). Thus, the full dataset comprised of muscle and joint reaction forces and femoral strains for 1000 frames (50 frames per trial for 20 trials, in total).
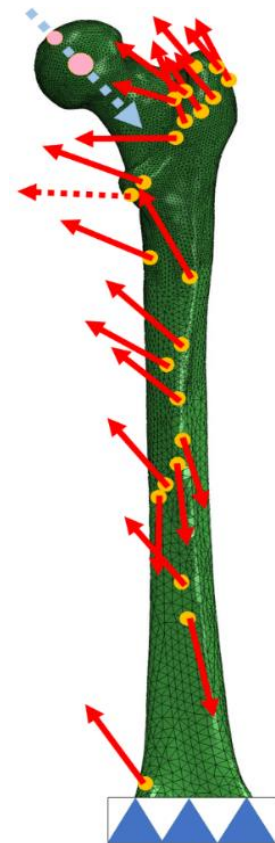
Figure 5.3: Schematic representation of the FE model and its boundary conditions, featuring the applied muscle forces (red arrows), muscle attachment points (orange circles), joint reaction force (blue dashed line), point of application of the joint reaction force on the femoral head surface (pink circle), femoral head centre (pink circle) and distal constraint (blue triangles).

Multi-variate linear regression surrogate model

A Latin hypercube (LH) sampling method was used to create the training set, which comprised of muscle forces, joint reaction forces and femoral strains for randomly selected frames of motion (Figure 5.4). The process was repeated to generate four training sets consisting of 50, 100, 200 and 300 frames, respectively. Training sets of similar size have been used to develop surrogate models in previous studies (Fitzpatrick et al., 2014; O'Rourke et al., 2016). The surrogate model, relating the magnitude of the applied forces to the equivalent von mises strain, was developed by fitting a MLR model for each element. Training the surrogate models returned the coefficients, which can be regarded as a link between the forces and the induced strain field. In other words, by showing the training data set to each element (as input variable) and the strain (as output), the response of each element was (the coefficients) obtained (Figure 5.4).
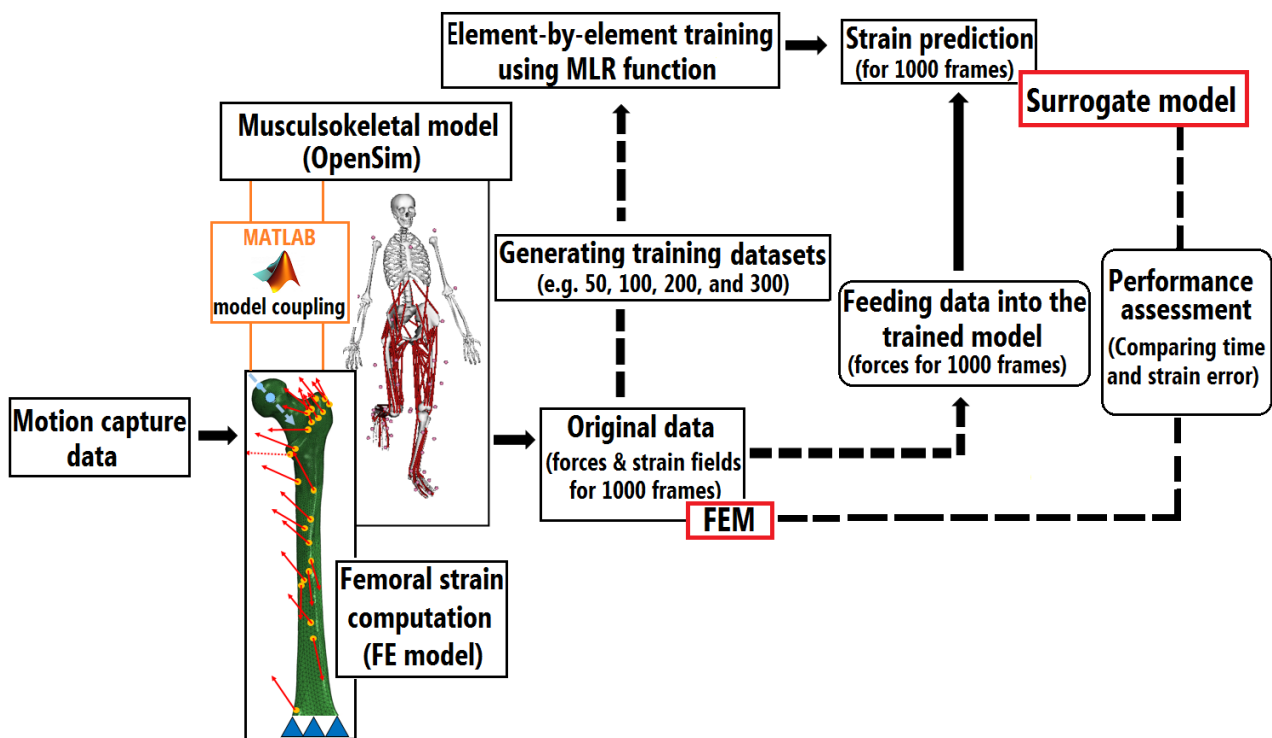
Figure 5.4: Flowchart illustrating the linear-based surrogate modelling approach used in the present study (Ziaeipoor et al., 2018).

The model took the form:

$$\varepsilon^{j,k} = \sum_{i=0}^{25}(c_i \times f_i^k); \ f_1^k, ..., f_{25}^k$$

Where $\varepsilon^{j,k}$ is the equivalent von Mises strain at element j for frame k, and c_i is the coefficient for the force i at frame k. The total number of forces applied to the finite-element model was 25, which included all the muscle forces in the musculoskeletal model acting on the femur and the hip reaction force. The strain field for all 1000 frames of motion was computed by multiplying the calculated coefficients c_i in the MLR model and the corresponding muscle and joint reaction forces (Figure 5.5).
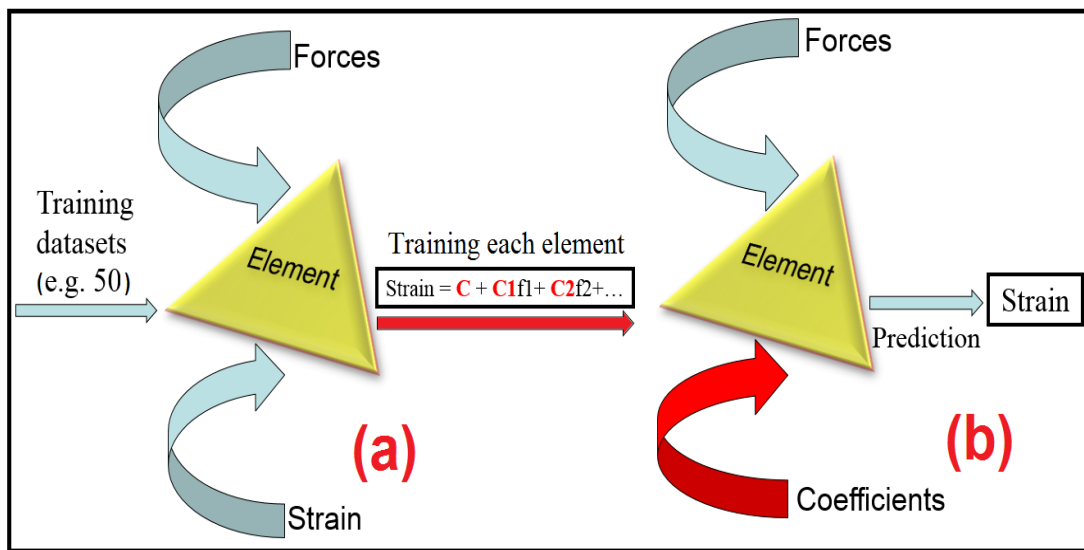
Figure 5.5: A schematic representation explaining the development of the surrogate model: (a) training, and (b) strain prediction for each element.

Metrics for assessing the performance of MLR model

Performance of the MLR regression models was assessed by calculating the coefficient of determination (R^2) and the slope of the linear regression between the strains predicted by the surrogate and finite-element models. CPU times needed to complete the finite-element analysis, train the MLR models, and calculate femoral strain using the MLR models were

compared on a standard desktop computer (8 CPUs Intel® Core(TM)® 3.4 GHz processor, 32 GB RAM). Strain error was calculated using the finite-element strain as a reference and evaluated using the Root Mean Square Error (RMSE) as well as the 95th percentile of the strain error distribution as an indicator of peak error. These parameters were analysed frame-by-frame within each trial (i.e. $RMSE_{Frame}; R^2_{Frame}$) by amalgamating all frames for each trial (i.e. $RMSE_{Trial}; R^2_{Trial}$) and for each activity (i.e. $RMSE_A; R^2_A$).

Results

The trial-by-trial comparison presented a good consistency for the coefficient of determination (R^2) and slope, ranging from $0.84 - 0.94$, and $0.97 - 0.99$, respectively. The performance of the MLR model is presented for a selected trial of normal walking as an exemplar activity (Figure 5.6 and Figure 5.8). Close visual agreement was observed between the strain distributions estimated by the surrogate model trained using 200 samples and those predicted by the FE model (Figure 5.8).
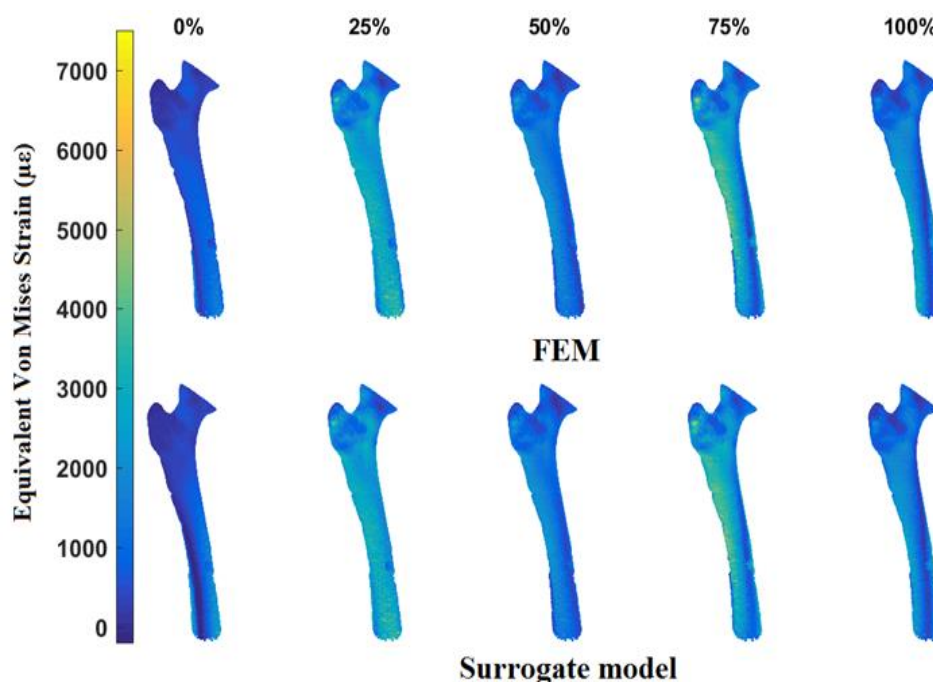
Figure 5.6: Contour plots showing the calculated femoral strain fields for normal walking obtained by applying finite element modelling (FEM) and MLR surrogate modelling. Results are shown at 25% intervals of the stance phase. 0% and 100% indicate the stance phase (Ziaeipoor et al., 2018).
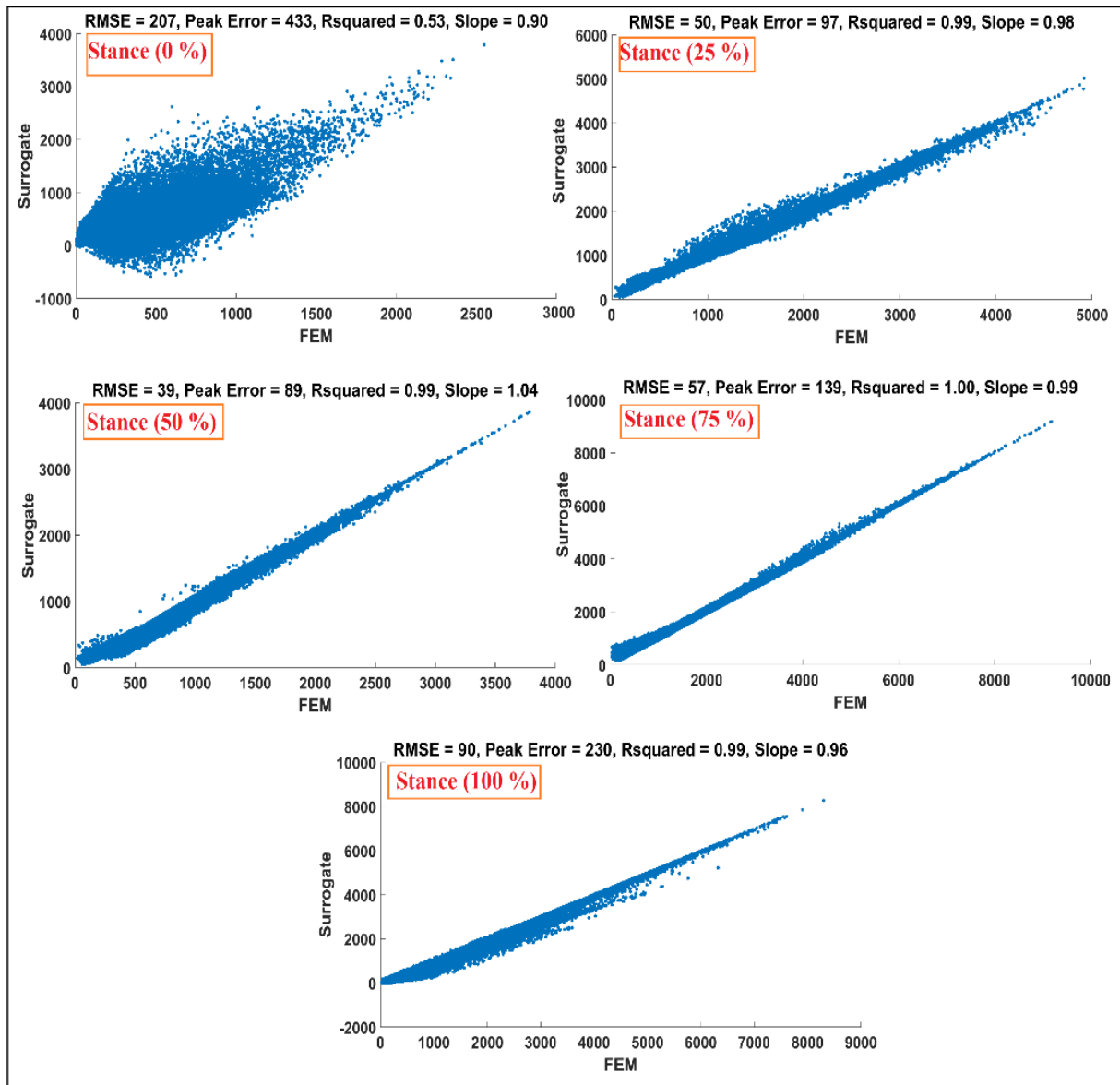
Figure 5.7: The results of the fitted regression line between surrogate modelling (MLR) and FEM during five different percentage of stance phase (normal walking), including RMSE (με); peak error (με); coefficient of determination and slope.

The average RMSE and peak error were 78 and 181 με, respectively, across different frames. RMSE reached 207 με during early stance and 140 με during late stance while the corresponding peak errors reached 433 με and 391 με, respectively, for early and late stance (Figure 5.8). The peak error was 8.6% of peak equivalent strain in the diaphysis, ranging from approximately 2920 to 5020 με during the stance phase of gait. The average coefficient of determination and slope were 0.97 and 0.99, respectively.
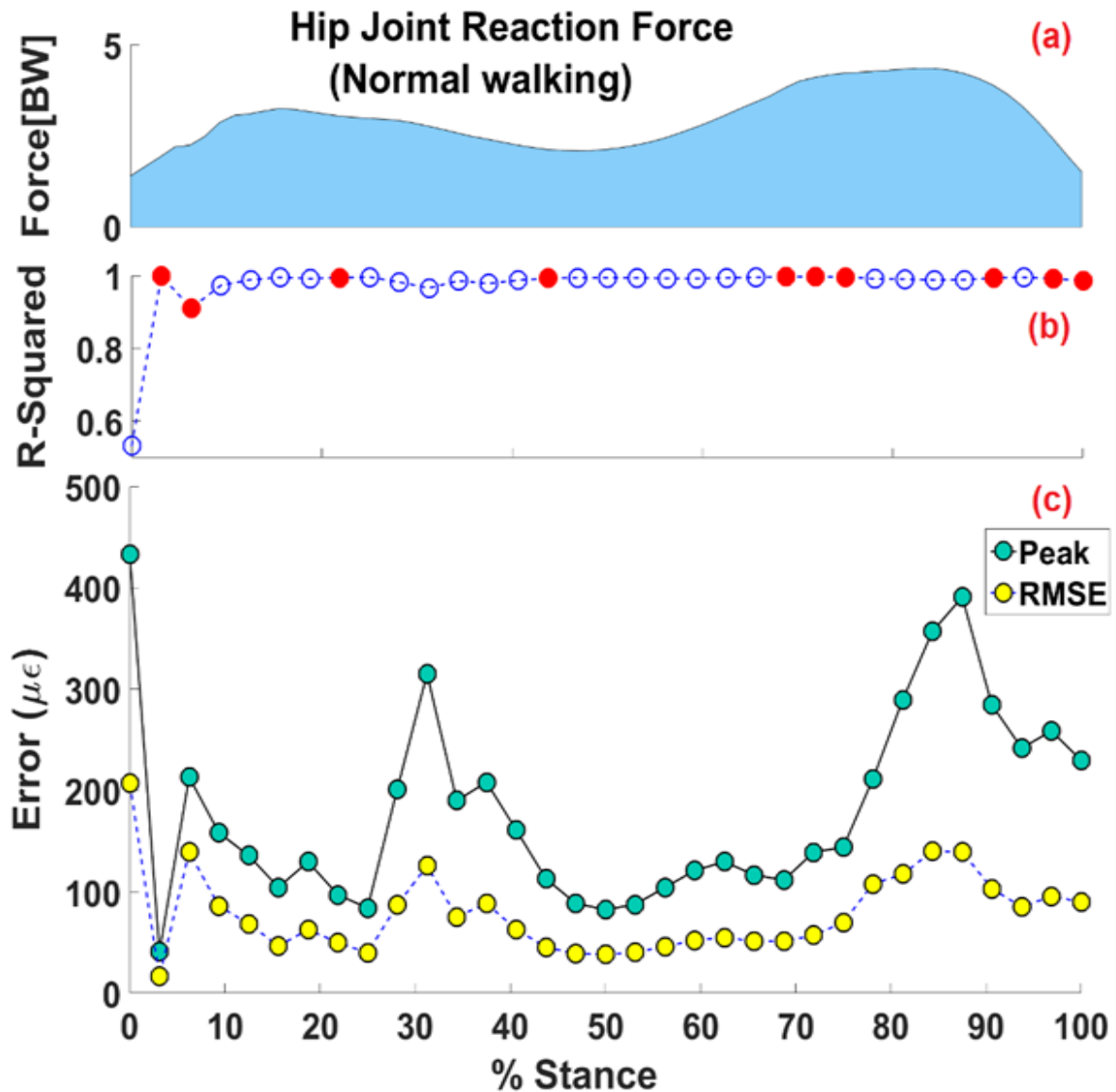
Figure 5.8: Evaluating the performance of the MLR surrogate model for normal walking: (a) pattern of the hip joint reaction force; (b) coefficient of determination (R^2_{Frame}); (c) peak error and root mean square error ($RMSE_{Frame}$) at each frame. BW in part (a) refers to body weight; the red (solid) dots shown in part (b) represent the frames used to train the surrogate model, and the blue (hollow) circles represents the coefficient of determination for those frames which has never used during the training process (Ziaeipoor et al., 2018).

Similar performance of the MLR model was observed among the different activities. The median $RMSE_A$ varied between 80 µε for normal walking and 124 µε for chair rise. Peak $RMSE_A$ varied from 163 µε for stair ascent to 389 µε for chair rise (Figure 5.9).
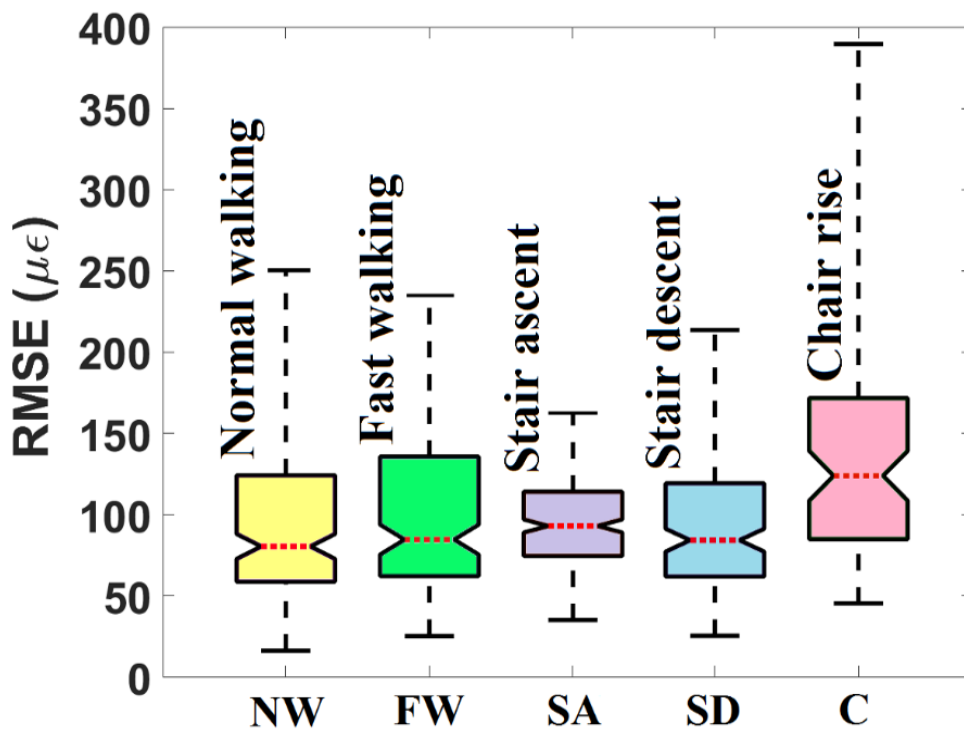
Figure 5.9: Box plots used to quantify the accuracy of model-predicted strains obtained from MLR surrogate modelling. The black box represents the range of the error between the 25th and 75th percentiles while the red horizontal dashed line represents the median error. The black dashed line represents the 95th percentile of RMSE_A for each activity (Ziaeipoor et al., 2018).

It was observed that the prediction error of the surrogate model was a function of the size of the training set. Increasing the size of the training set from 100 to 200 frames reduced the average RMSE across trials from 132 $\mu\varepsilon$ to 108 $\mu\varepsilon$, while a relatively small decrease in RMSE to 107 $\mu\varepsilon$ was obtained by increasing the training set size to 300 samples (Table 5-1).

Table 5-1: Effect of the size of training datasets on the accuracy of model-predicted femoral strains. Model accuracy was evaluated by computing the mean and peak error and the mean of coefficient of determination. These reported errors are based on pooled data.

Training Dataset	RMSE (με)		R^2	Training Time (min)
	Mean	95th perc.	Mean	
50	227,315	408,484	0.84	8.5
100	132	326	0.92	8.7
200	108	228	0.94	8.8
300	107	201	0.94	8.9

CPU time for predicting the full femoral strain for all 1,000 frames was 66,000 secs using the finite-element model alone (i.e., 55 minutes was required for predicting femoral strain for an entire activity of 50 frames). Training the MLR model required 13,200 secs for completing the 200 finite-element simulations in the training set, 528 secs for training and 100 secs for predicting all 1,000 frames, which corresponds to 5 secs for predicting femoral strain for an entire activity (50 frames). The MLR-based surrogate model was faster than finite-element analysis for solving 209 frames or more (Figure 5.10).
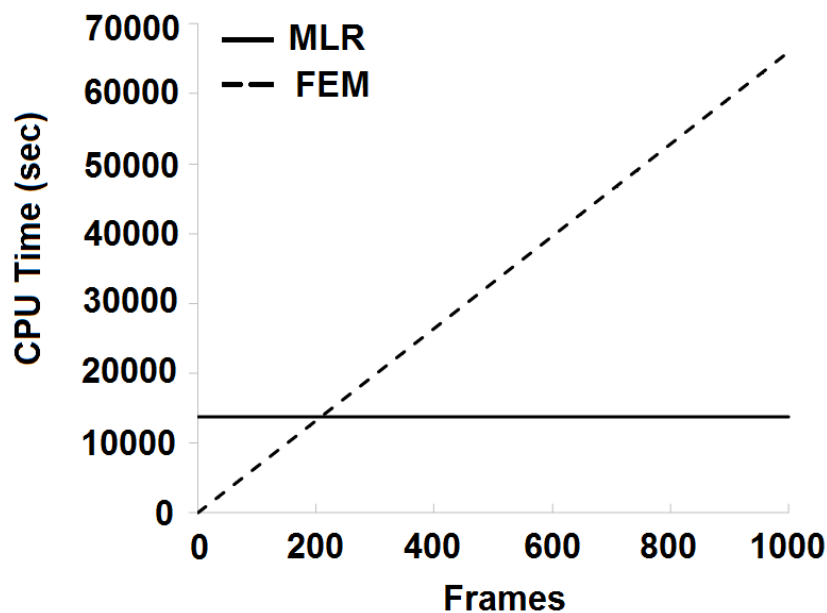
Figure 5.10: The CPU time required by the finite-element and the MLR model plotted against the number of frames (Ziaeipoor et al., 2018).

Discussion

The present chapter evaluated the performance of a multivariate linear regression surrogate model in approximating the full strain field of an intact femur during five different activities of daily living. We found that reliable predictions of femoral strain could be obtained across all five activities by training the surrogate model using 200 samples. The surrogate model closely reproduced the FE results at a low computational cost, with typical solution times of 5 secs per activity compared to 55 minutes needed for a finite-element analysis when 50 frames of motion were used to represent each activity.

The predicted strains from the MLR model were in close agreement with those obtained using the finite-element model. The peak error in the MLR model was 8.6% of the peak equivalent strain (5020 $\mu\varepsilon$), which is comparable to the error (i.e., 4.2 – 8.3% of peak strain on average) caused by material properties and geometry errors committed while generating the finite-element models from calibrated computed-tomography images (Taddei et al., 2006b). Furthermore, the average RMSE was 78 $\mu\varepsilon$, which is consistent with the average error (113 $\mu\varepsilon$) obtained when finite-element models are used to predict experimentally measured cortical strains (Taddei et al., 2006b). Therefore, MLR models represent valid surrogates of finite-element calculations of femoral strain during activity. The training sample size was similar to that reported in previous surrogate modelling studies in biomechanics: Fitzpatrick et al. (2014) required 100 – 200 samples for a MLR-based surrogate model; Taylor et al. (2017) needed 200 – 500 samples to train an artificial neural network; and Lin et al. (2009) required 300 samples to develop a kriging-based surrogate model. This supports the validity of the MLR model developed in the present study.

The current study is not without limitations. Firstly, Latin Hypercube sampling was used to generate the training datasets, but generating more uniformly distributed samples using other potential techniques may improve model accuracy. Secondly, the performance of the surrogate model was lowest during early stance where the coefficient of determination was only 0.53. The FEM model itself was a linear mode, so the error likely caused by the non-linear behaviour of the model arising, for example, from the location in the centre of femoral head which change during locomotion. Different surrogate methods (e.g. MARS, Gaussian Process and Artificial Neural Networks) may further improve model performance. Thirdly, the prediction time of the MLR model (0.1 sec per frame) was much faster than that of the finite-element model, although the MLR required 200 finite-element simulations for generating the training set and 528 secs for training the model. Thus, the MRL model is computationally advantageous relative to the finite-element model only when 209 frames of motion or more are to be analysed (Figure 5.10). Fourth, only normal activities were included in the reference study (Martelli et al., 2015b) to limit the risk of injury for the participants while executing demanding (e.g., sprinting) or para-physiological (e.g., falling) activities. Therefore, the validity of the present conclusion is limited to normal locomotion. Fifth, the MLR model was developed for a single healthy individual possibly limiting the generality of the present conclusions. However, the strain range predicted by the model (0 – 5020 $\mu\varepsilon$) spans a large portion of physiologically admissible strains (Bayraktar et al., 2004) and the loading conditions did span a broad range of normal activities, providing confidence on the performance of the MLR model over a relevant range of femoral strain and boundary conditions of the femur.

Conclusion

A Multivariate Linear Regression model was successfully developed for a single individual and used to rapidly predict the full femoral strain field for a range of activities of daily living. The MLR model was able to predict the femoral strain field for each studied activity within an error comparable to the intrinsic error in finite-element models based on clinical CT images and was computationally advantageous when 209 loading cases or more were analysed. Hence, MLR enables large statistical studies of femoral strain during activity. However, other potential techniques are required to be evaluated to compare the performance of each method.

Chapter 6 : A NOVEL TRAINING-FREE METHOD FOR REAL-TIME PREDICTION OF FEMORAL STRAIN

Introduction [2]

As discussed in the chapter 4, to reduce the computational cost of finite-element analyses, several surrogate methods have been used in computational biomechanics, including Artificial Neural Networks (Cilla et al., 2017; Eskinazi and Fregly, 2015; Taylor et al., 2017), Multi-linear Regression (Fitzpatrick et al., 2014), Multivariate Adaptive Regression Splines (Friedman and Roosen, 1995; Wang et al., 2014), Kriging (O'Rourke et al., 2016; Walter and Pandy, 2017) and Gaussian process modelling (Seeger, 2004). Multivariate Adaptive Regression Splines is an extension of the multi-linear regression method, which can be used to model the nonlinearities between variables by partitioning the training datasets into separate linear or cubic splines known as 'basis functions' (Friedman and Roosen, 1995). Gaussian process modelling, which provides a trade-off between fitting the data and smoothing, can handle noisy training datasets while capturing the precise trend of the data (Wang and Shan, 2006). Artificial Neural Networks provide an effective solution when the optimum number of artificial neurons needed for building the network structure can be determined *a priori*, for example, using trial-and-error approaches (Cilla et al., 2017; Tu, 1996). Kriging is best suited for nonlinear problems, but typically requires large training sets and is computationally expensive (Eskinazi and Fregly, 2015). Therefore, Multi-linear Regression (MLR), Multivariate Adaptive Regression Splines (MARS), and Gaussian process (GP) methods appear to be the best suited for predicting femoral strain during activity. However, the performance of each surrogate model is application-dependent and bounded by the scope of training data (Forrester and Keane, 2009; Jin et al., 2001). For

---

[2] The work presented in this chapter has been published in Journal of Biomechanics.

example, a surrogate model trained on data for level walking is unlikely to be as effective in predicting musculoskeletal loading patterns for activities with a higher degree of variability such as stumbling and jumping.

By leveraging the linearity of most models used to predict femoral strain (Fitzpatrick et al., 2014; Liang et al., 2018; Martelli et al., 2014a), the superposition principle can provide a solution that may outperform current surrogate methods while being applicable to every possible motor task or activity, without training. In the most general case, a muscle's contribution to femoral strain can be described by calculating the strain tensor generated by three independent nominal force vectors applied to each of the muscle's attachment points, and is therefore not related to a specific frame of motion. The displacement of the joint contact area during motion can be modelled by discretising the patch on the joint surface spanned by the joint contact force into a finite number of nodes. The strain tensor generated by the hip contact force can then be described by calculating the strain tensor generated by three independent nominal force vectors applied to each node in the patch. Femoral strain for a given frame of motion can be calculated by (1) matching the centre of pressure for the specific frame of motion using, for example, musculoskeletal modelling, and (2) determining the weights for the strain tensor generated by each nominal force component as the ratio between the amplitude of the actual force component and that of the nominal force applied. This model, henceforth referred to as the Superposition Principle Method (SPM), does not require training, and can be generated independently from motion analyses experiments.

The aim of the present chapter was to develop an SPM model for one representative individual and to compare its performance to that of MLR, MARS, and GP for the prediction of femoral strain for a range of activities and repetitions. The strain error and the CPU time required for solving the elastic problem of the femur by SPM, MLR, MARS, and GP methods

were computed and compared. We hypothesized that the Superposition Principle Model (SPM) would outperform popular surrogate methods for the calculation of femoral strain during activity in relation to both accuracy and total computational time required.

Building the surrogate methods

The data obtained from the previous chapter was used to build the models in this chapter. Marker trajectories and ground reaction force for a healthy woman (68 years of age, 53kg weight) during repetitions of normal walking, fast walking, stair ascent, stairs descent and chair sitting were taken from the previous work (Martelli et al., 2015b). As it was explained in the previous chapter, a coupled musculoskeletal and finite-element model was taken from an earlier study to calculate muscle and joint reaction forces and femoral strains for 1000 (Martelli et al., 2015b). Two sampling methods, Latin Hypercube (LH) and Design of Experiment (DOE), were used to generate training sets from the original data Latin Hypercube provided random samples while DOE provided samples that best spanned the variation in the original data (Han and Zhang, 2012). Training datasets of four different sizes (i.e., 50, 100, 200, and 300) required for developing MARS and GP methods were obtained for each mesh element and MLR was trained by taking the data from our earlier work (Ziaeipoor et al., 2018). The different in the distribution of samples for the training datasets with 200 samples are represented in Figure 6.1. All surrogate methods were implemented using custom code in Matlab (The Mathworks Inc., Natick, USA).
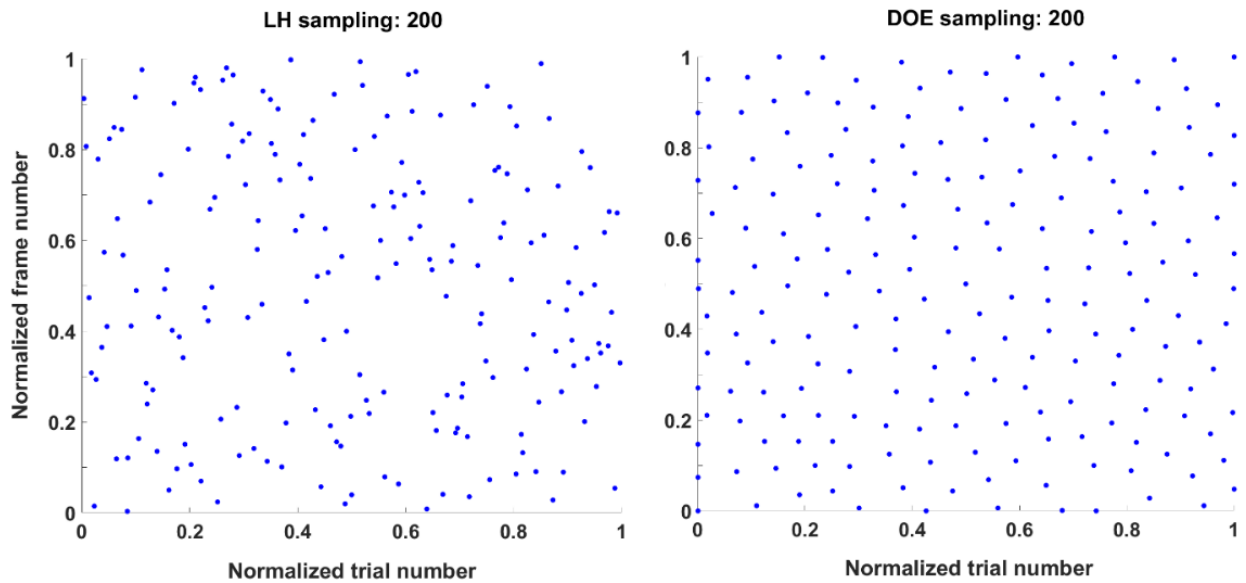
Figure 6.1: Generating training datasets using DOE and LH sampling (200 samples).

Superposition principle model

The Superposition Principle Model (SPM) was developed by leveraging the load-strain linear response in common finite-element models ensuring that every solution in the model can be expressed as a linear combination of a base of independent solutions. The SPM model was essentially a look-up table composed by a set of strain fields generated by nominal force vectors, each arbitrarily set to 100 N, applied to each muscle attachment and application point of the hip contact force. Finally, the strain tensor during a generic frame of motion was calculated as the sum of strain fields in the look-up table weighted by the ratio between the force intensity provided by the OpenSim model and the nominal force intensity (100 N).

For the 24 muscles in the model acting on the femur, the femoral strain in the look-up table was calculated by applying the nominal force along each of the three coordinate axes for each of the 24 muscle-attachment sites, resulting in 72 strain fields.

The displacement on the hip centre of pressure during movement was modelled by identifying the node patch on the femoral head spanned by the hip centre of pressure (Figure 6.2). The centre of pressure was assumed to be the intersection between the sphere that best fit the femoral head surface (i.e., the hip centre henceforth) and the hip contact force vector passing through the hip joint centre (Figure 6.2). The patch was composed by 101 nodes within the envelope of the trajectories of the hip joint centre of pressure across activities (Figure 6.2). For each node in the patch, the SPM model was completed by the strain field calculated using a nominal force vector $\overrightarrow{hf}v_z$ pointing to the hip joint centre. This condition represents a frictionless ball and socket joint consistent with a very low coefficient of friction characterising natural joints (Pawlak et al., 2015).
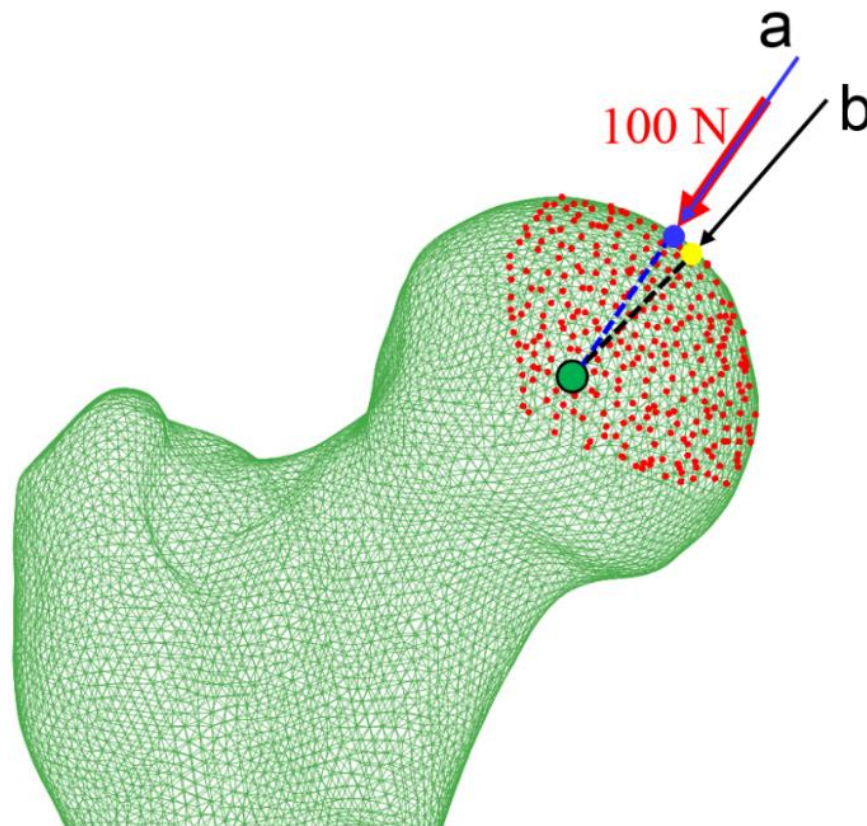
Figure 6.2: Matching the applied unit force vector (100 N) with two arbitrary forces named 'a' and 'b' vectors passing through the centre of femoral head. The distance between the blue and yellow circles is the error that may occur during matching the vectors to perform prediction using SPM method.

The total strain tensor $\bar{\bar{\varepsilon}}_i$ generated by both muscle and hip contact forces for a generic frame *i* of activity was given by:

$$\bar{\bar{\varepsilon}}_i = \sum_{j=1}^{24} \sum_{k=1}^{3} \frac{fm_{i,j,k}}{f_n} \times \bar{\bar{\varepsilon}}(fv_{j,k}) + \frac{fh_i}{f_n} \times \bar{\bar{\varepsilon}}(\overrightarrow{hf}v_{i,z})$$

where $fm_{i,j,k}$ is the magnitude of the force component *k*, muscle *j*, frame *i*, obtained using models of human motion (Martelli et al., 2015b); $\bar{\bar{\varepsilon}}(fv_{j,k})$ is the strain tensor generated by a nominal force *fn* applied at the muscle attachment point *j* along the coordinate axis *k*; *fh$_i$* is the magnitude of the hip contact force obtained using models of human motion (Martelli et al., 2015b) for frame *i*; and the nominal strain tensor $\bar{\bar{\varepsilon}}(\overrightarrow{hf}v_{i,z})$ was generated by a force vector $\overrightarrow{hf}v_z$ of magnitude *fn* applied to the node *z* at the femoral head surface. The node index *z* was dynamically determined by best matching the orientation of the hip contact force in the musculoskeletal model and that of the force $\overrightarrow{hf}v_z$.

Assessment of performance

The equivalent von Mises strain was calculated from the predicted strain tensor $\bar{\bar{\varepsilon}}_i$ to provide a compact assessment of the models' performance relevant to both tensile and compressive states. The strain error was calculated as the difference between the strain predicted by the surrogate and SPM methods and corresponding finite-element calculations of strains. For each surrogate method studied, the sample size and sampling method providing minimal strain error were identified. Surrogate and SPM models were compared using linear regression. The strain error was assessed at three levels: by pooling all the activities and repetitions together; activity-by-activity by amalgamating all the repetitions of each activity; and frame-by-frame. The Root Mean Square Error (RMSE) and 95th percentile of the strain

error distribution were used as indicators of mean and peak error. The coefficient of determination (R^2) and slope were used as indicators of goodness of fit. To gain insight into the source of error in the SPM method, the contribution to the total strain error in the SPM model of each muscle force and joint reaction force was calculated separately. Model efficiency was assessed using a standard desktop computer (Intel Core i7 processor, 8 CPUs, 32 GB RAM). Total CPU time included the time required for constructing the models, the time needed to execute the FE simulations in the training set, and the training time. The time required for predicting strain during an entire activity (50 frames) and the total time required for predicting strain for all the 1000 frames, including both model construction and prediction, were also compared.

Results

The DOE sampling method was superior to the LH method for each training sample size, with both methods showing only a marginal improvement in the mean and peak errors above 200 training samples (Table 6-1). Specifically, RMSE varied from 134 µε to 99 µε, 187 µε to 100 µε, and 91 µε to 53 µε for MLR, MARS, and GP, respectively, when 200 training samples were used. RMSE improved on average by less than 10 µε when the training sample size was increased to 300 samples. Peak error obtained for the MLR method with 200 training samples remained less than 521 µε, thus assessment of the performance of MLR, MARS and GP was based on the DOE method with a training sample size of 200 (Table 6-1).

Table 6-1: Mean and peak error for the different surrogate modelling methods (Multivariate Linear Regression (MLR), Multivariate Adaptive Regression Splines (MARS) and Gaussian Process (GP)) for increasing training set and different sampling methods, including Latin hypercube (LH) sampling and Design of Experiment (DOE). These reported errors are based on pooled data.

Training dataset	Methods	LH			DOE		
		Peak error$_{All}$	$RMSE_{All}$ (mean)	Training time (h)	Peak error$_{All}$	$RMSE_{All}$ (mean)	Training time (h)
50	MLR	1,082,306	227,315	0.14	911	134	0.14
	MARS	1,234,000	9,348,000	6.8	851	187	6.9
	GP	674	111	0.2	495	91	0.2
100	MLR	1021	132	0.14	697	109	0.14
	MARS	1422	508	23.0	678	133	22.7
	GP	461	75	0.3	556	83	0.3
200	MLR	540	108	0.15	521	99	0.15
	MARS	785	170	60.8	414	100	59.7
	GP	519	73	0.9	316	53	0.8
300	MLR	537	107	0.15	493	94	0.15
	MARS	441	106	93.5	385	90	91.7
	GP	528	62	2.9	280	46	2.1
*One processor used for training MARS and four processors used for MLR and GP							

Overall, SPM was found to be the most effective, showing the lowest mean (RMSE = 40 µε) and peak (PE = 256 µε) errors. By comparison, mean errors were 99, 100, 53 µε while peak errors were 521, 414, 316 µε for MLR, MARS and GP, respectively. Across activities, the strain error remained relatively constant showing a peak error consistently below 300 µε for all methods, except when MLR and MARS were applied to the chair rise task, where the peak error was higher than 350 µε. SPM performed best for the chair rise task (RMSE = 6 µε; PE = 47 µε) and showed similar performance to that of GP for the remaining activities (RMSE < 30 µε; PE < 172 µε) (Figure 6.3).
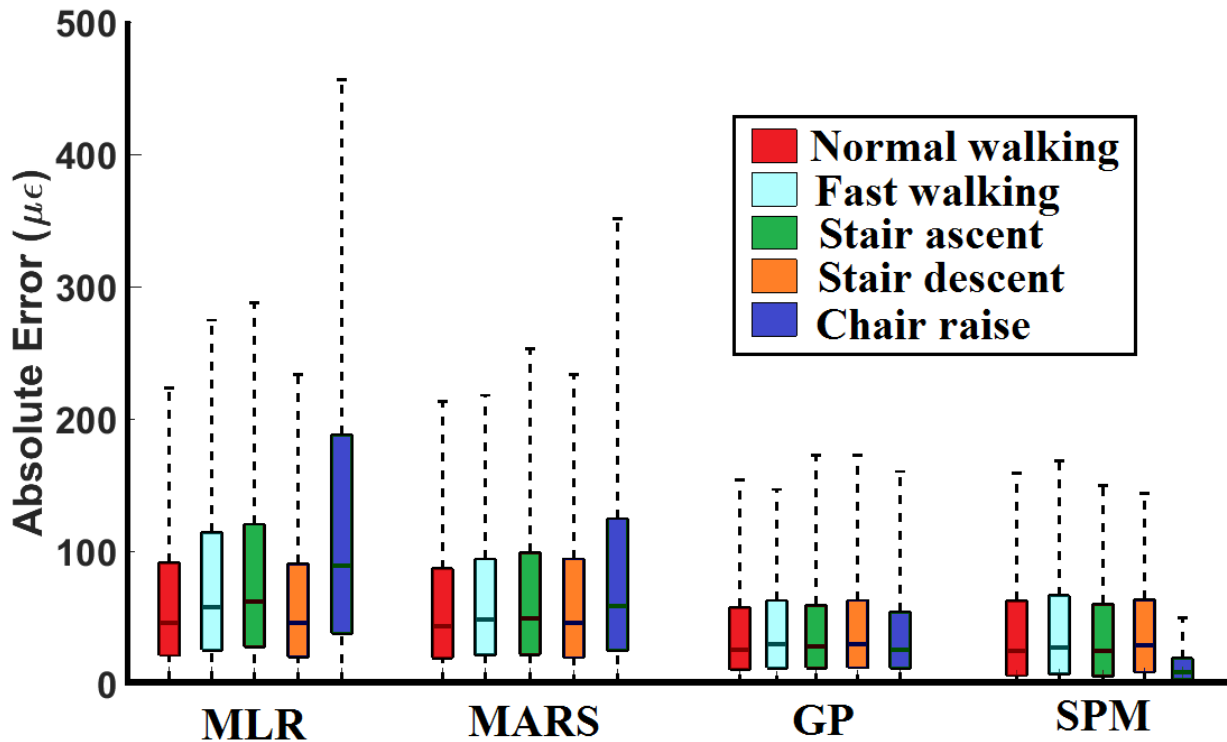
Figure 6.3: The strain error (median, 50th percentile and range) calculated for the different methods (MLR, MARS, GP, SPM) for each activity separately.

Comparing the performance of SPM and GP within a given activity, both models predicted femoral strains that were highly correlated to results obtained from corresponding finite-element calculations. The coefficient of determination (R^2) was $0.97 - 1.00$ for SPM and $0.88 - 0.99$ for GP. The slope of the linear regression was $0.96 - 1.08$ for SPM and $0.83 - 1.04$ for GP. The GP model showed higher RMSE and peak errors during early and late stance, reaching 153 µε and 380 µε, respectively, during late stance (Figure 6.4). The SPM model showed RMSE and peak errors of $0 - 96$ µε and $0 - 257$ µε, respectively, and presented a pattern across the different frames not visibly related to a specific gait phase (Figure 6.4).
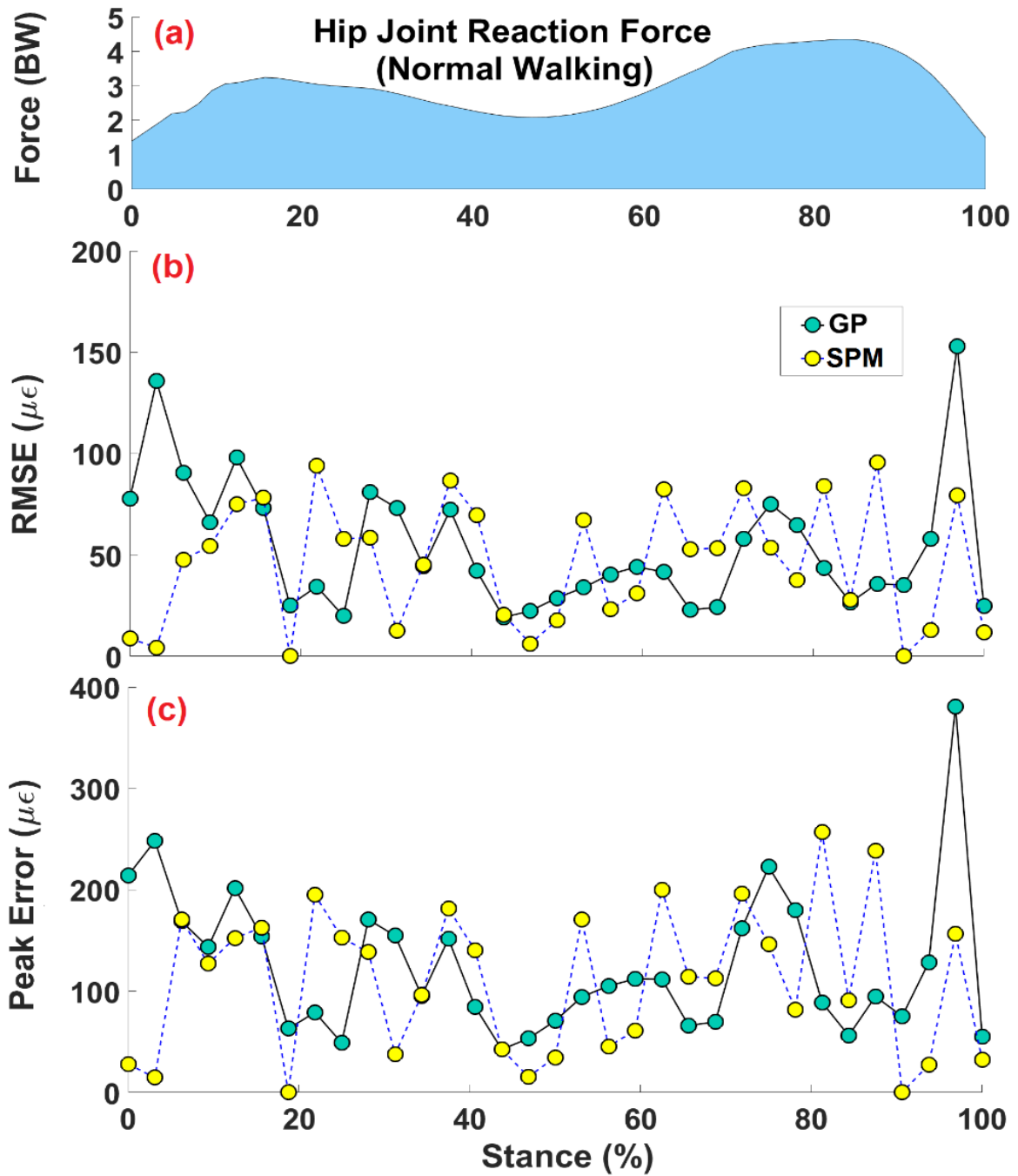
Figure 6.4: Comparison of the strain error in the SPM and GP methods for normal walking. Hip contact force during stance (a), frame-by-frame root mean square error (RMSE) (b), and peak error (c). Forces are expressed in body weight (BW) (Ziaeipoor et al., 2019).

The strain error distribution was located for the most part in the distal femur for both SPM and GP (Figure 6.5). The strain error measured for SPM was entirely associated with the hip contact force and zero error was observed for all muscle forces.
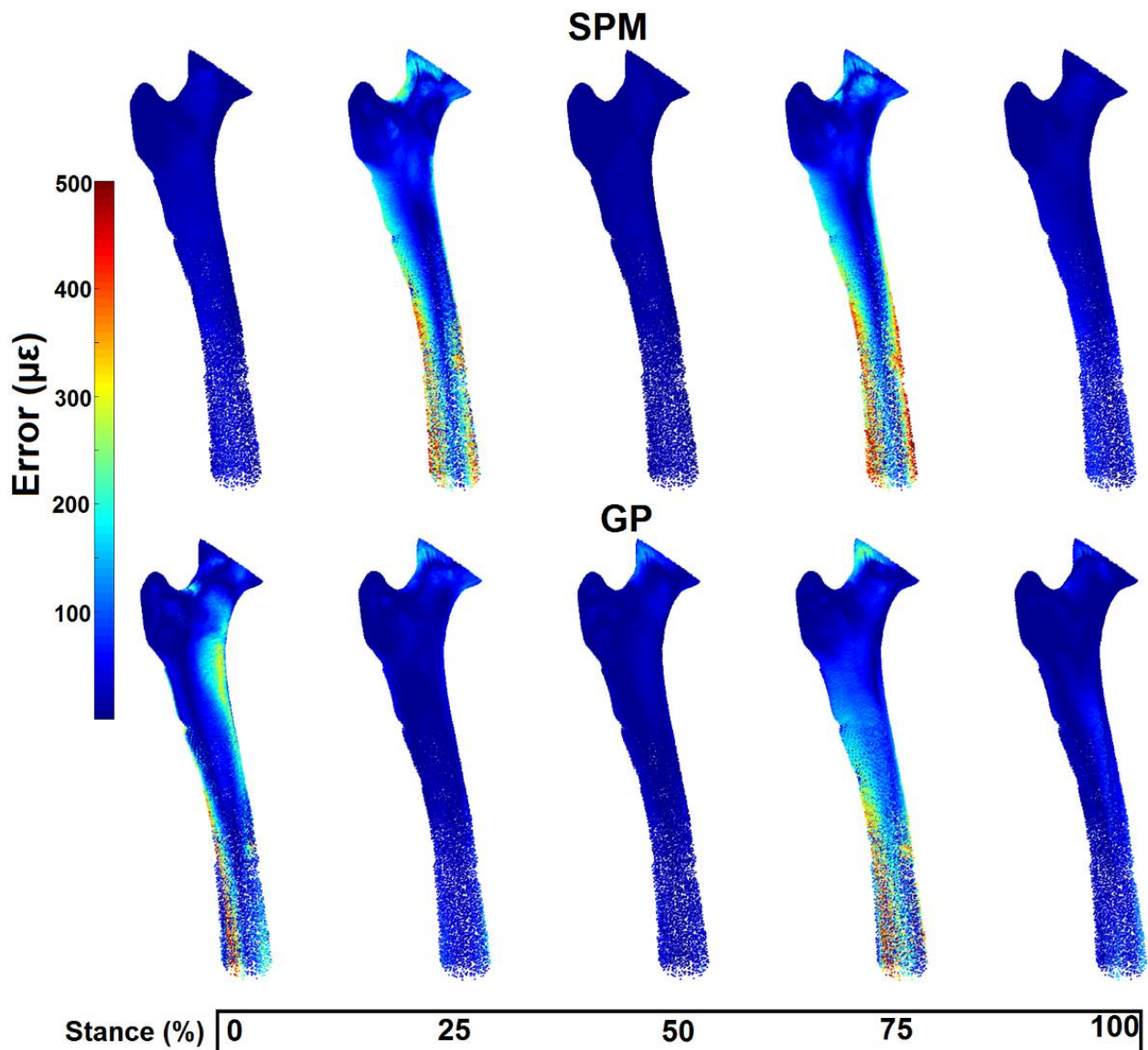
Figure 6.5: Error distribution in the SPM (top) and GP (bottom) methods for the stance phase of normal walking,(Ziaeipoor et al., 2019).

The SPM model provided the fastest construction time and the second fastest prediction time (Figure 6.6). Constructing the SPM model took 3.2 hours for solving 173 finite-element simulations. Constructing the surrogate methods took 3.66 hours for solving the 200 finite-element analyses in the training set and 0.15, 59.7 and 0.8 hours for training MLR, MARS, and GP, respectively. Predicting the femoral strain for an entire activity (50 frames) took approximately 36 s for SPM, and 6 s, 357 s and 1236 s for MLR, MARS, and GP, respectively.

When comparing the total time required by SPM, MLR, MARS, GP and a full finite-element analysis for predicting femoral strain for an increasing number of frames, SPM showed the fastest prediction time for all 1000 frames (3.4 hours) and outperformed a full finite-element analysis when 176 frames or more were analysed. MARS and GP always underperformed SPM due to a greater amount of time required for constructing the model and predicting strain whereas the number of frames above which the MLR model outperformed the SPM model was 3660 (Figure 6.6).
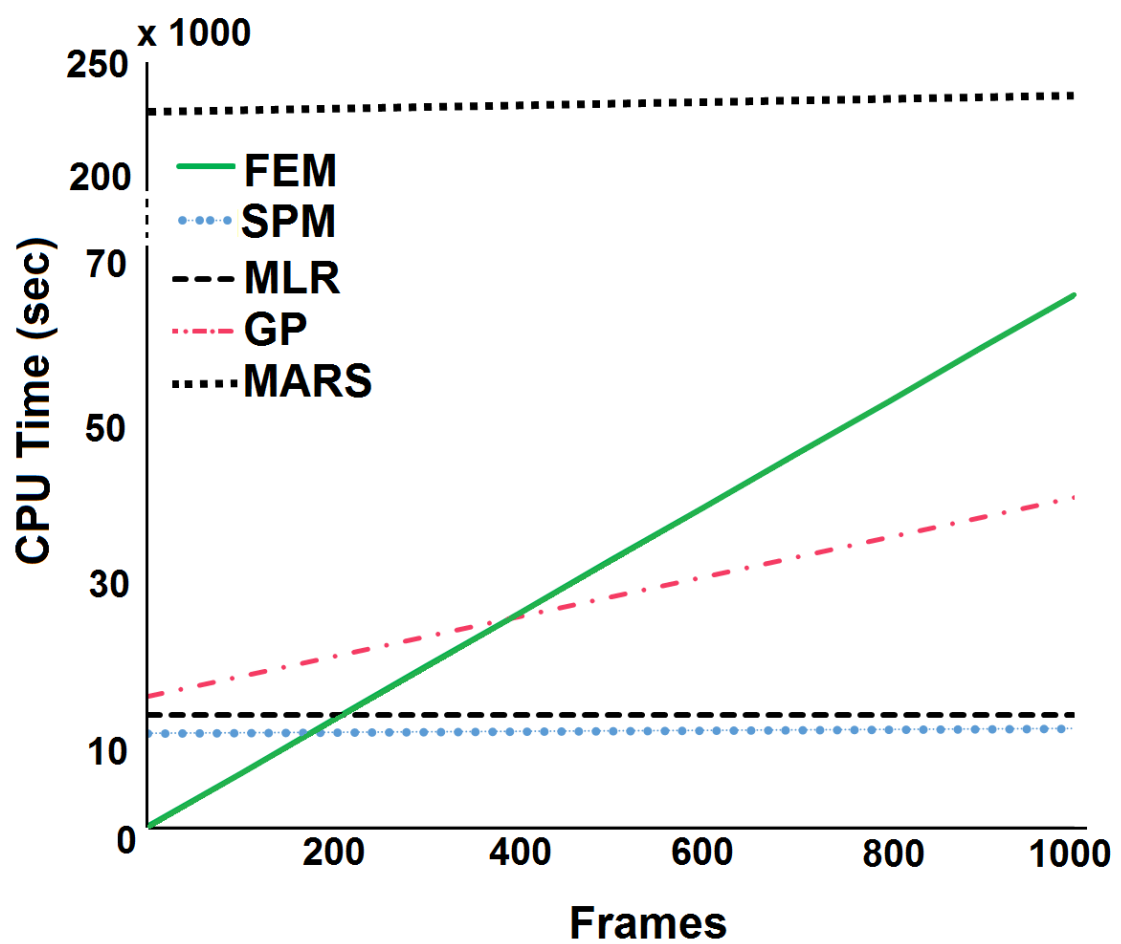
Figure 6.6: Total CPU time required by the full finite-element analysis and for model construction (i.e., solving 200 finite-element analysis and training) and predicting femoral strain using MLR, MARS and GP, (Ziaeipoor et al., 2019).

Discussion

We developed a superposition principle model (SPM) and compared its performance to that of multi-linear regression (MLR), multivariate adaptive regression splines (MARS) and Gaussian process (GP) for estimating the full-field strain in one human femur across a range of daily activities. The SPM model did not require training and showed the highest accuracy, the lowest total time for predicting femoral strain for all 1000 frames studied, the lowest model construction time, the lowest number of frames above which it outperformed corresponding full finite-element analyses, and the second-fastest prediction time relative to the MLR method. Thus, the SPM method offers a training-free approach while providing the highest accuracy and lowest prediction time for most foreseeable biomechanical applications.

The models studied for fast prediction of femoral strain produced an average strain error (RMSE = 40−100 με) over corresponding finite-element calculations that is comparable to the average strain error in current finite-element models (RMSE = 113 με; (Schileo et al., 2007)) hence supporting the use of SPM, MLR, MARS and GP models as valid alternatives to full finite-element analyses. Among the models analysed in the present study, SPM showed the lowest error (RMSE = 40 με), the fastest model generation time (3.2 hours), and the second-fastest prediction time per activity (36 s) after MLR (6 s), supporting the SPM method as a valid alternative for biomechanical applications requiring fast strain prediction time. The MLR method may outperform SPM when several thousands of loading cases are examined.

Differently from surrogate models, the SPM model can be developed independently from muscle and joint force analyses and later used to analyse any activity and without training, which incurs a high computational cost when developing a surrogate method. Therefore, SPM is a training-free method not bounded by the scope of the available motion data, often obtained by combining motion experiments and musculoskeletal modelling. Also, SPM provides the strain parameter of interest, i.e., the von Mises strain in the present study, through calculation of the full strain tensor, while surrogate methods are trained separately for each parameter in output. While this may explain the slower prediction time of SPM compared to MLR, the difference in the computational cost between these two methods decreases when multiple strain parameters are of interest.

Another difference between SPM and surrogate methods concerns the origin of the error. The SPM error reported here originated completely from the different algorithms used in the present study for defining the node of application of the hip contact force and that in the study of reference (Martelli et al., 2015b). Specifically, in the present study the node of application of the hip contact force was determined by matching the direction of the hip contact force vector calculated using OpenSim and the direction passing through the node and the hip centre whereas, in the study of reference, the node of application of the hip contact force was the node on the femoral head surface closest to the intersection between the hip contact force vector calculated using OpenSim and the femoral head surface. The different algorithms led to a mismatch between the point of application of the hip contact force in the two studies of up to the element edge length (2 mm in average) and zero-error when the hip force vector was applied to the same node in both studies. Thus, the accuracy of the SPM method can be improved using a smaller element size while the accuracy of

surrogate methods can only be moderately improved by increasing the training set size above 200 (Table 6-1).

Confidence in the validity and reliability of the present results may be gained through a comparison with previous studies. For example, the size of the training set in the present work is in agreement with earlier studies that used $100 - 200$ samples for training a MLR method (Fitzpatrick et al., 2014), $200 - 500$ samples for training an Artificial Neural Network (Taylor et al., 2017) and 300 samples for training a Kriging-based method (O'Rourke et al., 2016). Also, and in agreement with earlier studies (Wang et al., 2014), we found that DOE sampling systematically reduces both the mean and peak errors for all methods, particularly MARS (Table 6-1), as a broader distribution of samples is generated. These observations support the validity of the surrogate methods developed here. The principle of superposition has been long used in musculoskeletal modelling studies for determining the contribution of individual muscles to joint motion and loading, commonly referred to as muscle-induced acceleration analysis (Kersh et al., 2018; Pandy, 2001; Pandy and Zajac, 1991). The present study applies the same principle to the strain tensor in the human femur by combining the strain tensor generated by each separate force applied to the model rather than fitting the data by training a surrogate model. Therefore, SPM is better suited than surrogate models for studying the causal relationships between muscle force, joint contact force and femoral strain.

One limitation of the present study is that the time required for predicting strain for the 50 frames of an entire activity (i.e., 36 s for SPM and 6 s for MLR) was higher than the real-time duration of normal activities. Truly real-time analyses may be possible using alternative programming languages such as C++ or Fortran (Aruoba and Fernández, 2015) and/or by

determining the optimal mesh size and frame rate for the desired model accuracy and speed. A second limitation is that the SPM method was developed for an intact femur and may not outperform other surrogate models when highly non-linear problems such as joint replacement models and material non-linearity are of interest. Other surrogate methods might be better suited for addressing these types of problems. Finally, the SPM model was developed for one single femur, which may limit generality of the conclusions. However, the SPM method presented here can be generally applied to every linear-elastic and non-linear contact problem. Furthermore, the large range of loading conditions spanned by each model, separately generated for each element in the mesh, across a range of normal activities provides confidence on the SPM method's superiority over alternative surrogate methods.

Conclusion

In summary, the Superposition Principle Method (SPM) was developed for rapid prediction of femoral strain by leveraging the linear properties of common finite-element models of femoral strain and compared its performance to that of surrogate models, including MLR, MARS and GP. SPM required the lowest model generation time and provided the highest accuracy, the fastest total prediction time for all 1000 frames of motion studied, the second-fastest prediction time per activity, and did not require training. So, SPM offers the highest accuracy among common surrogate methods in predicting femoral strains over multiple activities and repetitions. However, MLR could provide a better outcome when several thousands of loading conditions are examined. Furthermore, the current chapter examined the applicability of the SPM method for one geometry, one set of material properties with no nonlinearity or history/time-dependent behaviour and well-defined loading locations. So, the SPM method needs to be developed further, so that it could be used for large-population-based studies by capturing variation between material properties and geometry of bones across a population, or, in clinical trials, where, for example, biofeedback is used in rehabilitation exercise.

Chapter 7 : EFFICIENT POPULATION-BASED STUDY OF FEMORAL STRAIN DURING PHYSICAL ACTIVITY

Introduction

The vast majority of traditional studies in orthopaedic biomechanics use a single (Noda et al., 2018; Taddei et al., 2006a; Taylor et al., 2012), or a few selected bones (Martelli et al., 2014a; Martelli et al., 2014b), and/or selected/often simplified loading conditions (Behrens et al., 2009; Bitsakos et al., 2005; Duda et al., 1998; Filardi, 2018) for the models related to femoral strain calculation (Martelli et al., 2014a; Martelli et al., 2014b), or implant design (Al-Dirini et al., 2019; Awadalla et al., 2018). The results then are extrapolated to a population as a whole. However, this approach sacrifices quantitative accuracy of bone analysis by disregarding the natural interpatient variability in shape and bone densitometry distribution (Bryan et al., 2010; Prendergast, 1997; Taylor et al., 2017). Furthermore, the muscle and joint reaction forces computed using musculoskeletal models vary between individuals (Martelli et al., 2015b). Consequently, there is an increasing need to move from individual-subject studies to multiple-subject studies (Bryan et al., 2012) in order to account for the variation in geometry, material properties and loading conditions within a cohort of patients. The computational cost required for solving single-subject studies of bone is generally low and does not raise specific issues for the majority of biomechanical studies (Taylor and Prendergast, 2015), however, building and solving a large scale-FE studies of femurs subjected to multiple time varying load cases takes considerable time and can be laborious. There are two major bottlenecks which prevent largescale implementation of patient-specific FE models becoming a commonplace approach in clinics. The first limitation is related to the ability to model a population by extracting the material properties and geometry of bone from the CT scans of each patient, a time-consuming and labour intensive task unless automatic segmentation techniques are available (Almeida et al., 2016; Ben Younes et al., 2014; Krčah et al., 2011). Statistical models can be developed as a source of data to produce synthetic populations. Although this could be a possible solution for reducing the cost of computation

required for large synthetic populations, FE models of each femur still need to be constructed and solved. Currently the solution phase of the problem is a major computational barrier, taking from minutes to days depending on the complexity, the scale and the number of frame of motions to be analysed using FE models. If the solution phase can be conducted within a reasonable time, like seconds or minutes, then the methodology can be used as a time-effective way to explore large-scale biomechanical analysis of bone, and also be valuable for real or near-time prediction of femoral strain in clinical environments.

Active shape and appearance models have been used as a technique to potentially reduce the dimensionality of a training database into linearly uncorrelated parameters, in order to describe the variation in the shape and modulus within a group of femurs. Once a statistical model is constructed, it can be used for producing a synthetic population which is needed for large FE models. This approach allows for the creation of femurs without taking the lengthy process required for generating bone models from CT data, leading to a considerable reduction in computational costs and the level of technical expertise. Principal component analysis (PCA) has been applied as a typical method to decompose the training population into its major components of variation in the shape and modulus. The PCA-based statistical model can create unique instances of synthetic femurs whose variation falls within the training population. The capability of PCA has been evaluated for various orthopaedic applications (Bryan et al., 2010; 2009, 2012; Nicolella and Bredbenner, 2012; Taghizadeh et al., 2017), such as studying the influence of femoral implant head size on the risk of fracture (Bryan et al., 2010), or for determination of the risk of femoral neck fracture within 1000 synthetic femurs as the representative of a population (Bryan et al., 2009). Although the statistical models can provide a source for constructing FE models of the femur, the problem with solution phase remains unsolved. This can be computationally expensive for

studies requiring 100s to 1000s of analyses where muscle and joint forces are assumed stochastic, rather than deterministic variables (Martelli et al., 2015a). Therefore, if bone models can be generated using automatic segmentation techniques, and the solution phase can be performed within a reasonable time period (in a few minutes rather than hours or days), and without sacrificing the accuracy of the model, then the strain calculations can be performed in clinics.

In the previous chapter, a novel computational approach called 'SPM' was discussed which has been developed based on the principle of superposition by leveraging the linearity of the FE models of bone (Schileo et al., 2007). SPM generally can be applied to any linear-elastic finite-element model and the models with low levels of non-linearity, not only to models of the human femur. The main conclusions drawn from this are that SPM is a training free method, it has a low error in comparison to alternative surrogate methods, and it is not bounded to the scope of the training data and would not be altered if more femurs were tested. Furthermore, both surrogate and SPM methods were created for each single element in the mesh spanning a broad range of physiological strain and loading conditions, hence providing confidence in the validity of the method for every foreseeable application of linear-elastic bone models (Schileo et al., 2007). In fact, the SPM model is comprised of a set of independent solutions, unrelated to activity and determined through finite-element analysis. For each frame and activity, solutions are then determined using linear combinations of base solutions, without any training or iterative learning approach for operators. However, this technique was constructed and tested based on a single bone, and hence, to perform the strain prediction for another femur, the model needs to be reconstructed. The current limitation with the SPM method needs to be eliminated so that it can be used for estimating femoral strain for arbitrary femurs.

The aim of current chapter is to integrate active shape and appearance models with the SPM method, so that it can be used for real or near-real time prediction of femoral strain. This can be achieved by taking three general steps: (1) establishing a correspondence between the members of training datasets using a registration procedure, (2) construction of a PCA based statistical model which can be fitted into the training dataset to explain the variation in the shape and modulus of a population by calculating the scores for principle modes of variation and standard deviations, and (3) finding the casual relationship between a set of applied force vectors and resultant strain distribution based on the principle of superposition across principle modes of variation, allowing to perform femoral strain for different random or real subjects during multiple physical activities. As previously stated in the current chapter, the principle of superposition will be applied for a population, hence the name of the technique, 'SPM', will be changed to 'SPM2'.

Materials and methods
Data acquisition

The active shape and appearance models of a femur were generated using a training set of 21 bones for healthy female subjects (65 ± 5 years; weight: 66 ± 12 kg, and height: 160 ± 7 cm) which were collected from a previous study (Martelli et al., 2015b). All patients were able to walk unassisted and did not have a history of musculoskeletal disease. Ethics approval was provided by the Human Research Ethics Committee at the University of Melbourne. The experiments and tools applied to collect CT scans of bones has been described earlier in Chapter 5. Furthermore, the muscle and joint reaction forces used to test the model was taken from Chapter 5 for a representative patient (68 years of age with a weight of 53kg) during the activities of normal walking, fast walking, ascending stairs, descending stairs and chair sitting.

PCA data registration

The main challenge to construct the PCA model is to reduce the dimensionality of the training data by establishing a point-to-point correspondence using a rigid and non-rigid registration procedure. This approach allows the morphing of a baseline mesh onto a target mesh by using the same number of nodes and elements. Before performing this registration scheme, a clean cut was made for each femur around the middle of femoral shaft using ScanIP (Simpleware, Exeter). A median length femur instance was then chosen as the reference femur, to minimise the distortion of elements while the surface of baseline mesh is being stretched or compressed to fit with the target surface. The baseline or reference femur was then meshed by changing the edge size of elements (1-1.5 mm) from the distal to proximal part, resulted in generating a fine mesh with 290,037 linear tetrahedral elements (C3D4: Four-node tetrahedral element) and 60,746 nodes.

Rigid registration was conducted by taking two steps to remove the variation in the size and location of the training data members caused during collecting the CT data. In the first step, the baseline mesh was scaled to the target mesh. The Iterative closest point (ICP) matching algorithms were then used (Besl and McKay, 1992) in MATLAB (The Mathworks, Natick, USA) to align the target meshes with the baseline mesh by performing a rigid transformation (three rotations and three translations), and the transformation matrices were stored.

A non-rigid registration algorithm which was developed earlier by Bryan et al., (2010), was re-coded in MATLAB (The Mathworks, Natick, USA) to establish a 3D point-to-point correspondence between members of the training dataset by taking a two-step procedure: (i) surface registration scheme, and (ii) volumetric meshing (Figure 7.1). The surface

registration was conducted to morph the surface of a baseline femur onto the surface mesh of a target femurs, while using the geometry of the target femurs as a boundary condition. To optimize the quality of the morphed surface and increasing the speed of the algorithm, a set of user-defined parameters, specifying the magnitude and speed of surface matching, were changed iteratively. More details about the surface registration can be found in the established procedure provided by Bryan et al., (2010).

In the next stage, the volumetric mesh-morphing of tetrahedral mesh was used by considering the registered target surface as a scaffold, permitting to define the coordinates of internal nodes of the mesh by computing the displacement vectors of all nodes (Bryan et al., 2010). This was achieved by implementing the diffusion-based mesh morphing scheme proposed earlier by Robertson and Sherwine (1999), which solves a set of Laplace equations using in input the baseline volume, the baseline surface and the target surface. Subsequently, the bones were re-scaled and transformed to the original position and the material properties of bones were re-assigned for each morphed mesh based through finding the closest point using linear-interpolation in MATLAB (The Mathworks, Natick, USA).
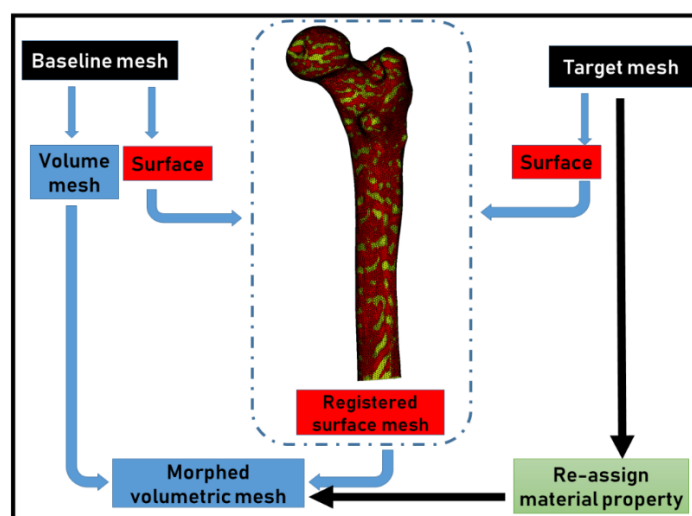
Figure 7.1: The procedure used for fitting non-rigid registration technique to morph a baseline mesh into a target mesh.

Mesh quality assessment

The success of the non-rigid registration technique was assessed by the evaluation of the quality of morphed mesh for each femur. The Normalised Shape Ratio (NSR) was computed for each registered femur as well as the initial baseline mesh as follows:

$$NSR = \frac{nr}{R}$$

Where, r is the radius of the element insphere, n is the number of dimensions being evaluated (e.g. 2 for surface elements, and 3 for solid elements), and R is the radius of the elements circumsphere (Field, 2000). This equation can yield a score ranging from 0 to 1 for each element, where the value of 1 shows perfect regularity. The NSR score was computed for each tetrahedron element by plotting a boxplot representing a different percentage of each element that was contained.

Construction of a statistical model using PCA

Principle component analysis (PCA) was used for building three types of statistical models, including active shape model (ASM), the active appearance model (AAM), and a combined active shape and appearance model. While the ASM and AAM models were developed based on either shape or modulus distribution of bones respectively, the so-called combined active shape and appearance (combined ASM and AAM) model was built by capturing the variation in the shape and modulus bones simultaneously.

To develop the statistical models, each femur was explained using a matrix containing the relevant information (e.g. shape, modulus, or both), followed by pooling data for all femurs to form a single training matrix. The PCA model was then fitted onto the matrix of training to determine the effect of each eigenmodes on the corresponding variation. For

example, to develop a combined active shape and appearance model, each femur was initially indexed using one column matrix (X_m), composed of both coordinates of nodes ($x, y, and\ z$) and the associated modulus of (E) at each element, and the corresponding nodes ($1, 2 \dots n$), which can be concisely presented in the form below:

$$X_m = [x_1, y_1, z_1, E_1, \dots, x_n, y_n, z_n, E_n]^T$$

Where, n is the number of nodes, each member of training dataset (ranging from one to N) was then combined in the following format to produce the training dataset required for building the PCA model:

$$A = [X_1, X_2, X_3 \dots, X_N]$$

The PCA was then applied onto the A matrix to describe the members of the training datasets as follows:

$$x = \bar{x} + \sum_{i=1}^{m} c_i X_i$$

Where x is a produced femur instance; $\bar{x}$ is the mean shape and modulus of the training dataset; X_i represents a basis vector containing orthonormal modes and c_i is a set of weighting coefficients describing the contribution of the first considered modes (m) to the shape and modulus of the bone (Bryan et al., 2010). Using this relationship, it is possible to create legal or permissible synthetic femurs by altering the component weighting coefficients. For instance, the mean femur can be produced using $c_i = 0$. Furthermore, the number of principle components to include, m, can be defined based on cumulative variance (cumulative energy curve) which determines the number of modes needed to represent a desired percent of variation in the training member (Campbell and Petrella, 2016).

Examination of PCA model

The quality of the statistical model in generating synthetic femurs was evaluated using compactness, generalisation ability and visual assessment. Compactness refers to the number of PCA modes needed to represent a certain percentage of variation within a population and can be evaluated by calculating the cumulative energy for ASM and AAM models (Bryan et al., 2010). The generalisation ability can be evaluated through quantification of the error occurred during reconstruction of unseen femurs (Bryan et al., 2010; Hawkins et al., 2003). To ensure that the combined ASM and AAM model has a consistent performance during a re-construction test, a Leave-one-out (LOO) approach was used (Bryan et al., 2010; Hawkins et al., 2003). In this case, the PCA model was built by leaving one subject out, and calculating the associated scores for the left subject using the known the built PCA model. The scores were then fitted onto the statistical model to perform prediction for the femur which was not used earlier for PCA construction, followed by determination of the difference between the reference bone and PCA-predicted values based on an element-by-element approach. The LOO approach was used iteratively until every femur was analysed and the error associated with the reconstruction of geometry and shape was determined. Finally, the combined ASM and AAM model was used to visually explore the variation in the shape and modulus of produced bones across the first three modes.

PCA results
Mesh quality

The quality assessment of the morphed mesh using normalised shape ratio (NSR) showed a mean score of 0.87 across all target femurs, as compared to the score computed for baseline mesh which did not go through the mesh-morphing procedure (Figure 7.2). The

maximum and minimum values calculated for the volume of the 5 to 95 percentiles of the

elements varied from 0.62 to 0.96, compared to the baseline mesh ranging from 0.7 to 0.96.
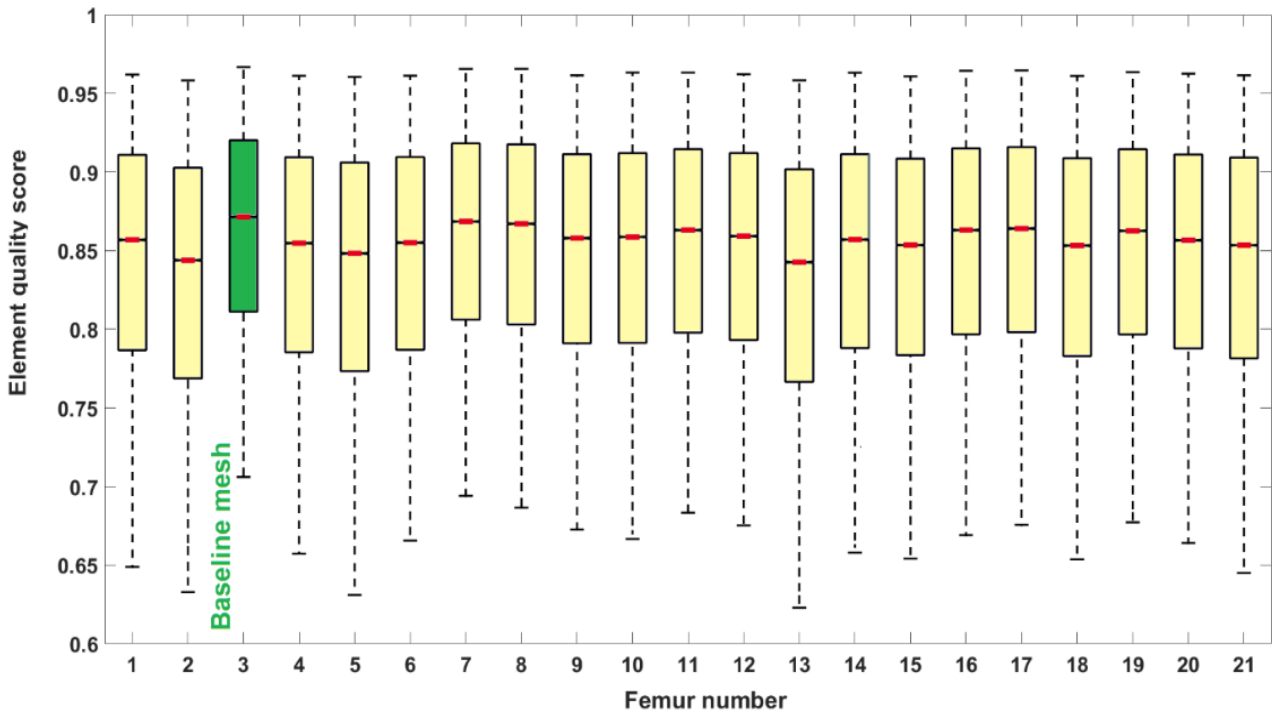
Figure 7.2: Mesh morphing quality assessment for all femurs. The black box represents the range of the error between the 25th and 75th percentiles while the red horizontal dashed line shows the median error. The lower and upper bounds show 5th and 95th percentile of volume of mesh. The yellow box represents the target morphed meshes, and the green box represents the baseline mesh used as template for mesh-morphing.

PCA performance analysis

The evaluation of principal components' cumulative energy for ASM showed a better

capability for capturing the corresponding variation in the training data when compared with

AAM and the combined ASM and AAM model which presented identical results with no

difference across different models. So, for the sake of simplicity, only the performance of

AAM was compared against the ASM model (Figure 7.3). The first mode of ASM was the

prevalent mode by accounting for over 82% of the shape variation, requiring at least three

and five PCA modes to preserve 92% and 95% of variation respectively. In contrast, the first

mode of AAM was able to describe only 27% of the modulus variation, maintaining 44% and

53% of modulus variation, respectively, for three and five PCA modes.
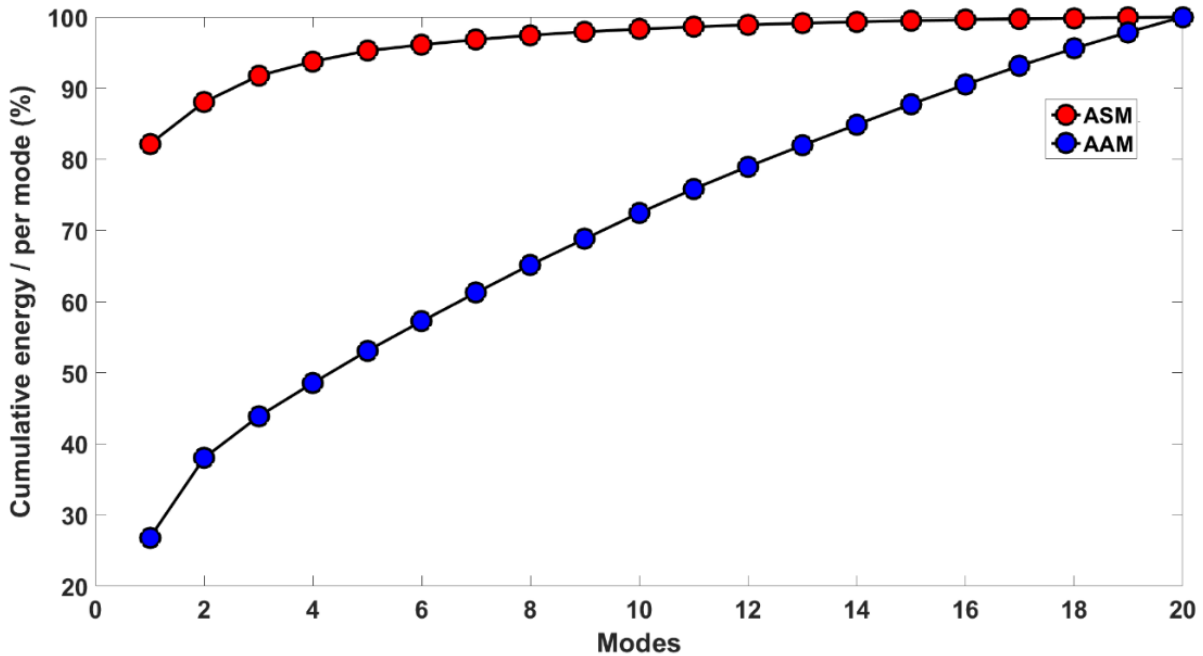
Figure 7.3: Plot of the cumulative energy/per mode, representing the capability of ASM and AAM models to capture the corresponding variation across different modes. The cumulative energy refers to the sum of the energy content across all of the investigated eigenvalues. As the cumulative energy for the AAM and the combined AAM and ASM models were identical, the plot was only provided for AAM model.

Re-construction error

The evaluation of the geometry and modulus reconstruction error was calculated for each

femur using the developed PCA model by considering the modes of variation (17 modes).

The reconstruction of geometry showed a peak error ranging from 2.9 – 11.5 mm and a

median error ranging from 1.1 – 4.6 mm (Figure 7.4 – a). The modulus reconstruction error

provided a peak error varying from 3,100 – 4,400 MPa and a median error within the range

of 720 – 1,210 MPa (Figure 7.4 – b).
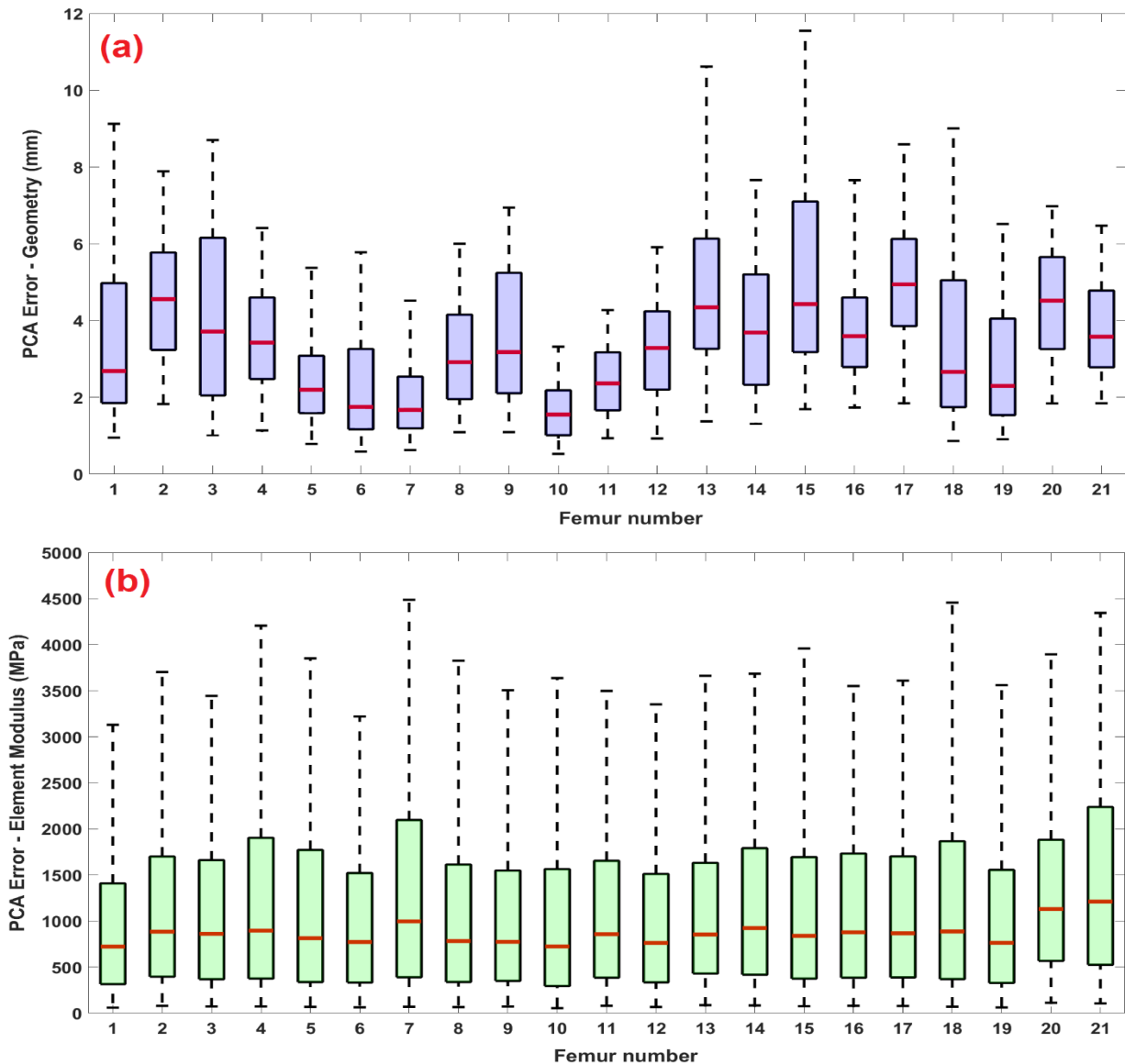
Figure 7.4: The PCA reconstruction error calculated for each femur on the basis of leave-one-out approach: (a) the geometry error measured by comparing the coordinates of element centroid between the original and reconstructed femur; and (b) the modulus error calculated for each element. The lower and upper bounds show 5th and 95th percentile of error; the red lines show the median error (50th percentile).

Visual interpretation of principle modes

The visual evaluation of a combined statistical shape and appearance model showed that the first mode appears to be a scaling mode with a noticeable increase in the anteversion angle, femoral head size, modulus, as well as a decrease in the femoral length (Figure 7.5). By the second mode, a little variation was noticed for femoral length and neck-shaft angle, however, a considerable change was noticed for bone modulus and anteversion angle.

Mode three experienced a little change in the anteversion angle, and a little increase in the bone modulus, while the length of the femoral shaft was almost constant across different standard deviations.
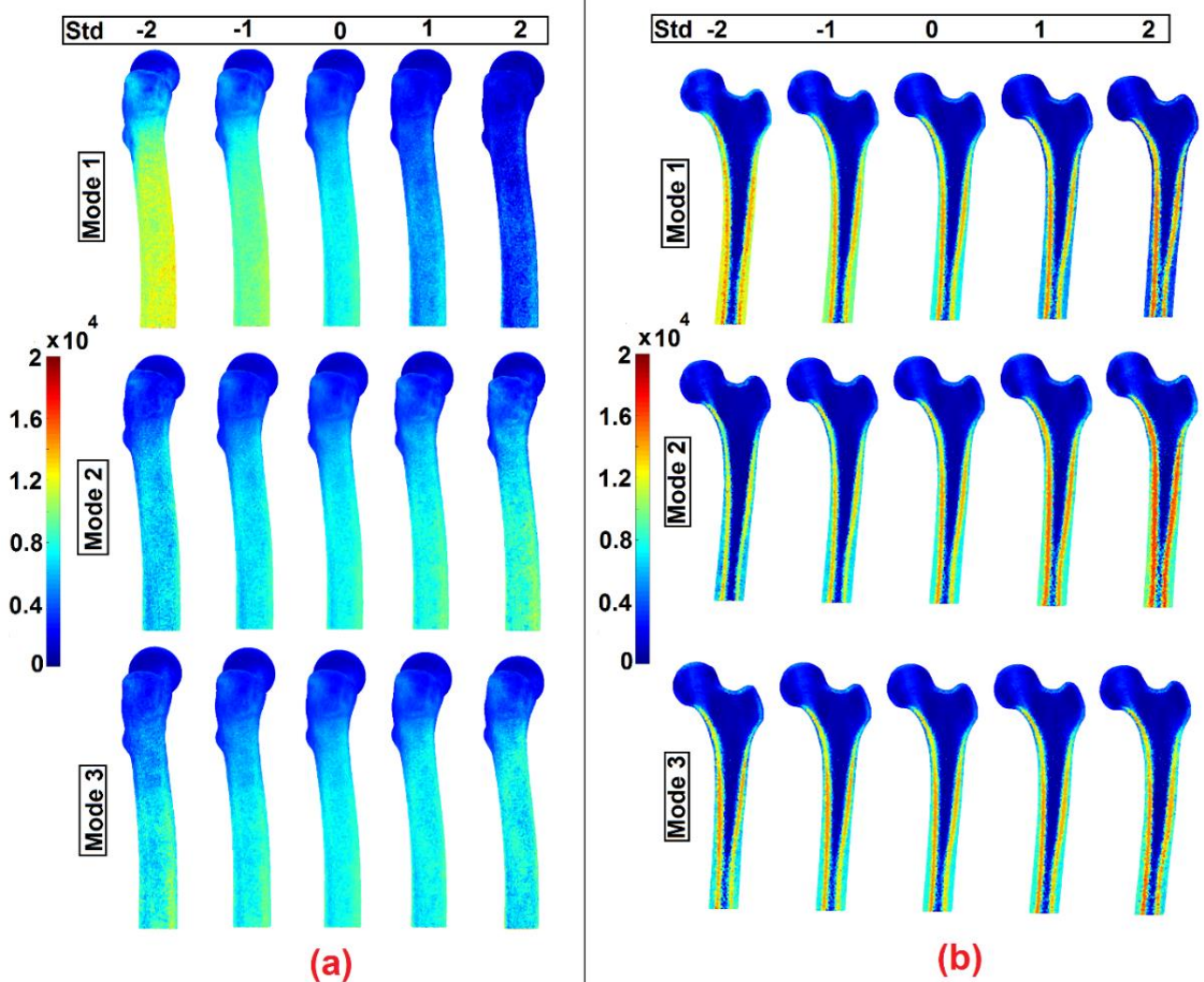
Figure 7.5: The changes in the shape and modulus of the bones generated by PCA (combined ASM and AAM models) for the first three modes and the standard deviations (±2).

Comparison of the current PCA model with previous studies

The compactness assessment showed that ASM was the most compact model when compared with the AAM, or combined ASM and AAM models. The first mode was found to be the dominant mode, which explained about 82% and 27% of variation respectively in the ASM and AAM models. This was comparable with previous findings, explaining the 35%

(Sarkalkan et al., 2014a) and 50% (Taghizadeh et al., 2017) of shape variation in the ASM model and about 35% of modulus variation in the AAM model. Furthermore, to explain 75% of the variation, the current combined ASM and AAM model needed at least 11 modes, or 55% of total PCA modes, compared with a previous study which needed at least 8 modes, or 17% of total PCA modes (Bryan et al., 2010). According to the leave-one-out test of the training dataset, the average distance error ranged from 1.3 – 4.9 mm, comparable with previous studies ranging from 0.88 mm (Vaananen et al., 2012) to 1.22 mm (Grassi et al., 2014). The peak error was shown to be 11.5 mm, which was higher than the previous findings, ranging from 5.6 mm (Vaananen et al., 2012) to 16 mm (Grassi et al., 2014). The modulus reconstruction error for each element showed a fairly high range of error with the mean ranging from 1,040–1,570 MPa and a peak error reaching to 4,400 MPa. This was more likely related to the relatively small size of the training dataset (20 femurs) used for the reconstruction of the modulus in the AAM model, compared with a PCA study built using 46 femurs, representing lower error with mean = 500 MPa and peak = 1,400 MPa (Bryan et al., 2010). When femur instances were visualised for the first three modes, a realistic bone material distribution was noticed (Bryan et al., 2010; Vaananen et al., 2012). The major source of error for ASM and AAM models were likely related to either the linear PCA procedure which is commonly used by the research community, or the limited number of training datasets which were used for building the PCA model. Hence, further research is needed to improve the accuracy of the current statistical models.

Prediction of femoral strain using SPM2

In the previous chapter, it was shown that Superposition Principle Method (SPM) can be used to accurately and efficiently predict femoral strain for a single subject while performing various physical activities. However, in order to transfer from a single-subject study to a

population-based one, the SPM and PCA methods need to be integrated. A flowchart explaining the construction and testing phase of the integrated PCA and SPM methods, referred to 'SPM2' is represented in Figure 7.6.
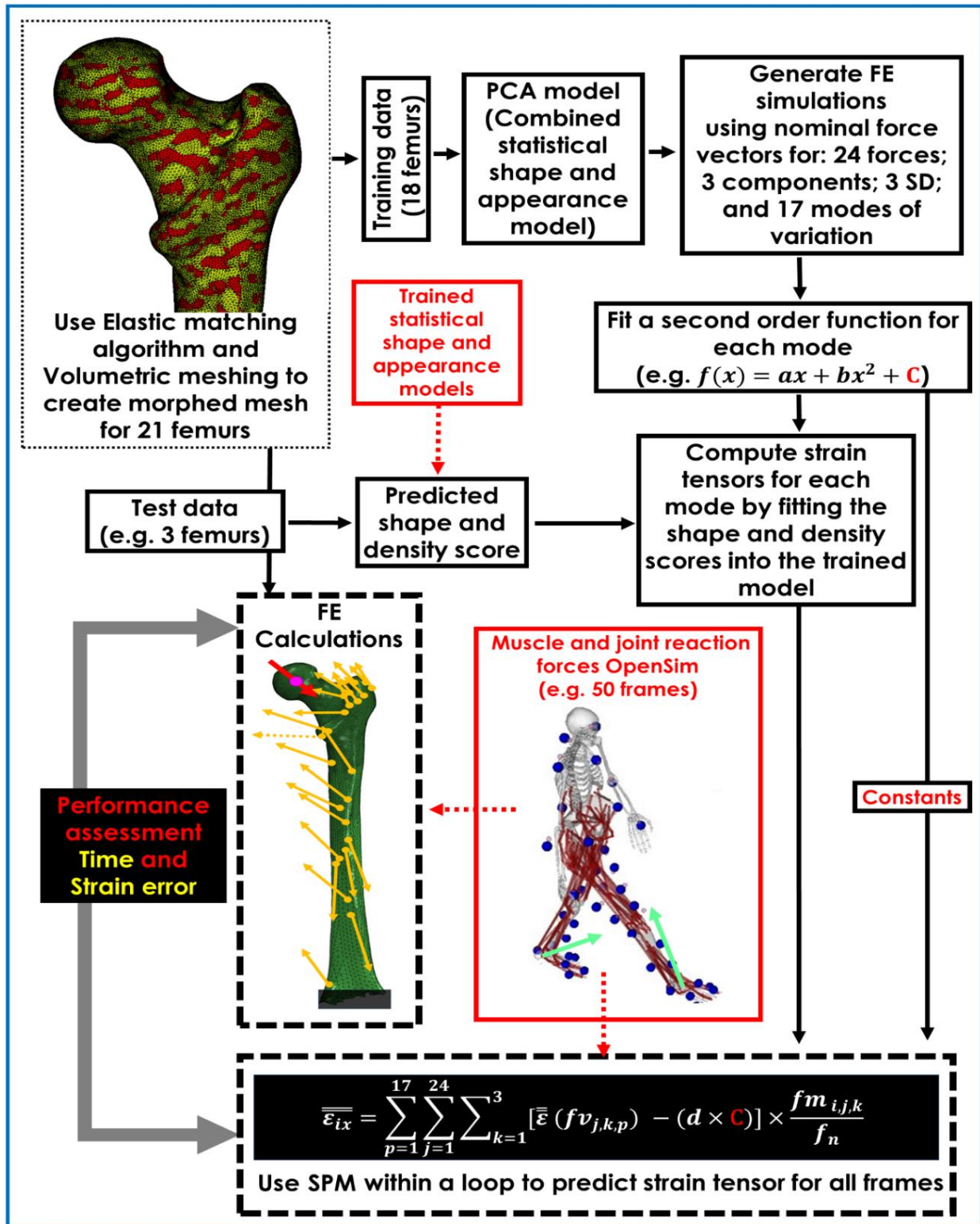
Figure 7.6: A flowchart presenting the general approach needed for computing femoral strain within a population using an integrated version of SPM and PCA, called 'SPM2'.

Construction of SMP2

The PCA model was generated using 18 of the 21 participants according to an established procedure (Bryan et al., 2010). Three randomly selected participants were excluded from the training set and used as independent target instances for testing the performance of PCA model. The output of the PCA model was a (17x18) matrix, where each femur was represented using a vector of scores containing 17 numbers. The PCA scores generated for each femur ranged from -3.3 to 2.4, explaining the modulus and the shape of femurs for that particular mode and standard deviation. To explain 95% of variation, mode weights were constrained to -2 to +2 standard deviations (SDs) and the rest of variation in the training dataset was excluded from further consideration. While all PCA scores were plausible for reproducing bone instances, in order to reduce computational costs, only the extreme and mean standard deviation (SDs = 0 and ±2) were used, which resulted in building a look-up table composed of a set of bone instances (17 x 3). For each synthetic bone instance, a set of individual FE simulations were created by applying a nominal force vector, each arbitrarily set to 100 N, applied along each of the three coordinate axes for each of the muscle attachment sites (23) and the hip centre of the femoral head, resulting in 72 finite element simulations per femur. The bone instance for the mean standard deviation was the same for all modes. Hence, to reduce the number of simulations, the FE simulation for mean case was only generated once.

The location of muscle attachment sites and centre of pressure was obtained from previous work (Martelli et al., 2015b) for the baseline femur, and the identified loading points were used for all femurs. For each simulation, the equivalent von Mises strain was calculated at the element centroid using the linear-elastic solver implemented in Abaqus (Dassault Systems, USA). The FE model of bone was locally isotropic, unstructured mesh consisting of 290,037 linear tetrahedral elements (C3D4: Four-node tetrahedral element) and 60,746

nodes that were fully constrained at distal region (Figure 7.6). As a result of generating and solving the total of 2,520 FE simulations, a full dataset comprised of the force components and their corresponding tensor of strains with six components (i.e. exx, eyy, ezz, exy, exz and eyz) were obtained, which allowed for calculation of principle or equivalent strain distribution. Furthermore, there was an upfront computational cost for building SPM2, requiring approximately 38 hours to create and solve all the FE simulations using a standard desktop computer (Intel Core i7 processor, 8 CPUs, 32 GB RAM).

As a function of the change in mode weight, there was a weak, non-linear behaviour of the predicted strain at the element level. To capture such a non-linearity within each mode, a second-order function was fitted onto the strain components of each element across three standard deviations, and the resultant coefficients and constants were saved (Figure 7.6). This training process led to the determination of the causal relationship between the normal applied force (100 N) and the resultant strain tensors within each PCs. However, like the training phase, only three standard deviations were used, and an error occurred for each element (Figure 7.7).
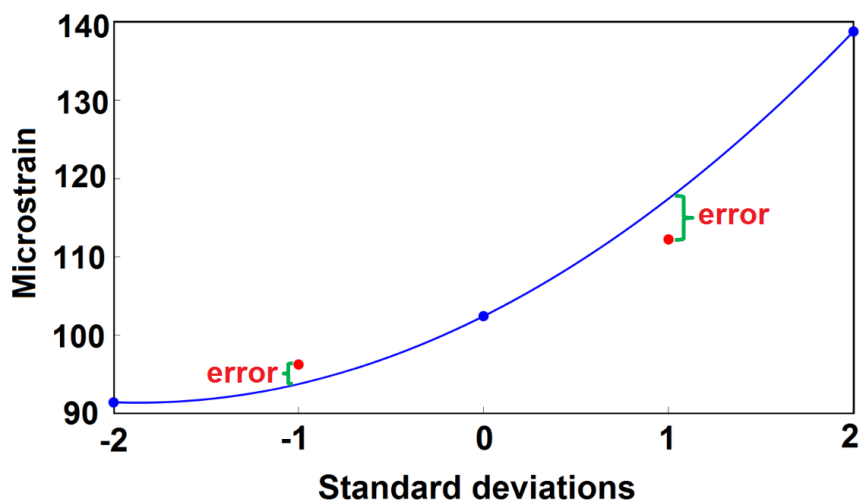
Figure 7.7: The interpolation error occurred during fitting a second-order function for each element across each mode. The blue dots represent those three standard deviations (0 and ± 2) which was used for building the model while the red dots refer to those which were excluded from consideration. The region shown in green represents the error occurred during interpolation for the representative element.

Strain prediction using SPM2

The total strain tensor ($\bar{\bar{\varepsilon}}_i$) for a given bone instance (x) and an arbitrary frame of motion (i) was computed as the sum of strain fields in the look-up table weighted by the ratio between the force intensity derived from OpenSim and the nominal force intensity as follows:

$$\overline{\overline{\varepsilon_{ix}}} = \sum_{p=1}^{17} \sum_{j=1}^{24} \sum_{k=1}^{3} [\bar{\bar{\varepsilon}}\,(fv_{j,k,p}) - (d \times c)] \times \frac{fm_{i,j,k}}{f_n}$$

Where $fm_{i,k,p}$ is the magnitude of force computed by OpenSim for a given muscle or joint reaction force j, along the coordinate axis k, and mode of variation p; $\bar{\bar{\varepsilon}}(fv_{j,k,p})$ is the strain tensor computed by the nominal force vector of f_n with an arbitrary magnitude set to $100\ N$, and c refers to the constants computed for each element through the fitted second-order function, and $d = t - 1$, where t is the total number of modes in the PCA model.

To predict the total femoral strain for a given frame of motion, a vector of scores representing the shape and modulus of a testing femur was fitted onto the constructed PCA model to produce a new bone instance. Subsequently, the basis strain tensors for each force component was then estimated by fitting the known scores onto the trained second-order functions of each PCs. Finally, by iterative use of SPM2 formula, the strain field for component of the look-up table was computed through scaling the strain fields with regard to the applied force obtained from OpenSim and adding up the scaled strain tensors (Figure 7.6).

Performance analysis of SPM2

The accuracy of the SPM2 method was investigated by comparing the predicted strain fields with the corresponding FE results. To achieve this, two sources of errors were evaluated: interpolation error and reconstruction error. The interpolation error referring to the error

which occurred during the fitting of the second-order function was evaluated by calculating the strain error for a synthetic population consisting of 50 femurs randomly produced using the PCA scores. The interpolation error was further investigated by representing the PCA scores across different modes of variation in the shape and modulus of the statistical model. The reconstruction error in the case of the PCA model was evaluated by measuring the strain error for the reproduced femurs. This was achieved by extracting the scores for three unseen femurs using the available PCA model and reconstructing the bone instances using the obtained PCA scores. The FE simulations were then generated and solved for each of the reconstructed and original femurs and the equivalent strain fields were compared.

To ensure that the SPM2 method had a consistent response across different loading conditions, two different sets of loads were taken from a single subject from chapter 6, including: (i) the full stance phase of normal walking as a representative activity, and (ii) 50 random frames of normal walking, fast walking, stair climbing, stair ascent, stair descent, and chair sitting which were taken from the previous chapter. The accuracy of predictions were evaluated by fitting a linear regression line between the predicted strain fields and the FE results. The predictions were evaluated by taking two approaches: (i) frame-by-frame assessment of normal walking as the representative activity, and (ii) by pooling the entire frames of motion. The predictions were assessed either for each femur individually or by pooling the results for three femurs altogether. The Root Mean Square Error (RMSE) and 95th percentile of the strain error was used as indicators of mean and peak error. The coefficient of determination (R^2) and slope were used as indicators of the quality of fitted regression line. The efficiency of SPM2 method was compared with the results of FEM by recording the computational time needed for the prediction of femoral strain for a full activity cycle using a standard desktop computer (Intel Core i7 processor, 8 CPUs, 32 GB RAM).

SPM2 results
The performance of SPM2 for a synthetic population

The SPM2 method was able to calculate the full femoral strain for 40 frames of motion in 3 minutes (on average) compared with 44 minutes for FEM. In terms of accuracy, when the error associated with interpolation was evaluated for the synthetic population and 40 pooled frames of motion (normal walking), a consistent trend was noticed with the mean error of 89 µε. The median error (50th percentile) ranged from 19 µε to 78 µε across the whole synthetic population (Figure 7.8). However, a lower consistency was observed when the peak error (95th percentile) was reported, reaching to 725 µε as the worst scenario, followed by the second peak with 624 µε, and reached 124 µε as the best femoral strain prediction.
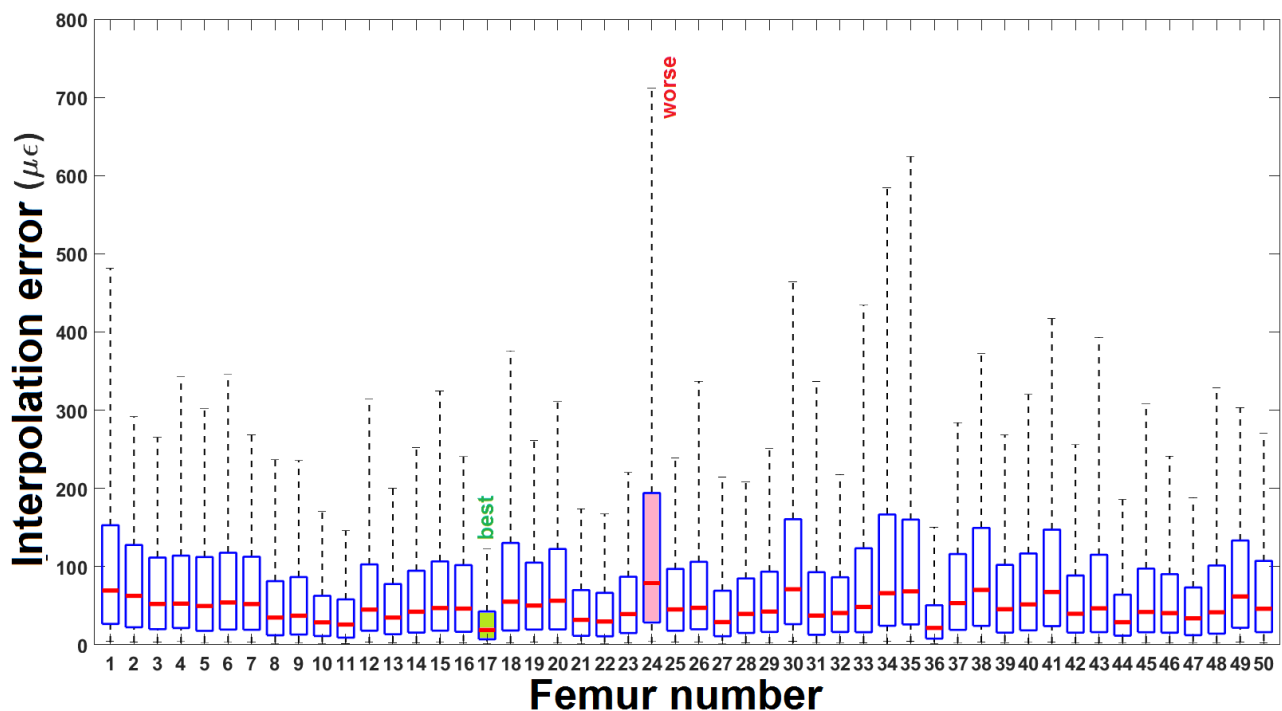
Figure 7.8: Boxplots illustrating the interpolation error in SPM2 method for a population composed of 50 synthetic femurs. Each boxplot shows the strain error for 40 pooled frames of normal walking. The lower and upper bounds show 5th and 95th percentile of error, while the red horizontal line represents the median error (50th percentile).

The visual investigation of the femurs shows no specific pattern or location of curve fitting error for both the worst and best scenarios (Figure 7.9). Furthermore, it was noticed that the error tended to occur at higher loads, by presenting a lower error at the early and later stance phase, and a higher error at mid-stance phase (e.g. 25 and 75% of stance). However, the peak strain error calculated for the worst scenario was less than 5% of the peak equivalent strain across different frame of motions (Figure 7.10).
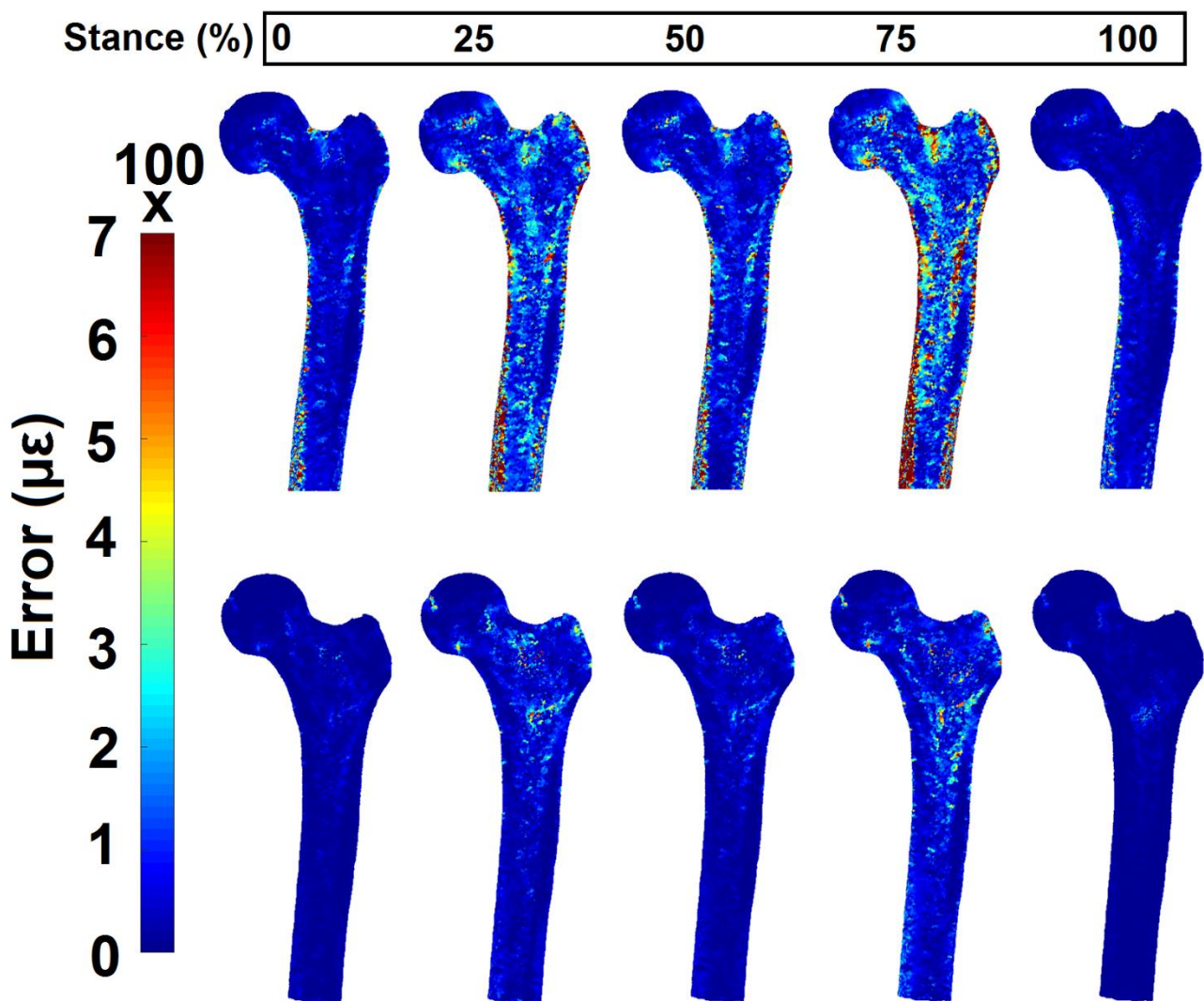
Figure 7.9: The distribution of interpolation error in SPM2 method for the worst (top) and the best (bottom) case during the stance phase of normal walking. Results are presented at 25% intervals of the stance phase.
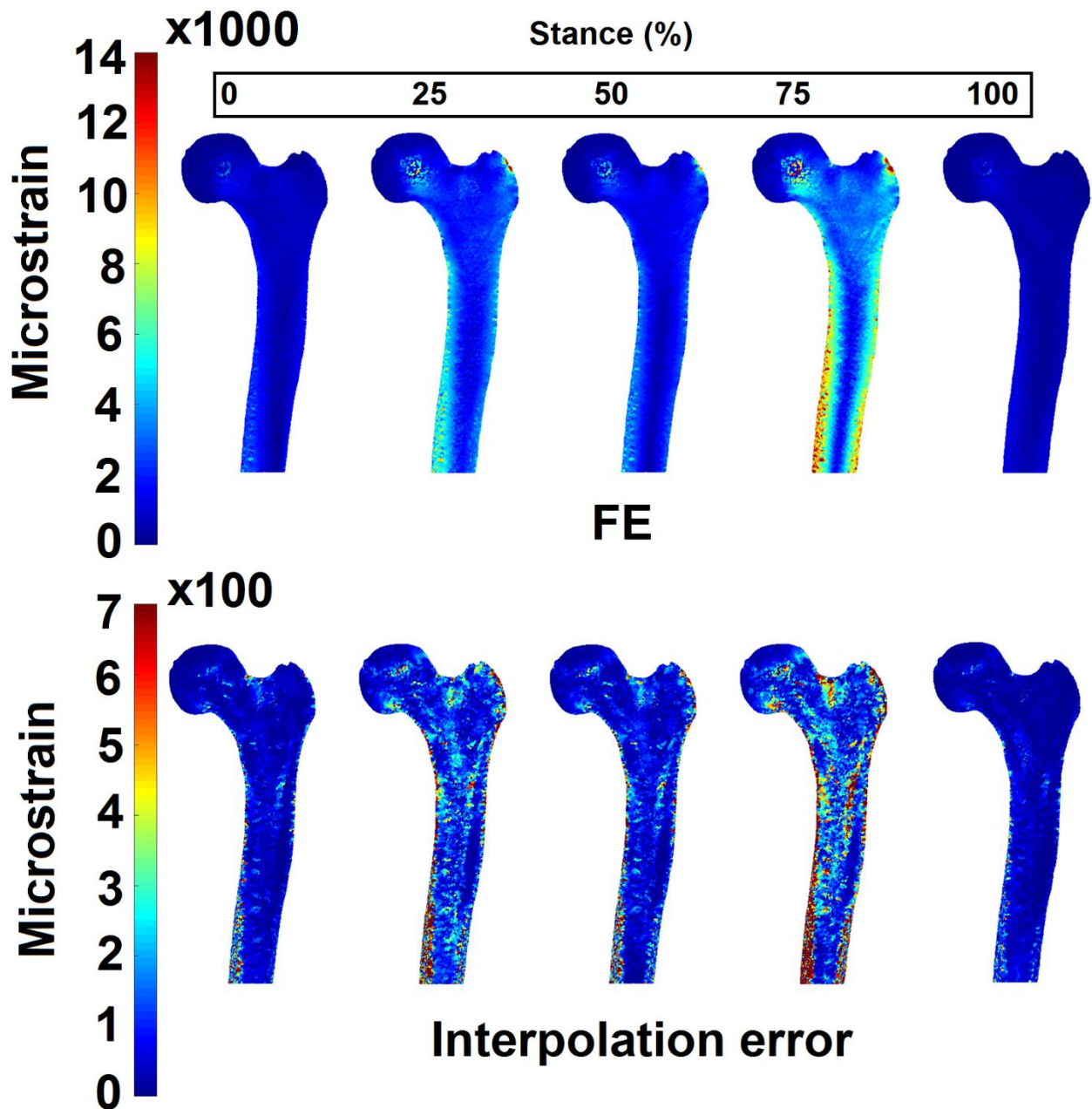
Figure 7.10: Contour plots representing the distribution of femoral strain in FEM (top) and the strain error in SPM2 method (bottom) occurred due to the interpolation. The results are provided for the synthetic bone with the worst prediction.

Fitting a linear regression between the strain predictions of SPM2 and FE results showed a good correlation for a given activity. Comparing the predictions for the best case against worst case showed a variation from 81 με to 399 με for RMSE, a variation from 0.95 to 1.00 for coefficient of determination (R^2), and a variation from 0.93–1.00 for the slope of the regression line (Figure 7.11).
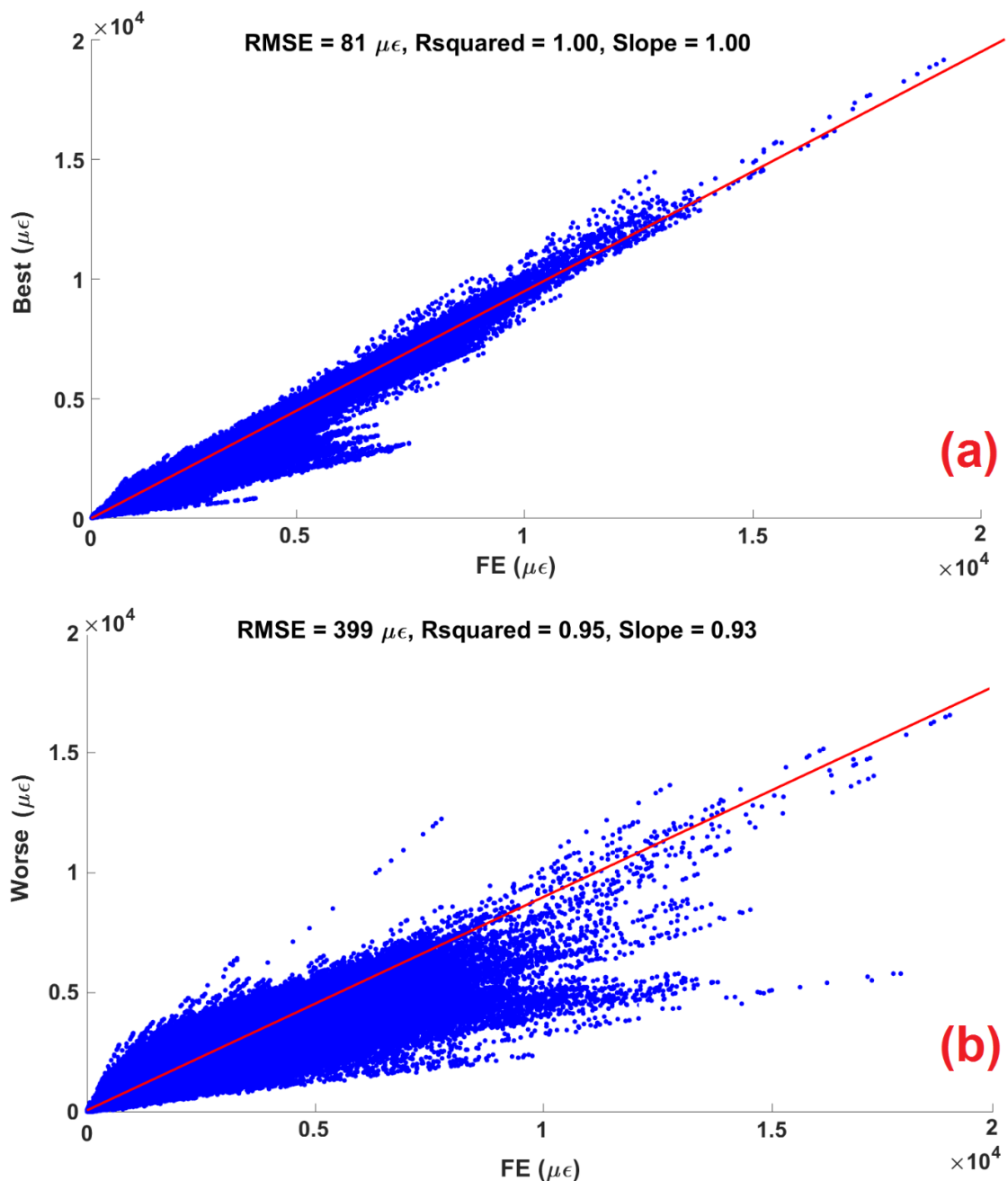
Figure 7.11: Comparing the performance of the SPM method against FEM for femoral strain calculation for a pooled 40 frames of motion (normal walking). The best and the worst predictions across the synthetic population are reported. The best prediction refers to the femur instance with the lowest error, while the worst prediction refers to the femur instance with the highest error.

The frame-by-frame assessment of the SPM2 method of an exemplar activity (normal walking) showed that the error was a function of the hip joint contact force (Figure 7.12). For example, for the worst case prediction, the highest peak error reached to 1,293 με at mid-

stance phase, and reduced to 152 με at late stance. Moreover, RMSE error for the worst scenario varied from 90 to 675 με, compared with a more consistent variation obtained for the mean and best predictions with the range of 35 – 274 με, and 19 – 124 με respectively.
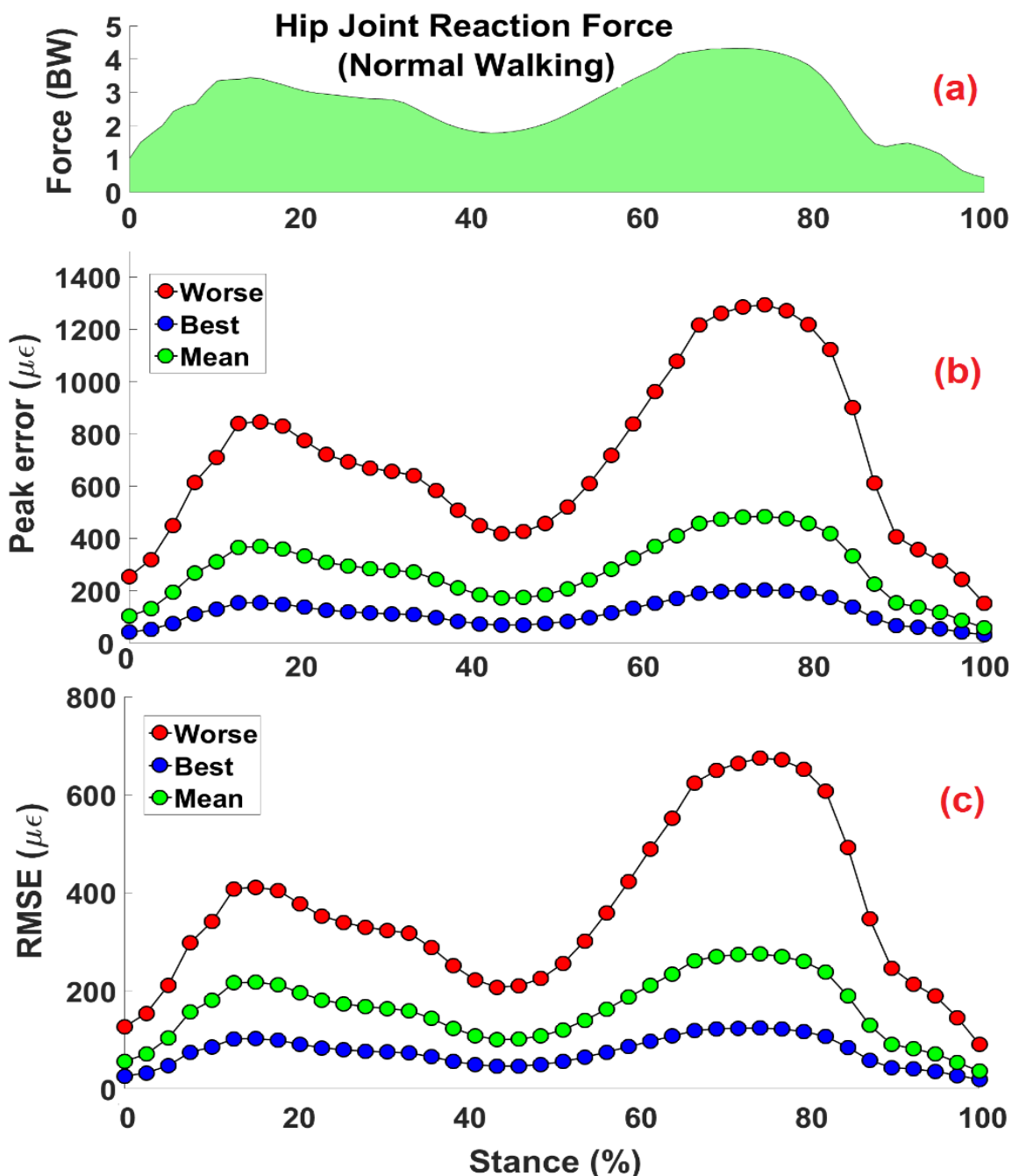
Figure 7.12: Frame-by-frame analysis of SPM2 across different frames of stance phase (normal walking (a)) for the worst, best and mean cases by calculating peak (b) and RMSE (c) errors. The worst and best predictions are provided for the cases with the highest and lowest error, respectively, and the mean error refers to the average error which was measured by accounting the whole population.

When the computed microstrain error was normalized for different frames of motion, a high consistency was observed for the whole population with a mean RMSE and peak error was always lower than 1.6% and 2.9%, respectively (Figure 7.13 and Table 7-1). For the worst predictions, the RMSE and peak error were consistently lower than 2.2% and 4.9%, comparing with the corresponding results for the best-case predictions, yielding 0.9% and 1.4% respectively. More details about this frame-by-frame assessment is provided in Table 7-1.
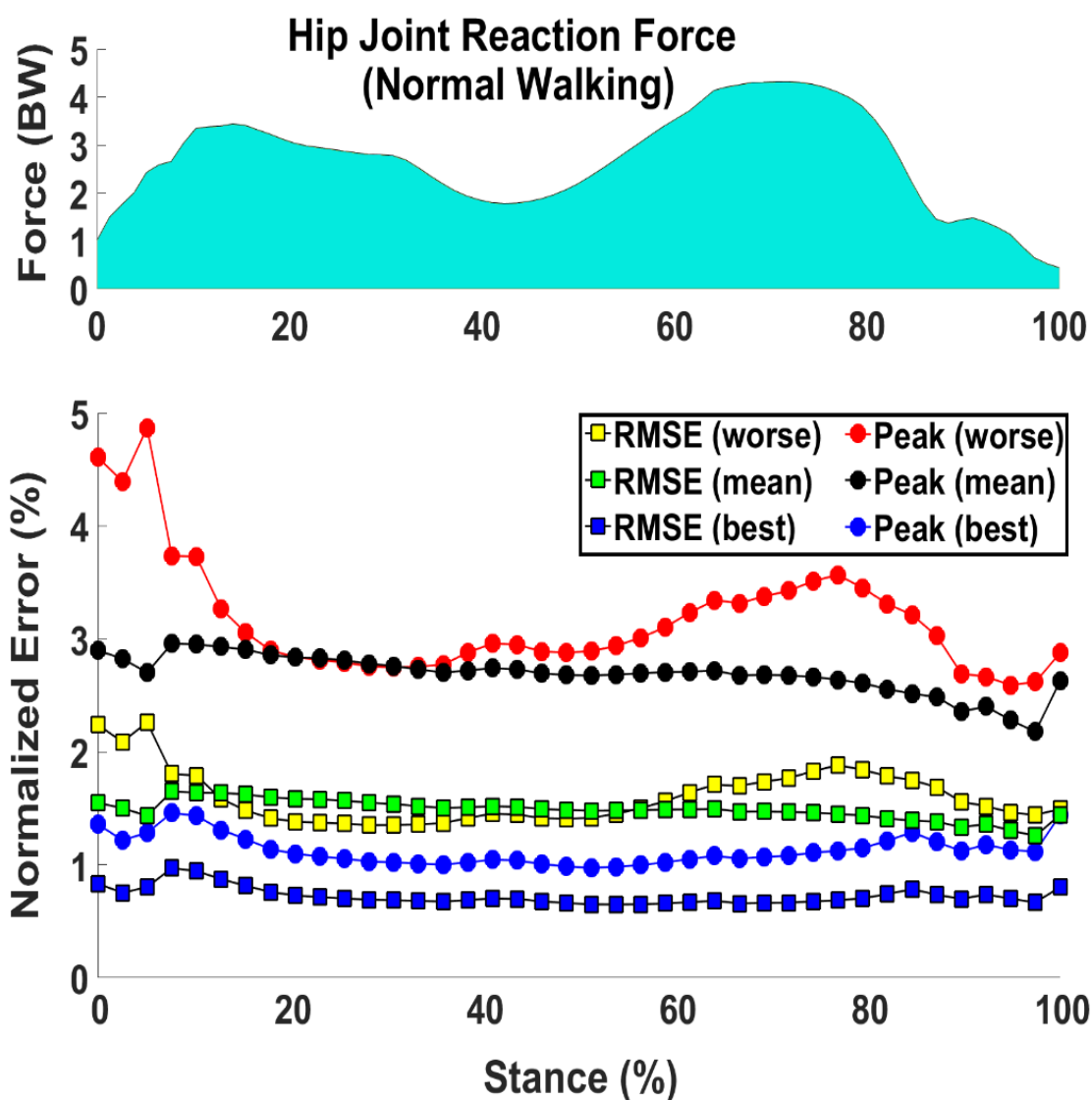
Figure 7.13: The normalised error reported for SPM2 across different frames of motion in normal walking (a). The peak and RMSE errors are provided for best, mean and the worst scenarios (b).

Table 7-1: Performance assessment of SPM2 for computing femoral strain during locomotion. The reported errors are based on the full stance phase.

Case	Mean RMSE (με)	Mean Normalised RMSE (%)	Peak Error (με)	Peak Normalised Error (%)	Mean R^2	Mean Slope
Best	74	0.7	202	1.4	0.99	0.99
Mean	162	1.4	484	2.9	0.97	0.99
The worst	361	1.6	1, 293	4.9	0.93	0.92

The interpolation error was further investigated by calculating the PCA score of synthetic femurs for the worst and best scenarios across the entire principle modes of variation (Figure 7.14). It was observed that the PCA scores of the best prediction were closer to the mean (SDs = 0) when compared with the worst case, particularly during the first three modes, which explain about 44% of variation in the shape and modulus of the population. For example, as a predominant mode, the PCA score of the first mode was 0.14 for the best scenario, compared with the corresponding PCA score of 1.77 obtained for the worst case (Table 2).
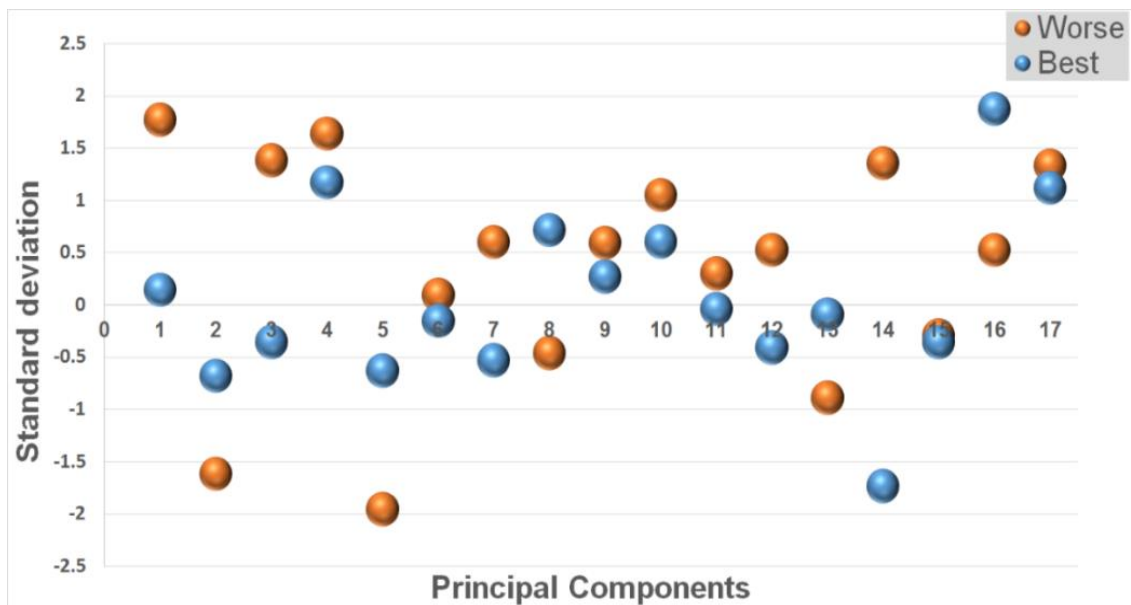
Figure 7.14: PCA scores generated randomly for creating synthetic femurs. The worst and best refers to the femurs with the highest and lowest error obtained from SPM2 calculations.

Accuracy of SPM2 for unseen femurs
Frame-by-frame assessment

When the femoral strain prediction was compared between SPM2 and FEM methods by

accounting for both reconstruction and interpolation error, a close agreement was observed

for the strain distribution for all three unseen femurs across the entire activity (Figure 7.15).

However, a noticeable difference was observed in terms of the magnitude of the femoral

strain, particularly during the later stages of stance phase (Figure 7.15). For example, when

the strain predictions were visualised for Femur 3, a noticeable strain difference was noticed

between FEM and SPM2 results, particularly at distal femur.

(a) : Femur 1
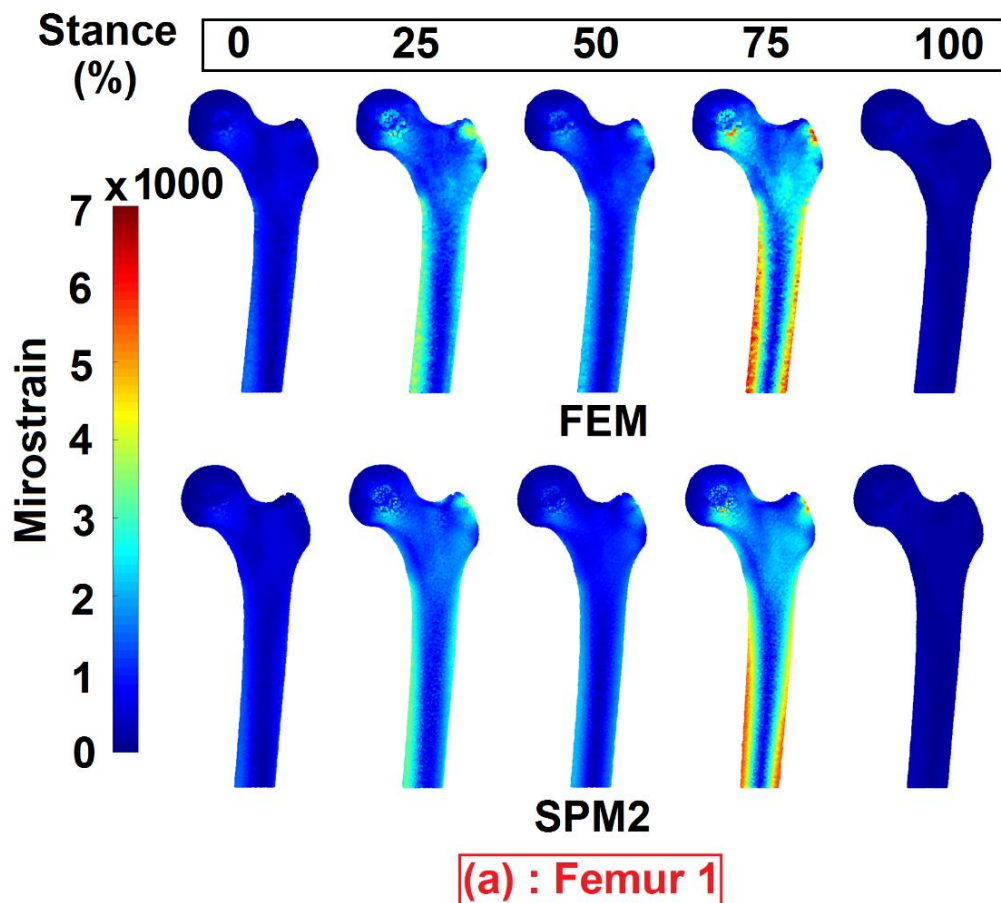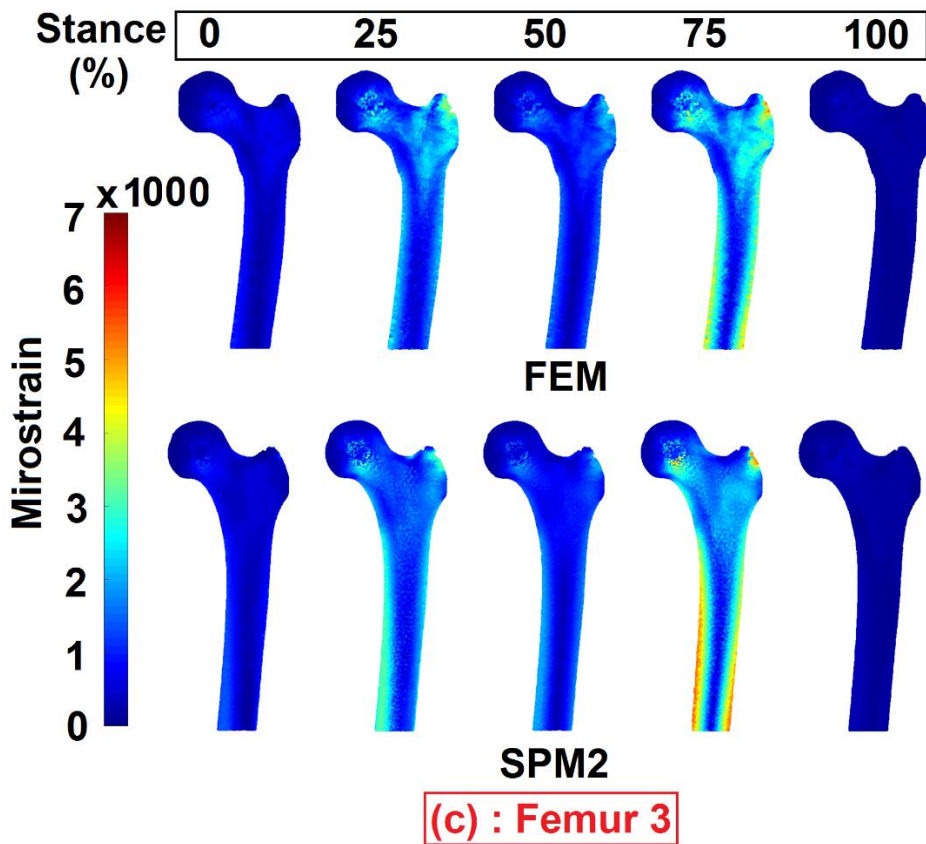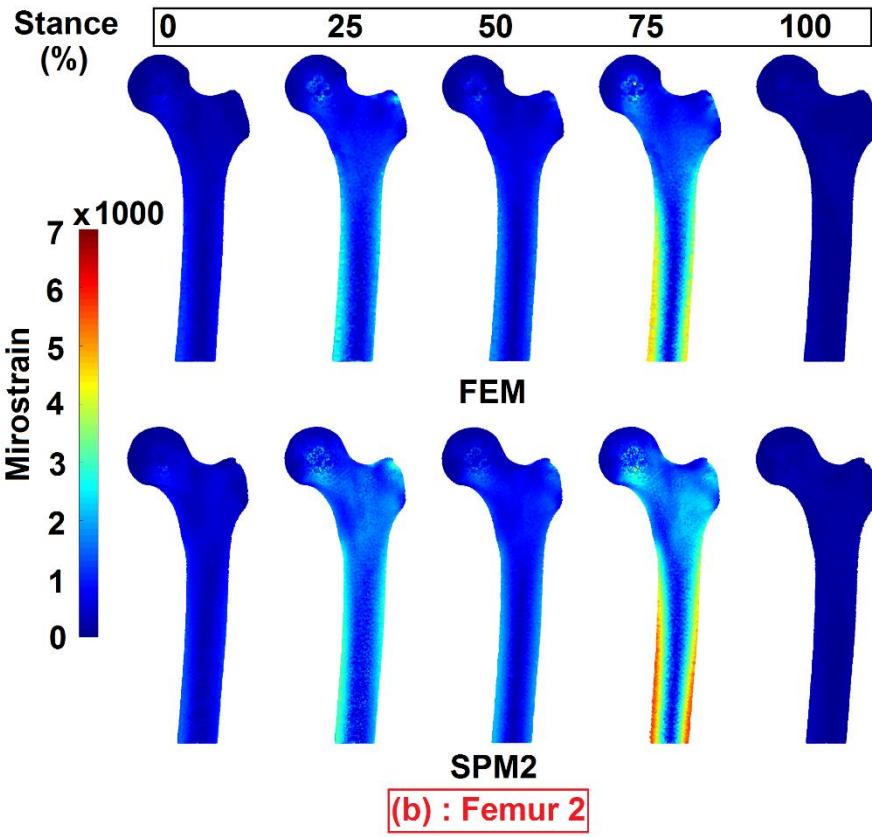
Figure 7.15: Comparing the SPM2 predictions against FE results of three randomly selected participants which were not included in the training datasets used for building PCA model (i.e., the CT-based model instances henceforth).

Quantification of SPM2 error for unseen femurs presented a higher strain error for higher loads across different frames of the representative activity (Figure 7.16). For example, for Femur 3, the worst case, the RMSE and peak errors ranged from 215 and 501 during early stage of stance phase to 904 and 1,776 at mid stance phase, and decreased to 93 and 129 at late stance phase, respectively. Furthermore, when the SPM2 predictions were investigated for Femur 1, the best case, an improvement in the accuracy of predictions was noticed with an RMSE ranging from 64 to 530 and peak error ranging from 128 to 1,133. In addition, while the mean coefficient of determination was 0.83 for the worst case, a better correlation was noted for the best scenario with the average R^2 of 0.94 (Table 7-2). The slope of the fitted regression line between the prediction of SPM2 and FE results was always greater than 0.91 for all investigated cases (Table 7-2).
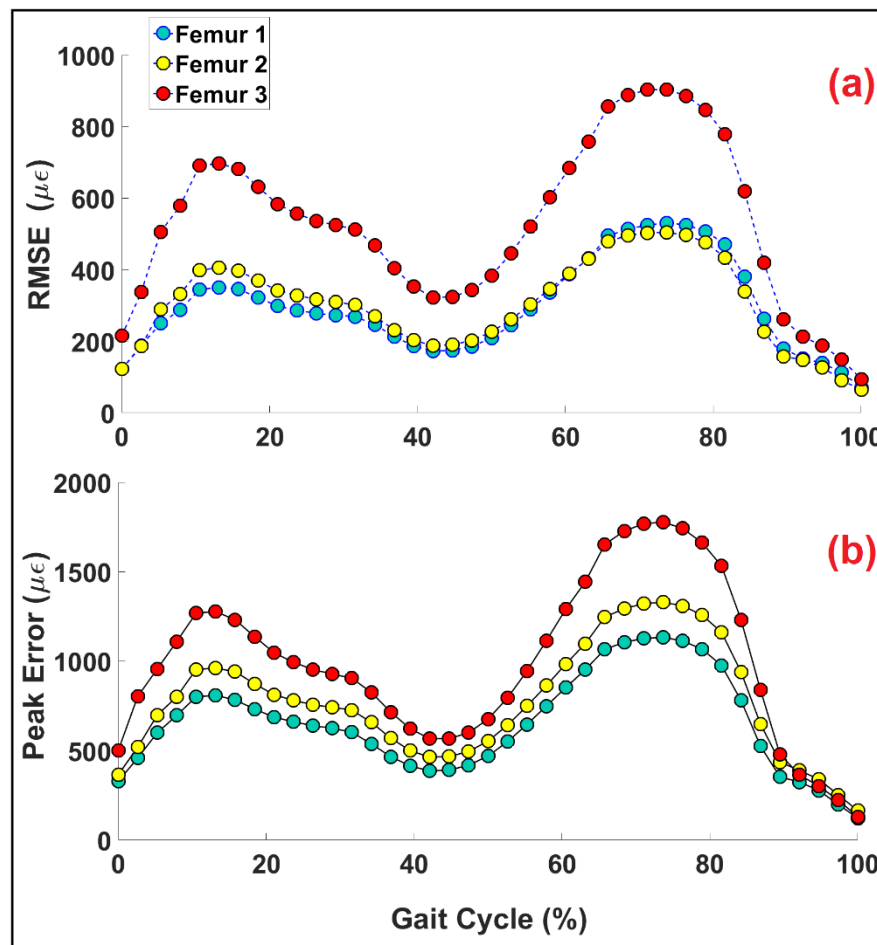
Figure 7.16: Frame-by-frame analysis of SPM2 method for three unseen femurs by measuring (a) RMSE and (b) peak errors across different frames of normal walking as the representative activity.

Table 7-2: Performance assessment of SPM2 for three unseen femurs.

Method	Unseen Femurs	Mean RMSE (µε)	Peak RMSE (µε)	Peak Error (µε)	Mean R^2	Mean Slope
SPM2	Femur 1	296	530	1, 133	0.94	0.91
	Femur 2	304	504	1, 328	0.92	1.23
	Femur 3	530	904	1, 776	0.83	0.97

As discussed in the previous section, the distribution of PCA scores could be a parameter that influences the accuracy of predictions gained from the SPM2 method. Therefore, it would be interesting to see how the PCA scores are distributed for major principle modes of variation. Comparing the PCA score for the first five modes of variation (which can explain over 53% of variation in the population) revealed that the PCA scores of Femur 1 with the lowest error was closer to the mean (SDs = 0) than Femur 3 with the highest SPM2 error (Figure 7.17). For example, for Femur 1, the weights of the principle components of first, second and the third mode were 0.04, 0.36 and 0.13, respectively, compared with the corresponding principle components of -0.69, 0.72 and 0.36 gained for Femur 3.
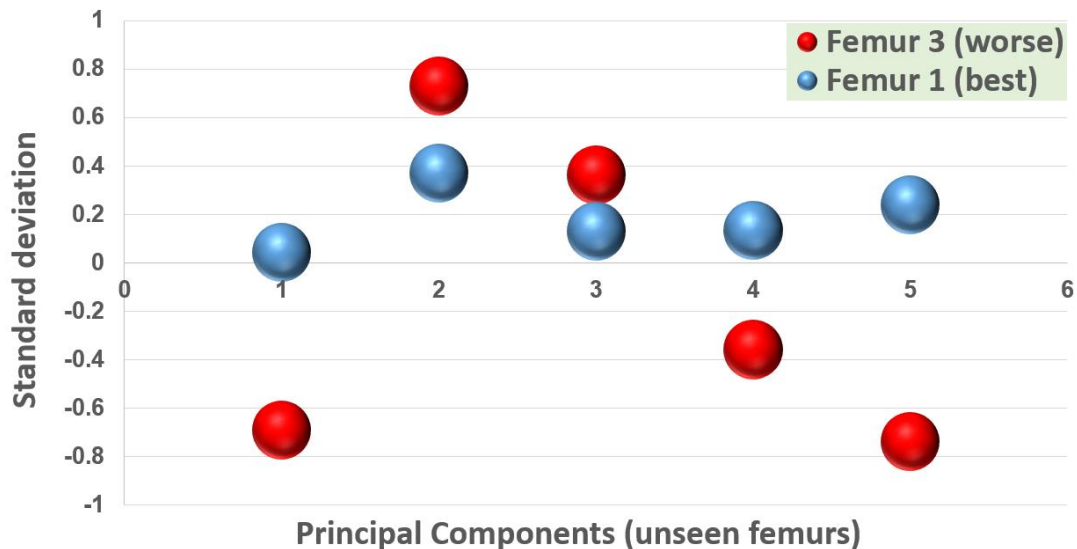
Figure 7.17: PCA scores of two unseen femurs (best and the worse cases) which were used for calculating femoral strain using SPM2 method.

Analysis of bones pooled

The capability of SPM2 was further confirmed when the accuracy of predictions was evaluated for three bones pooled together and using 50 random frames of motion. Similar to the previous section, a low range of interpolation error was observed for the investigated testing data by showing a median (50th percentile) and peak error (95th percentile) of 4 and 49 με, respectively (Figure 7.18). The major source of strain error was related to the reconstruction of geometry and modulus of femurs using the PCA model, representing a median and peak error of 166 με and 945 με, respectively. However, when both interpolation and reconstruction error was taken into account, the total error remains identical, showing a median error of 163 με and peak error of 931 με.
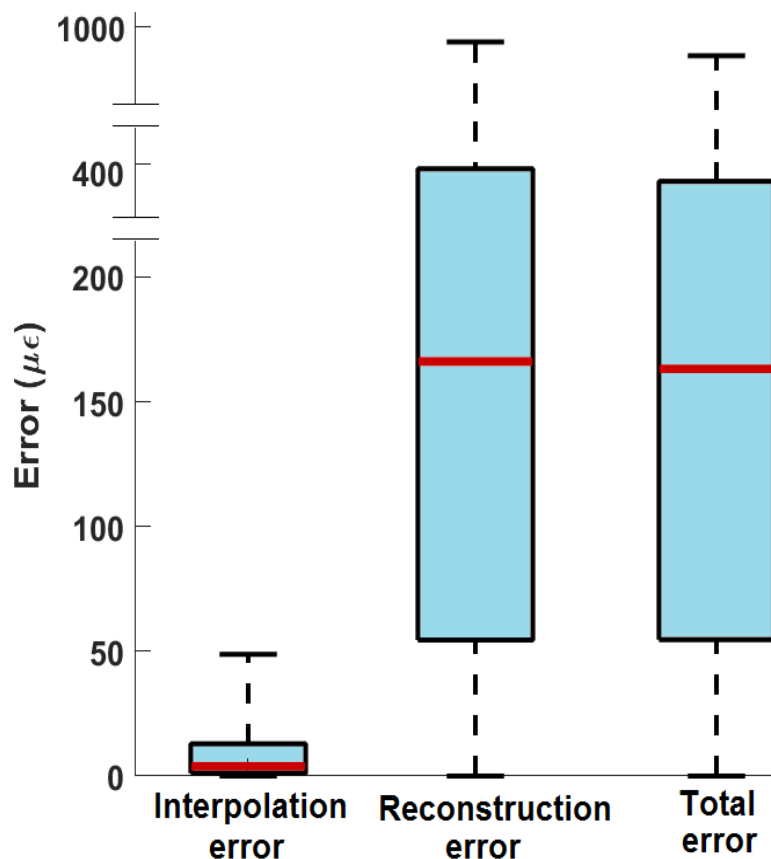
Figure 7.18: Comparing the contribution of two source of errors, interpolation and PCA reconstruction error, and the total error obtained when the femoral strain was computed for three unseen femurs and 50 random frames of motions. The blue box represents the range of the error between the 25th and 75th percentiles while the red horizontal line represents the median error (50th percentile). The lower and upper bounds show the 5th and 95th percentiles of error.

For the three pooled femurs and 50 pooled frames of motion, the equivalent strain was calculated with an RMSE of 480 µε, a determination coefficient (R^2) of 0.9, and a regression slope of 1.00 (Figure 7.19). When validating each femur individually, RMSE was ranged from 310 to 569 µε, R^2 was ranged from 0.86 to 0.96, while the regression slope was close to unity for all cases (Figure 7.20).
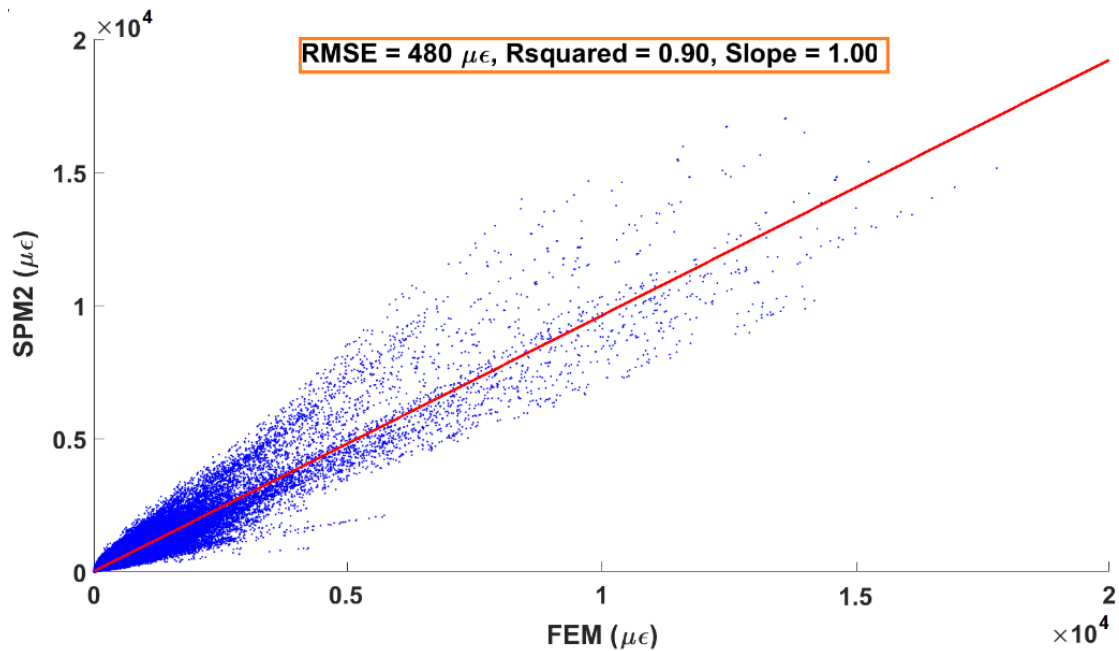
Figure 7.19: Comparison of the strains predicted by SPM2 with the strains calculated using FE method on the corresponding three pooled bones and during 50 random frames of motions.
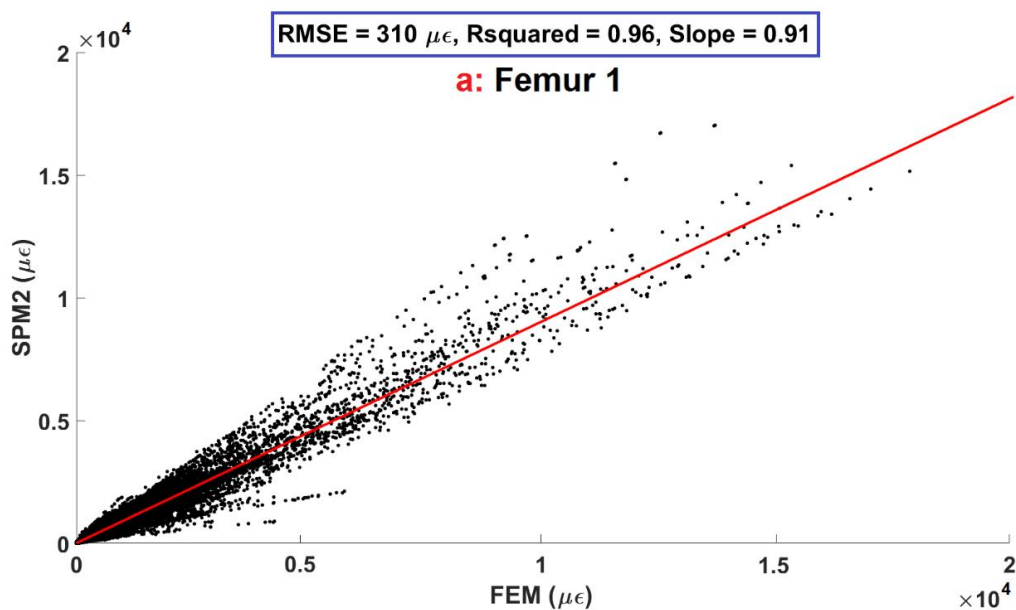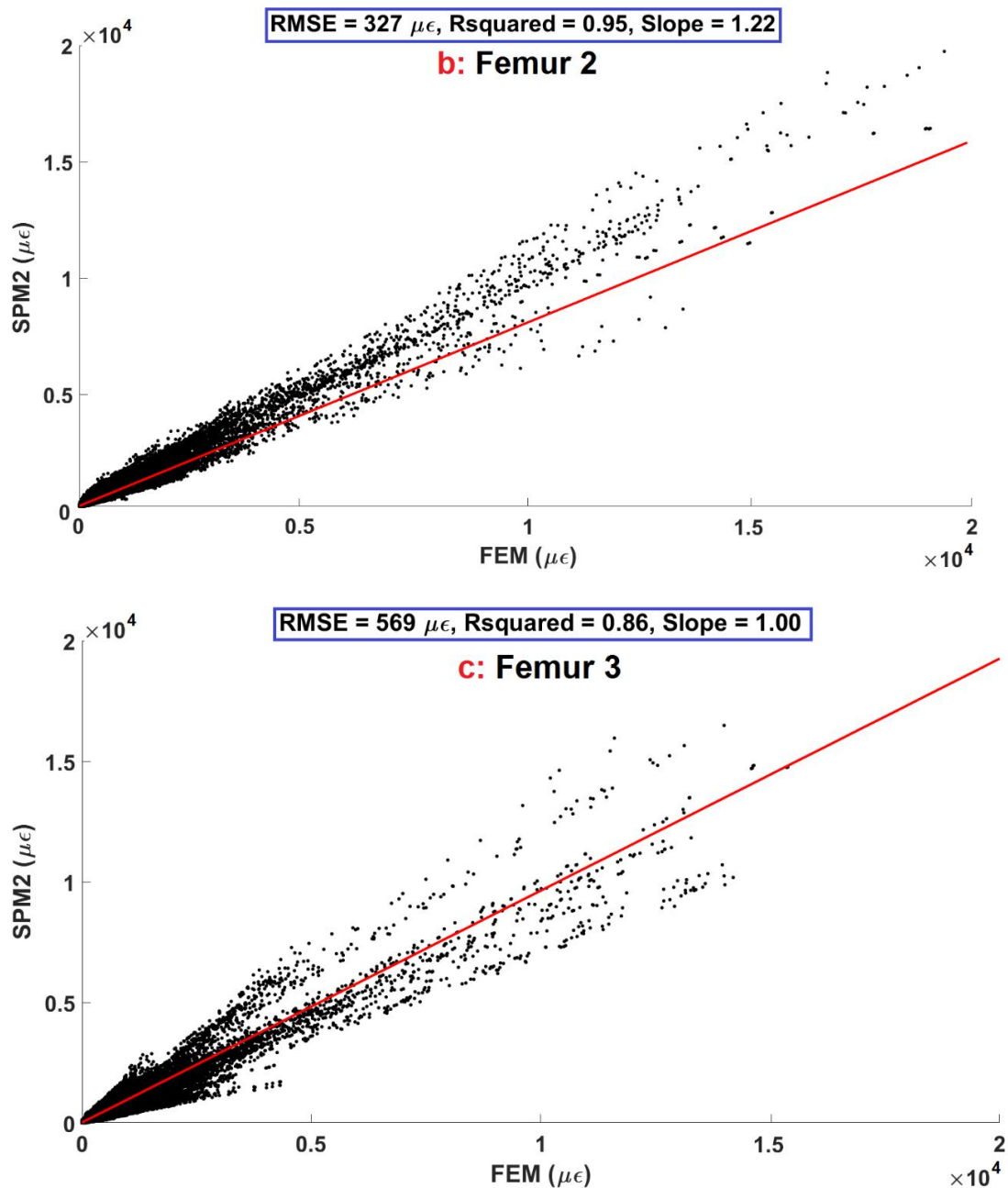
Figure 7.20: Individual validation of SPM2 for each unseen femur (a, b, c). The analysis was performed by considering 50 random frames of motion.

The validation of the single femurs presented a significantly lower error when the interpolation error in SPM2 (using the same femur geometry and material property distribution as the FE model) was compared against PCA reconstruction error (using femur geometry and material property distribution estimated from the combined ASM and AAM model) across different frames of investigated representative activity (Figure 7.21). The

median of interpolation error ranged 3 to 5 µɛ, while its peak error ranged from 48 to 50 µɛ.

The evaluation of PCA reconstruction error for each individual femur also presented a

median error changing from 146 to 191 µɛ and a peak error changing from 920 to 1,010 µɛ.
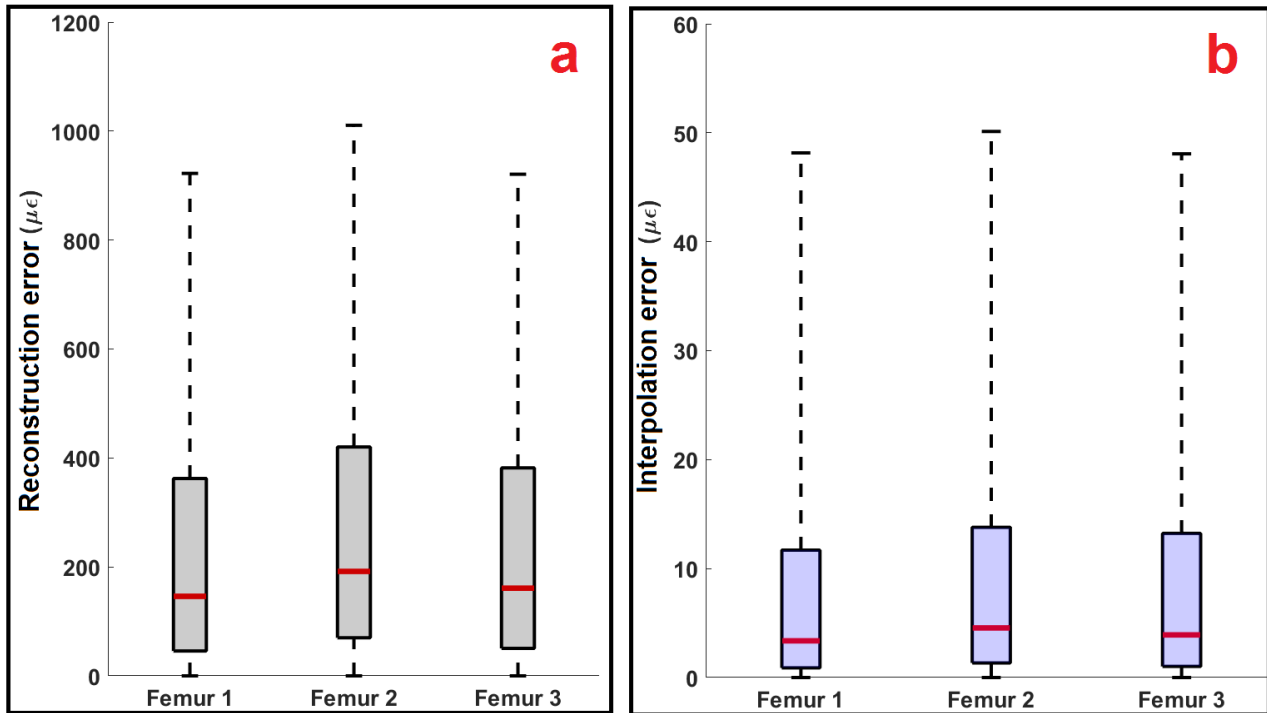
Figure 7.21: The range of (a) PCA reconstruction and (b) interpolation errors calculated for each individual unseen femurs during 50 frames of motion. Each boxplot represents the range of the error between the 25th and 75th percentiles. The red horizontal line represents the median error (50th percentile). The lower and upper bounds show the 5th and 95th percentiles of error.

The geometry and modulus reconstruction error

As discussed previously, the inaccuracy of the calculated strain fields in SPM2 was mostly

related to the reconstruction of femurs using the PCA method. For example, for a combined

statistical shape and appearance model, the PCA model yielded an RMSE and peak error

of 488 µɛ and 945 µɛ respectively (Figure 7.22). However, when the PCA-based statistical

model was built based on geometry and the material properties from the original femur used,

the computed RMSE and peak strain error were 261 µɛ and 493 µɛ respectively. Prediction

made with the original femur geometry and modulus assigned from the AAM model resulted

in RMSE and a peak strain error of 340 µɛ and 600 µɛ (Figure 7.22).
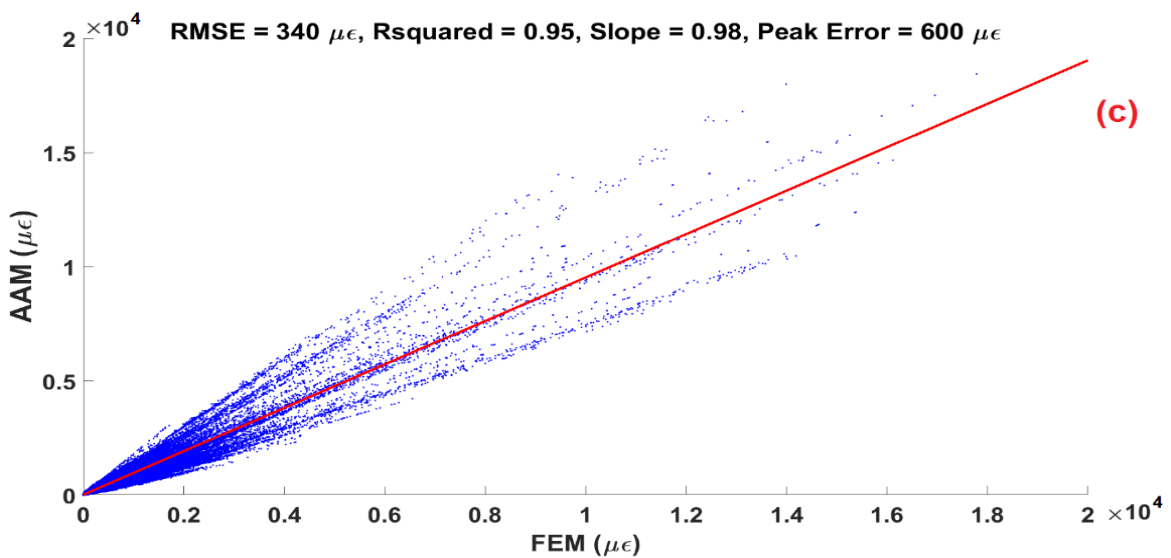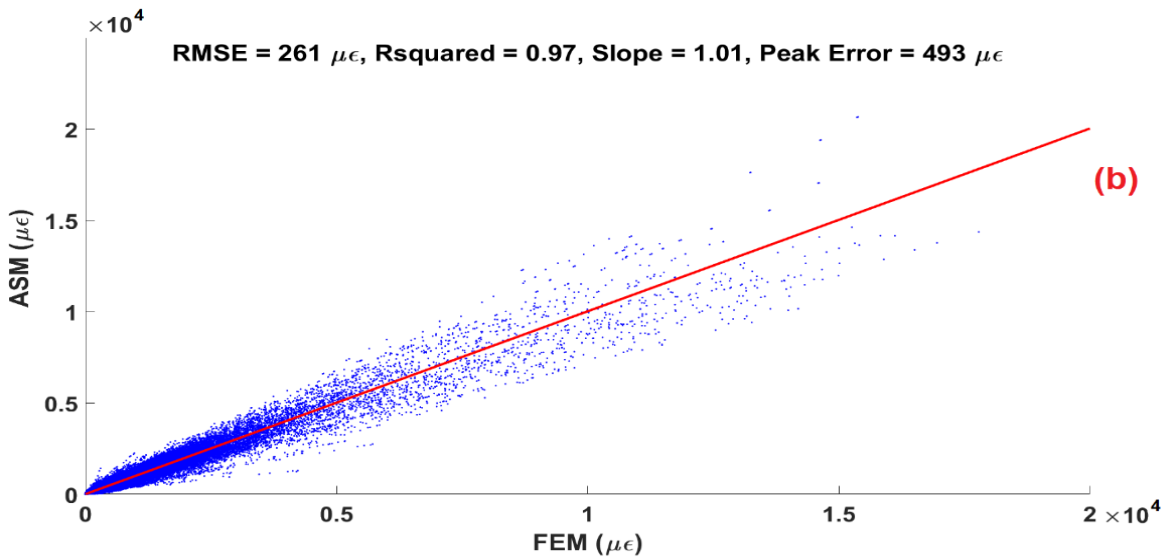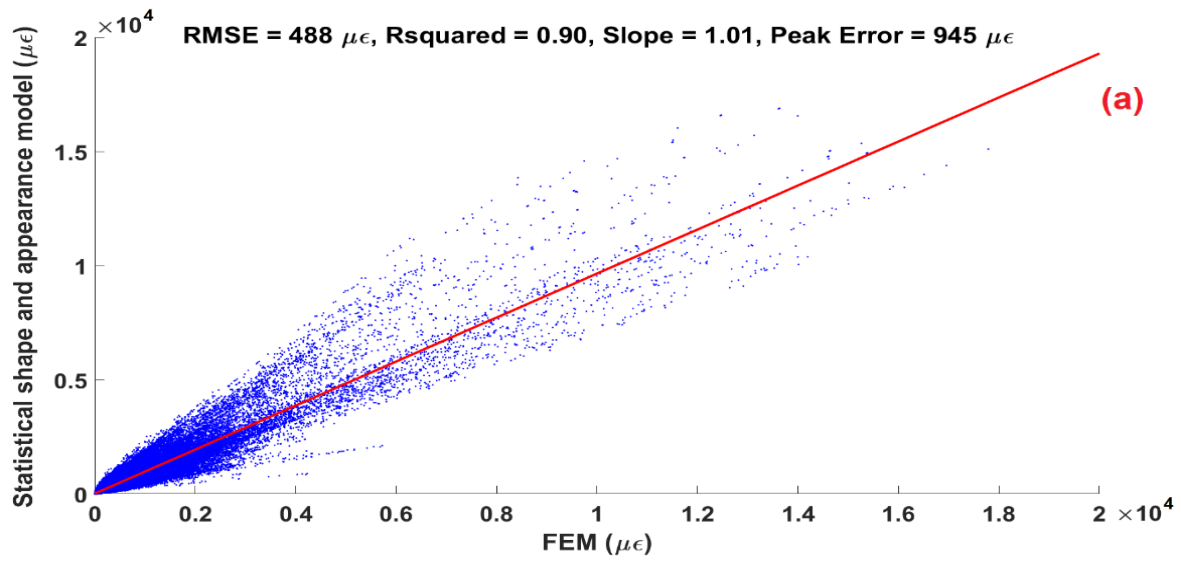
Figure 7.22: Femoral strain prediction accuracy for FE models constructed based on synthetic femurs reproduced by three PCA models: (a) Combined statistical shape and appearance model; (b) Statistical shape model (ASM); and (c) Statistical appearance model (AAM).

Discussion

Real-time prediction of femoral strain can promote large studies of bone, like assessing the risk of bone fracture (Bessho et al., 2009; Fuchs et al., 2017; Zani et al., 2015) and improving the biomechanical behaviour of implantable devices (Chanda et al., 2015; Helwig et al., 2009; Small et al., 2016). Unlike the popular surrogate modelling techniques which are bound by the training datasets, the Superposition Principle Method (SPM) is a training-free method which can be used for the rapid prediction of femoral strain during any physical activity. However, the applicability of this technique needs to be extended from one single subject to larger studies (e.g. a population-based study) to understand how the variability on the geometry and material quality between individuals would influence the performance of the technique. Therefore, the aim of the current chapter was to develop and test a novel computational method termed SPM2 for efficient calculation of femoral strain in a cohort of patients. To develop SPM2, a combined statistical shape and appearance model was integrated with the principle of superposition to capture a compact load-strain linear response in a set of basis FE simulations generated for each PCA mode of variation. The strain prediction of a given frame was then calculated within each mode by scaling the computed strain tensors with regard to amplitude of the actual force component and that of the nominal force applied (e.g. 100 N), and followed by adding the scaled strain tensors across different modes. The accuracy of the femoral strain computed by SPM2 method was then evaluated using two sets of data: (i) a synthetic population to explore the effect of anatomical variability and (ii) three unseen femur to examine the applicability of SPM2 method for real femurs. As a result of this analysis, two sources of errors (Interpolation and reconstruction errors) were identified and compared across different physical loading conditions (e.g. 50 random frames of motion and a full activity cycle).

The SPM2 method was used successfully for accurate prediction of femoral strain during motion when it was applied for both synthetic and unseen femurs. For the synthetic population, the peak error changed from 1.4% (for the best case) to 4.9% (for the worst case), in agreement with the error (i.e., 4.2 – 8.3% of peak strain on average) caused by the geometry and material properties of the FE models constructed from CT images (Taddei et al., 2006b). Such a consistency in strain error was also observed with a low RMSE of 81– 399 $\mu\varepsilon$ (equal to 0.7 to 1.6% of peak strain), in agreement with the average RMSE of 113 $\mu\varepsilon$ achieved when the FE calculations were compared with the corresponding experimental measurements (Taddei et al., 2006b). This source of error occurred due to fitting the second-order function to the strain tensors across different modes, resulting in an accumulated strain error over the entire modes. Furthermore, when the applicability of SPM2 method was examined for each unseen femur not belonging to the training dataset, a reasonable strain prediction was noticed (RMSE < 10% of peak strain, R^2 > 0.86). These results were comparable with the outcome of PCA-based FE studies created from CT data, reporting normalised RMSE of 11 – 13% (Grassi et al., 2017) and 11 –15% (Grassi et al., 2016), and coefficient of variation (R^2) greater than 0.88 (Grassi et al., 2017) and 0.89 (Grassi et al., 2016). From the reported strain differences for pooled unseen femurs, the PCA reconstruction error was the major source of strain error (median error = 166 $\mu\varepsilon$ and peak error = 945 $\mu\varepsilon$), as compared with the negligible interpolation error (median error = 4 $\mu\varepsilon$ and peak error = 49 $\mu\varepsilon$), highlighting the importance of the PCA method for accurate prediction of femoral strain in the SPM2 method. In addition to this, when the PCA scores of both synthetic and unseen femurs were investigated, a lower strain error achieved for those bone instances with the PCA scores near to the mean standard deviation (SD = 0). This finding was more important for the first three modes, which could explain about 44% of variation in the shape and modulus of the population.

Further analysis of the PCA method revealed that a higher portion of strain error was related to the reconstruction of femurs using the Active Shape Model (ASM) rather than the Active Appearance Model (AAM). For example, when the strain calculations of statistical-based FE models were compared with the corresponding FE models of the (original) three bones pooled, the error for geometry reconstruction (peak error = 493 $\mu\epsilon$, RMSE = 261 $\mu\epsilon$) was lower than the error computed for modulus reconstruction (peak error = 600 $\mu\epsilon$, RMSE = 340 $\mu\epsilon$). Furthermore, the coefficient of determination for ASM (R^2 =0.97) was marginally higher than AAM (R^2 =0.95), as compared with previous findings, with R^2 of 0.89 and 0.88, respectively. (Grassi et al., 2017). This evidence suggests that the error in the reconstruction of modulus could influence the accuracy of strain calculations more than the geometry reconstruction. Thus, further improvement is required for statistical models, particularly for reconstruction of material properties which is likely prone to higher errors.

The present work has some limitations. The SPM2 was developed and tested for calculation of femoral strain on the basis of a relatively small size of training data with 21 healthy women (65 ± 5 years). While the leave-one-out approach was used for reporting the reconstruction error of PCA model, to save the computational costs, and avoid re-building the SPM2 method, 18 femurs were used for building the SPM2 model, and three femurs were randomly selected for testing. To gain more confidence in term of the strength of the proposed technique, a larger population needs to be used by incorporating a larger variation in material characteristics and femoral anatomy (Austman et al., 2008; Bah et al., 2015a; Bryan et al., 2010; Oftadeh et al., 2015). The PCA predictions was restricted to ±2 standard deviations, covering about 95% of the variation within each mode, and ignoring the remaining percentage. To cover the variation near to boundaries (SDs = ±3), the size of the training dataset needs to be increased to provide enough data representing the entire

variation within each mode. In term of efficiency, the SPM2 method is faster than the FE method by a factor of 15 times. However, further improvement is achievable either by coding the MATLAB programs using more efficient programming languages such as C++ and Fortran (Aruoba and Fernández, 2015), or optimising the element size which was used for statistical shape and appearance models. For synthetic femurs, a physiologically less realistic (peak error = 14,000 – 20,000 με) strain fields was observed. This could, most likely, be related to, the magnitude of muscle and joint reaction forces that were taken from one single-subject and applied for all femurs. So, to explore the applicability of SPM2 for particular applications, like assessing the risk of femoral fracture (Martelli et al., 2014b), the applied forces needs to be scaled based on the body-weight of patients. While this would help to estimate a physiologically more realistic femoral strain fields, the main conclusions that SPM2 can be applied to any linear-elastic finite-element model would not be altered. Furthermore, the current study used a linear-based PCA model for the development of statistical shape and appearance model. However, more improvement, could likely be achieved by testing other alternative solutions, particularly, non-linear PCA methods, such as Kernel PCA (Chaber et al., 2018), Independent Component Analysis (Li et al., 2010), or non-linear classification techniques (Heimann and Meinzer, 2009; Lu and Pandolfo, 2011; Rasoulian et al., 2013).

The SPM method was applied in the previous chapter by varying the point of application of the hip contact force during locomotion, and the current chapter used a constant point to apply the joint reaction force. This led to ignoring the error associated with linearising the surface of the femoral head. Hence, the SPM2 method needs further changes so that the variation in the location of hip contact force can be considered. Finally, the SPM2 method was explored as a suitable technique for applications with linear systems like the

calculation of strain for intact femurs during motion (Kersh et al., 2018; Martelli et al., 2014a; Taylor et al., 2017), or relatively low non-linear models like the calculation of micromotion between bone and implant (Fitzpatrick et al., 2014). However, this method would not be appropriate for the prediction of outcome of interest in highly non-linear models, such as predicting the pattern of strain or wear for knee joint (Kazemi et al., 2013) with a complex dynamic system during locomotion (Walter and Pandy, 2017).

Conclusion

Large finite-element studies of bone have been hampered by their expensive computational costs, leading to a limit of the adaptation of FE analysis for this particular application which needs more efficient techniques. The current work developed and applied a novel computational method called SPM2 as a viable technique to bypass the computational complexity of current population-based studies of bone. The SPM2 method would be capable to predict femoral strain for a synthetic population with an average correlation coefficient of 0.97, allowing performance for particular applications such as assessing the risk of fracture in a population. However, the accuracy of predicted strain fields for unseen femurs was reduced slightly by showing the minimum correlation coefficient of 0.83. Two major sources of errors were identified during prediction of strain via the SPM2 method: interpolation error and reconstruction error. While the interpolation error could be reduced by increasing the number of standard deviations used within each PCA mode, the reconstruction error could be improved by either increasing the size and the variability of training dataset, or implementing other potential statistical models (e.g. non-linear PCA), which would enable a person to reconstruct the geometry and material properties of bone with higher accuracy. Therefore, to improve the robustness of the SPM2 method for strain

calculation, more advanced statistical shape and appearance models are needed to eliminate the PCA reconstruction error as the major source of error.

In conclusion, the proposed training-free computational method can provide a promising path for real, or near-real-time, biomechanical analysis of intact or implanted femurs for large population-based studies and various physical activities. However, the performance of the Active appearance model still needs further improvement, either by testing other methods or increasing the size of training datasets, to provide a consistent and low strain error for a set of independent femur instances.

Chapter 8 : DISCUSSION, CONCLUSIONS, AND FUTURE WORK

Background, aim and significant findings

The currently-used workflow for calculation of femoral strain in FE models includes segmentation of bone from CT images; mesh generation; assignment of material properties; the definition of loading condition; and submitting models to FE solvers (i.e. implicit or explicit solutions), as well as post-processing the obtained results. However, the current workflow, from building to solving the models, is a time-consuming and labour-intensive process, requiring a skilful operator. While statistical shape and appearance models are viable solutions for reducing the computational expenses of building FE models of a large cohort/population, the solution phase is still a computational barrier where 100s to 1000s of bone models are analysed. Current FE models are less attractive for clinical applications, where solution times of seconds to a few minutes are required.

The aim of this thesis was to develop a novel computational method for biomechanical analysis of bone, enabling rapid prediction of femoral strain distribution which would be applicable to multiple subjects and various loading conditions. The potential techniques were developed and the performance of each method was evaluated by measuring the solution time and strain error. The significant findings of this work are summarised below.

In Chapter 5, the efficacy and efficiency of Multi-Linear Regression (MLR) for computation of femoral strain during five different physical activities (normal walking, fast walking, stair ascent, stair descent, and chair rise) for a single healthy individual was explored. The MLR was able to predict femoral strain for a full activity cycle up to 200 times quicker than FE model. RMSE ranged from 1.2% to 1.3% while peak error ranged from 2.2% to 3.6% of the maximum micro-strain (5,020 $\mu\varepsilon$), followed by presenting lower accuracy when the magnitude of the applied load was lower, (e.g. in early and late stance phase) with

RMSE of 4.1% and a peak error of 8.6% of the maximum computed micro-strain. Therefore, MLR-based surrogate model could be applied as an efficient computational approach for predicting strain fields over the entire volume of long bones and across a range of normal physical activities.

In Chapter 6, by leveraging the linearity of most biomechanical studies of bone, a newly developed training-free method was developed, based on the superposition principle (Superposition Principle Method, SPM). The performance of this technique was then compared against three popular surrogate models: Multi-Linear Regression, Multivariate Adaptive Regression Splines, and Gaussian Process by measuring the time and strain error. The main advantage of the SPM method was related to its construction phase, permitting the building of a model independent from motion analyses experiments. The theory behind this relied on finding the causal relationship between a set of nominal applied forces and the resultant strain fields. Once constructed, the model was able to predict full tensor of femoral strain for a given frame of motion by scaling the known strain fields with regard to the corresponding force components, followed by adding the computed femoral strain for each force component. Among the surrogate methods, it was found that 200 DOE samples consistently provided low error (RMSE < 100 με), with model construction time ranging from 3.8 to 63.3 h and prediction time ranging from 6 to 1,236 seconds per activity. Furthermore, compared with surrogate models, a better performance was observed from the SPM method, by producing the lowest strain error (RMSE = 40 με), the fastest model construction time (3.2 hours) and the second fastest prediction time per activity (36 seconds) after Multi-Linear Regression (6 seconds).

The SPM error originated completely from the different algorithms used in the present study and in the study of reference (Martelli et al., 2015b) for matching the nodes on the

femoral head surfaces and the hip force vector calculated using OpenSim. Specifically, in the present study the hip contact force vector was applied to the node on the femoral head surface by matching the direction of the hip contact force vector calculated using OpenSim and the direction through the node and the hip centre. While, in the reference study (Martelli et al., 2015b), the hip contact force vector was applied to the node on the femoral head surface closest to the intersection between the hip contact force calculated using OpenSim and the femoral head surface. The different algorithms led to a mismatch between the point of application of the hip contact force in the two studies of up to the element edge length (2 mm in average) and to zero-error when the hip force vector was applied to the same node in both studies. The SPM error attributable to each muscle in the model was systematically zero because muscle attachment points were fixed throughout the activity. Therefore, while the error surrogate models could only be reduced marginally by increasing the training set size above 200, the error in the SPM method could be reduced without a significant computational cost by generating smaller elements on the surface of the femoral head.

It was demonstrated that surrogate models are application-based and the performance of these techniques is bounded by training dataset, meaning that a surrogate model trained on data for level walking is unlikely to be as effective for activities with a higher degree of variability, like jumping. In contrast, the SPM model is comprised of a set of independent solutions, unrelated to activity, determined through finite-element analysis. For each frame and activity, solutions are then determined using linear combinations of base solutions, without training or any iterative learning approach. Therefore, the SPM method is a training-free method which could be applied for any activity without the need to re-train the model, provided that the predicted strains are within the linear elastic region.

In Chapter 7, a novel computational approach called 'SPM2' was developed and the performance of this technique was examined for a population-based study by considering the variation in anatomy and bone distribution. This was achieved by amalgamating the Principle of superposition and a combined statistical shape and appearance model. The accuracy of predicted femoral strain was explored for two sets of data, including synthetically generated population and three unseen femurs. For a synthetic population generated using random PCA scores, the SPM2 method was able to reliably predict the femoral strain compared with the corresponding FE method across the whole population and for randomly selected frames of motion. The peak error ranged from 1.4 – 4.9 % (of maximum strain), while the RMSE varied from 0.7 to 1.6% (of maximum strain), which was consistent with previous findings (Grassi et al., 2014; Taddei et al., 2006b). While the variation within each mode is currently only described by three points (Standard deviations), increasing the number of points may help to reduce the error. However, as a result of this change, the number of simulations needed for building the SPM2 will increase accordingly, requiring the solution of an additional 2,448 simulations, which ultimately increases the computational cost.

When the applicability of SPM2 was examined for unseen femurs, a lower accuracy was noted, mainly due to a poor performance of PCA during reconstruction of femurs. The average of shape reconstruction error in the ASM model was ranged from 1.3 – 4.9 mm, corroborating previous studies with an average error of 1.22 (Grassi et al., 2014), 0.88 mm (Vaananen et al., 2012) and 1.64mm (Rao et al., 2013). Furthermore, while the elemental modulus reconstruction error showed a fairly high average error (860 MPa) compared with a previous study (500 MPa), a realistic modulus distribution was noticed when the first few modes of PCA were visualised. Prediction of femoral strain using reconstructed femurs

showed a normalised RMSE error of 9% (of peak strain) for AAM and 5% (of peak strain) for ASM models. This was comparable with previous findings, reporting the normalised RMSE of 10% and 8% respectively for AAM and ASM-based FE models when compared with experimental measurements (Grassi et al., 2017). However, according to previous research (Bryan et al., 2010; Grassi et al., 2017; Vaananen et al., 2012), increasing the sample size up to a certain level (e.g. 40 – 100 femurs) could help to tailor further development of AAM models as the major source of error.

Additionally, detailed analysis of strain error for unseen femurs presented a higher amount of strain error resulting from the reconstruction of the modulus distribution as compared to the reconstruction of the shape. This finding could be justified by looking at the compactness test, where PCA needed a higher number of modes to explain a certain percentage of variation for modulus as compared to the shape. Thus, caution is needed when building statistical models using PCA, particularly for statistical appearance models which could potentially generate a higher range of error during model reconstruction, leading to strain predictions using SPM2 with higher errors. Another finding worth mentioning was related to the PCA scores and their effects on the measured strain errors. It was noted that when PCA scores for both synthetic and unseen femurs are close to the mean femur (with standard deviation = 0) of the population, a lower error could be achieved. This could likely be related to building the SPM2 method based on the PCA scores of the mean femur across different modes of variation, and further improvements may be achieved, if further standard deviations were accounted for in the construction of SPM2.

Limitations

The quality of a statistical shape and appearance model is dependent on the training datasets which have been used to build the model. In the present work, the size of training datasets used to build the statistical model was restricted to 21 healthy women (age range = 60 – 74). Due to this relatively small sample size, the range of femurs which were used for the construction of statistical shape and appearance models could reflect the small sample size and its potential bias. Furthermore, analysis of the PCA model using a compactness test and reconstruction error showed a better performance for ASM than AAM. For example, using the first five PCA modes, the ASM model was able to preserve around 95% of existing variation, whereas the AAM model was only able to capture 53% in the first five modes. Therefore, more caution needs to be taken while constructing the AAM models from CT images, and the statistical model needs to be constructed using a sufficient number of bones to provide a better representation of the whole population.

The statistical shape and appearance model, which is the foundation of the SPM2 method, has been constructed using a linear-based PCA method. The motivation to use this statistical model could be related to its two major features: compactness and reversibility. The compactness allows the PCA method to explain the main features of a training dataset by the projection of a high dimensional space into lower dimensional space. This capability allows the method to explain the shape and material properties of each bone using a limited set of PCA weights, without which a point-to-point training process would be needed to explain the variation in the shape and material properties of bone, making it too difficult to explain large population-based studies with a wide variety set of bone models. The reversibility is another feature of the PCA method which allows it to either reconstruct a femur from a set of known weights or extract the weights for a given femur. This feature is

an important requirement, particularly when the aim is to use PCA weights in large studies of bone or clinical applications, allowing the examination of the performance of an established PCA model by assessing the errors occurring during the reconstruction of shape and material properties, and thus evaluating the resultant strain error occurring in SPM2.

The PCA method has been used in a vast majority of statistical models as the preferred method for describing the shape of a population, while presenting a difficulty explaining the variation in material properties (Bryan et al., 2010; Bryan et al., 2012; Vaananen et al., 2012). This was further confirmed through the current study by showing the difficulty the PCA method has capturing the variation in material properties for unseen femurs, while better performance was noted for the reconstruction of shape in unseen femurs. While increasing the sample size is suggested as a potential solution (Sarkalkan et al., 2014b) for improving the performance of the active appearance model (AAM), another possible solution which needs to be explored, is the use of smaller elements. This might be effective on the distribution of material properties, particularly when the material properties of bones are re-assigned from the original mesh to the morphed mesh.

Another major limitation with PCA is its algorithm, which uses a least-square estimation and assumes that data are distributed normally, while the principle modes are orthogonal to each other (Linting et al., 2007). This could lead to the outliers associated with realistic training datasets being ignored and the generation of bone instances with implausible shape and material properties, specifically when the size of the training dataset is not large enough. To circumvent this limitation, it is essential to consider other potential classification methods to understand how the accuracy of the current AAM-based statistical models could be improved. Independent component analysis (ICA) is an extension of PCA (Hyvärinen, 2012;

Tumer et al., 2019), which has been explored successfully for different fields of science and technology, including biomedical engineering, either for explaining the material properties (Üzümcü et al., 2003), for 3D shape analysis , or; removal of artefacts using simulated data (Djuwari et al., 2005). However, unlike the PCA model which provides a natural ordering of the eigenvectors according to the associated eigenvalues, a typical ICA method can explain the variation within a dataset via a set of independent factors, making it impossible to describe the variation within population in an appropriate format as required for SPM2. Therefore, if the generated independent components obtained from ICA could be ordered meaningfully, then this method could potentially be used as an alternative to current PCA models. Kernel PCA is a generalisation of PCA and has been proven to be a powerful classification technique for nonlinear dimensionality reduction of high-dimensional feature space and has claimed success in machine learning and pattern recognition problems (Deng and Tian, 2013; Peter et al., 2019). A standard PCA uses a linear algorithm to project the data into a straight line, affecting the accuracy of the model when the datasets are not distributed normally in the design space (Bishop, 2006). For example, when the shape and distribution of material properties in one specific bone is different from others, linear PCA may not be the best option to capture such a different property, leading to the loss of the variation within the population and making some errors for the reconstruction of the corresponding femur. In this case, Kernel PCA, which uses a non-linear algorithm, allows for the description of these small variations during the reduction of a high dimensional space into multiple low dimensional subspaces. Another potential method which could be used for improving the performance of AAM models could be Autoencoders which is developed based on the theory of neural networks to reduce a high-dimensional observation to a lower-dimensional representation space. While this technique is able to describe the non-linearity of the given training data, due to the reduction of the number of layers during finding the

relationship between input and output layers using an optimising function, a perfect reconstruction of all vectors of material properties may not be possible (Bishop, 2006). Therefore, a correct choice of method needs to be established by testing these potential methods to understand which of them is more suitable for the construction of AAM models as the major source of error, and to investigate how the obtained AAM weights could be combined with ASM weights produced from a linear-PCA model as a suitable technique for describing shape with a population.

When the SPM method was developed for single subject study during motion, the centre of pressure was assumed to be the intersection between the sphere that best fit the femoral head surface and the hip contact force vector passing through the hip joint centre. This assumption led to the generation and solving of 101 individual simulations for those nodes located within the envelope of the trajectories of the hip joint centre of pressure across activities. However, for the sake of simplicity, the SPM2 method was applied for population-based study by assuming that the location of applied joint contact force is constant across different subjects during motion. While this may increase the computational costs significantly due to creating and solving a large number of individual simulations for three components (e.g. x, y, and z) of joint contact force across the entire standard deviations and modes of variation, this would not affect the validity of the concept used in the SPM2 method. It could be advantageous if the centre of pressure could be varied during motion within the population-based study, helping to physiologically better describe the distribution of femoral strain during different loading conditions.

The SPM2 method showed a great potential for reducing the computation required for calculation of femoral strain. The current solution time in the SPM2 method for activity cycle discretised into 40 frames of motion is approximately 15 times quicker than the FE method.

However, the analysis time could be reduced further by rewriting the codes using more efficient programming languages, like C++, which is almost 11 times quicker than MATLAB (Aruoba and Fernández, 2015). This would allow the performance of strain prediction in a few seconds, which is a requirement for clinical applications and large studies of bone.

The current statistical model was developed based on the shape and material properties of bones derived from CT images. However, the CT images are not standard of care, due to some limitations, such as high operational costs and exposing patients to significant doses of radiation, making them less attractive for clinical-based studies, like assessing the risk of femoral fracture (Grassi et al., 2016; Vaananen et al., 2012). The capability of planar dual-energy X-ray absorptiometry (DEXA) has made it popular for FE studies of bone (Grassi et al., 2017) as well as the establishment of statistical shape and appearance models (Sarkalkan et al., 2014b; Vaananen et al., 2012). Although statistical models built from these quick and non-invasive DEXA images is in early stages and the accuracy of generated 3D models projected from 2D images needs to be improved, (Grassi et al., 2017; Vaananen et al., 2012), combining these DEXA-imaged based statistical models, with real-time musculoskeletal models (Durandau et al., 2018; Pizzolato et al., 2017a; Samy et al., 2019), and using the SPM2 method would potentially permit the determination of the distribution of femoral strain in clinics without harm to patients.

The data used in this study was obtained from previous work (Martelli et al., 2015b), where the bones were segmented manually. For future work, fully automatic segmentation approaches could be coupled with the current SPM2 workflow, allowing it to include a wider variation in the shape and material properties of bones by enlarging the size of training datasets up to thousands of CT images. This could, ultimately, improve the robustness of

PCA-based statistical models by incorporating a wide variation in the shape and material properties of bone within the population (Bryan et al., 2010; Vaananen et al., 2012).

Applications and future work

The aim of this thesis was to develop an efficient computational model for calculation of femoral strain during motion in large bone studies. This aim has been achieved by developing and testing the SPM2 method for a linear-elastic problem, while capturing the non-linearity of joint contact force during motion. However, this technique has greater capabilities and with further development could be used for: (i) assessing the risk of fracture on the femoral neck for a large number of activity regimes across a representative patient population; (ii) real or near-real time calculation of femoral strain while patients are exercising or performing physical activates; and (iii) assessing the primary stability of an implant design by evaluating the effect of several patient and surgical factors on the interfacial micromotion and strain between bone and implant within the populations.

The current study used a limited set of normal activity for testing the performance of SPM2. However, by accounting a large space of potential or physiologically plausible forces, it is clearly feasible to study femoral neck mechanics. To generate such physiologically plausible muscle forces, the available full-body musculoskeletal models need to be coupled with potential statistical approaches (e.g. Bayesian statistics) and sampling methods (e.g. Markov chain Monte Carlo). The obtained data can then simply be fed into the SPM2 method to explore the risk of femoral fracture within a representative or real population by ranking a variety of physical activities based on their effect on the risk of fracture.

Recently, real-time musculoskeletal modelling pipelines are suggested for the direct calculation of forces in the lower limb (Durandau et al., 2018; Pizzolato et al., 2017a; Samy et al., 2019). These force estimation approaches which are typically developed based on EMGs and motion-capture data, are able to provide a real-time bio-feedback for different participants and physical activates in clinics. So, by coupling these musculoskeletal models and having a set of segmented CT data, it is feasible to fit the input data (forces and PCA weights representing the material properties and shape of bone) into the SPM2 method to compute femoral strain in a time-effective manner. Thus, translation of this rapid computational method to the clinical environment could be beneficial for various applications including: establishing personalised treatments after surgery (e.g. total hip replacement); improvement of rehabilitation systems by providing real-time biofeedback about the effect of forces acting on bone during daily activities; improving the accuracy of musculoskeletal models in their estimation of muscle and joint reaction forces by efficiently refining the models based on the predicted femoral strains; and also in sport biomechanics, for enhancing the performance of athletes during exercise (e.g. running and cycling) or examining the risk of bone injury, like assessing the risk of bone stress injury (BSI) as a common problem among runners.

The current study used the SPM2 method for calculation of femoral strain in intact femurs. However, in future research, it would be interesting to look at the performance of SPM2 for implantable devices. For example, this could be a useful tool for investigating the interface conditions between the interface of bone and a designed implant, allowing the understanding of the primary stability of implanted bones across a large population, and ultimately helping to optimise the design of implants by accounting for both anatomical (Bah et al., 2015b) and surgical variabilities (Al-Dirini et al., 2019; Bah et al., 2011). To achieve

this, the available automated implantation approaches (Al-Dirini et al., 2019) could be coupled with large FE studies of bone (Bryan et al., 2012; Galloway et al., 2013) to synthetically generate populations which are implanted in the ideal position in hosting bone, leading to the generation of the training data required to build the SPM2 method. However, the major challenge would be related to establishing a suitable algorithm so that the size and shape of an implant design could be matched with the corresponding hosting bone across different standard deviations and modes of variation. If this problem could be solved, then the methodology could be used as an effective solution for comparative assessment of implant designs for large population based-studies.

In conclusion, the Superposition principle method (SPM) is a training-free method providing solutions of femoral strain during activity that outperform common surrogate models both in terms of error and computational time. The combination of superposition principle and the PCA-based statistical model is computationally an effective solution for running population-based simulations of femoral mechanics during activity. With further development, this approach could potentially be used for other applications, such as improving the design of implantable devices, either using a real or representative population, and providing biofeedback to patients while performing physical activates in clinics.

REFERENCES

Abrahamsen, B., van Staa, T., Ariely, R., Olson, M., Cooper, C., 2009. Excess mortality following hip fracture: a systematic epidemiological review. Osteoporosis International 20, 1633-1650.

Acciaioli, A., Lionello, G., Baleani, M., 2018. Experimentally Achievable Accuracy Using a Digital Image Correlation Technique in measuring Small-Magnitude (<0.1%) Homogeneous Strain Fields. Materials (Basel) 11.

Ackermann, E.R., Villiers, J.P.d., Cilliers, P.J., 2011. Nonlinear dynamic systems modeling using Gaussian processes: Predicting ionospheric total electron content over South Africa. Journal of Geophysical Research 116, A10303.

Adams, D.J., Spirt, A.A., Brown, T.D., Fritton, S.P., Rubin, C.T., Brand, R.A., 1997. Testing the daily stress stimulus theory of bone adaptation with natural and experimentally controlled strain histories. Journal of Biomechanics 30, 671-678.

Al-Dirini, R.M.A., Martelli, S., O'Rourke, D., Huff, D., Zhang, J., Clement, J.G., Besier, T., Taylor, M., 2019. Virtual trial to evaluate the robustness of cementless femoral stems to patient and surgical variation. Journal of Biomechanics 82, 346-356.

Almeida, D.F., Ruben, R.B., Folgado, J., Fernandes, P.R., Audenaert, E., Verhegghe, B., De Beule, M., 2016. Fully automatic segmentation of femurs with medullary canal definition in high and in low resolution CT scans. Medical Engineering & Physics.

Anderson, F.C., Pandy, M.G., 2001a. Dynamic optimization of human walking. Journal of Biomechanical Engineering 123, 381-390.

Anderson, F.C., Pandy, M.G., 2001b. Static and dynamic optimization solutions for gait are practically equivalent. Journal of Biomechanics 34, 153-161.

Anthony Giunta, S.N.L., Steven Wojtkiewicz, S.N.L., Eldred, M., 2001. Overview of modern design of experiments methods for computational simulations. 41st Aerospace Sciences Meeting and Exhibit.

Ardestani, M.M., Moazen, M., Chen, Z., Zhang, J., Jin, Z., 2015. A real-time topography of maximum contact pressure distribution at medial tibiofemoral knee implant during gait: Application to knee rehabilitation. Neurocomputing 154, 174-188.

Arnold, A.S., Salinas, S., Asakawa, D.J., Delp, S.L., 2000. Accuracy of muscle moment arms estimated from MRI-based musculoskeletal models of the lower extremity. Computer Aided Surgery 5, 108-119.

Arnold, E.M., Ward, S.R., Lieber, R.L., Delp, S.L., 2010. A model of the lower limb for analysis of human movement. Annals of Biomedical Engineering 38, 269-279.

Aruoba, S.B., Fernández, V., J., 2015. A comparison of programming languages in macroeconomics. Journal of Economic Dynamics and Control 58, 265-273.

Ashman, R.B., Cowin, S.C., Van Buskirk, W.C., Rice, J.C., 1984. A continuous wave technique for the measurement of the elastic properties of cortical bone. Journal of Biomechanics 17, 349-361.

Austman, R.L., Milner, J.S., Holdsworth, D.W., Dunning, C.E., 2008. The effect of the density–modulus relationship selected to apply material properties in a finite element model of long bone. Journal of Biomechanics 41, 3171-3176.

Awadalla, M., Al-Dirini, R.M.A., O'Rourke, D., Solomon, L.B., Heldreth, M., Taylor, M., 2018. Influence of varying stem and metaphyseal sleeve size on the primary stability of cementless revision tibial trays used to reconstruct AORI IIA defects. A simulation study. J Orthop Res.

Bah, M.T., Nair, P.B., Taylor, M., Browne, M., 2011. Efficient computational method for assessing the effects of implant positioning in cementless total hip replacements. Journal of Biomechanics 44, 1417-1422.

Bah, M.T., Shi, J., Browne, M., Suchier, Y., Lefebvre, F., Young, P., King, L., Dunlop, D.G., Heller, M.O., 2015a. Exploring inter-subject anatomic variability using a population of patient-specific femurs and a statistical shape and intensity model. Medical Engineering & Physics 37, 995-1007.

Bah, M.T., Shi, J., Heller, M.O., Suchier, Y., Lefebvre, F., Young, P., King, L., Dunlop, D.G., Boettcher, M., Draper, E., Browne, M., 2015b. Inter-subject variability effects on the primary stability of a short cementless femoral stem. Journal of Biomechanics 48, 1032-1042.

Bayraktar, H.H., Morgan, E.F., Niebur, G.L., Morris, G.E., Wong, E.K., Keaveny, T.M., 2004. Comparison of the elastic and yield properties of human femoral trabecular and cortical bone tissue. Journal of Biomechanics 37, 27-35.

Behrens, B.A., Nolte, I., Wefstaedt, P., Stukenborg-Colsman, C., Bouguecha, A., 2009. Numerical investigations on the strain-adaptive bone remodelling in the periprosthetic femur: Influence of the boundary conditions. Biomedical Engineering Online 8.

Ben Younes, L., Nakajima, Y., Saito, T., 2014. Fully automatic segmentation of the Femur from 3D-CT images using primitive shape recognition and statistical shape models. International Journal of Computer Assisted Radiology and Surgery 9, 189-196.

Bergmann, G., Bender, A., Dymke, J., Duda, G., Damm, P., 2016. Standardized loads acting in hip Implants. Plos One 11, e0155612.

Bergmann, G., Deuretzbacher, G., Heller, M., Graichen, F., Rohlmann, A., Strauss, J., Duda, G.N., 2001. Hip contact forces and gait patterns from routine activities. Journal of Biomechanics 34, 859-871.

Bergmann, G., Graichen, F., Rohlmann, A., 1993. Hip joint loading during walking and running, measured in two patients. Journal of Biomechanics 26, 969-990.

Bergmann, G., Graichen, F., Rohlmann, A., 1995. Is staircase walking a risk for the fixation of hip implants? Journal of Biomechanics 28, 535-553.

Bergmann, G., Graichen, F., Rohlmann, A., 2004. Hip joint contact forces during stumbling. Langenbeck's Archives of Surgery 389, 53-59.

Besl, P.J., McKay, N.D., 1992. A method for registration of 3-D shapes. IEEE Transactions on Pattern Analysis and Machine Intelligence 14, 239-256.

Bessho, M., Ohnishi, I., Matsumoto, T., Ohashi, S., Matsuyama, J., Tobita, K., Kaneko, M., Nakamura, K., 2009. Prediction of proximal femur strength using a CT-based nonlinear finite element method: Differences in predicted fracture load and site with changing load and boundary conditions. Bone 45, 226-231.

Bettamer, A., Allaoui, S., Hambli, R., 2017. Using 3D digital image correlation to visualise the progress of failure of human proximal femur. Computer Methods in Biomechanics and Biomedical Engineering: Imaging & Visualization 5, 233-240.

Bevill, S.L., Bevill, G.R., Penmetsa, J.R., Petrella, A.J., Rullkoetter, P.J., 2005. Finite element simulation of early creep and wear in total hip arthroplasty. Journal of Biomechanics 38, 2365-2374.

Bieger, R., Ignatius, A., Decking, R., Claes, L., Reichel, H., Durselen, L., 2012. Primary stability and strain distribution of cementless hip stems as a function of implant design. Clinical Biomechanics 27, 158-164.

Bishop, C., 2006. Pattern recognition and machine rearning, Information Science and Statistics.

Bitsakos, C., Kerner, J., Fisher, I., Amis, A.A., 2005. The effect of muscle loading on the simulation of bone remodelling in the proximal femur. Journal of Biomechanics 38, 133-139.

Bowman Jr, K.F., J. Fox and J. K. Sekiya, 2010. A clinically relevant review of hip biomechanics. Arthroscopy: The Journal of Arthroscopic & Related Surgery 26, 1118-1129.

Boyd, S., Shrive, N., Wohl, G., Muller, R., Zernicke, R., 2001. Measurement of cancellous bone strain during mechanical tests using a new extensometer device. Medical Engineering and Physics 23, 411-416.

Brand, R.A., Pedersen, D.R., Friederich, J.A., 1986. The sensitivity of muscle force predictions to changes in physiologic cross-sectional area. Journal of Biomechanics 19, 589-596.

Brekelmans, W.A., Poort, H.W., Slooff, T.J., 1972. A new method to analyse the mechanical behaviour of skeletal parts. Acta Orthopaedica Scandinavica 43, 301-317.

Bryan, R., Mohan, P.S., Hopkins, A., Galloway, F., Taylor, M., Nair, P.B., 2010. Statistical modelling of the whole human femur incorporating geometric and material properties. Medical Engineering and Physics 32, 57-65.

Bryan, R., Nair, P.B., Taylor, M., 2009. Use of a statistical model of the whole femur in a large scale, multi-model study of femoral neck fracture risk. Journal of Biomechanics 42, 2171-2176.

Bryan, R., Nair, P.B., Taylor, M., 2012. Influence of femur size and morphology on load transfer in the resurfaced femoral head: A large scale, multi-subject finite element study. Journal of Biomechanics 45, 1952-1958.

Byrne, D.P., Mulhall, K.J., Baker, J.F., 2010. Anatomy & biomechanics of the hip. The Open Sports Medicine Journal 4, 51-57.

Campbell, J.Q., Petrella, A.J., 2016. Automated finite element modeling of the lumbar spine: Using a statistical shape model to generate a virtual population of models. Journal of Biomechanics 49, 2593-2599.

Carballido-Gamio, J., Bonaretti, S., Saeed, I., Harnish, R., Recker, R., Burghardt, A.J., Keyak, J.H., Harris, T., Khosla, S., Lang, T.F., 2015. Automatic multi-parametric quantification of the proximal femur with quantitative computed tomography. Quantitative Imaging in Medicine and Surgery 5, 552-568.

Carbone, V., Fluit, R., Pellikaan, P., van der Krogt, M.M., Janssen, D., Damsgaard, M., Vigneron, L., Feilkas, T., Koopman, H.F., Verdonschot, N., 2015. A comprehensive musculoskeletal geometry dataset for subject-specific modeling of lower extremity. Journal of Biomechanics 48, 734-741.

Carlson, C.E., Mann, R.W., Harris, W.H., 1974a. A look at the prosthesis-cartilage interface: Design of a hip prosthesis containing pressure transducers. Journal of Biomedical Materials Research 8, 261-269.

Carlson, C.E., Mann, R.W., Harris, W.H., 1974b. A radio telemetry device for monitoring cartilage surface pressures in the human hip. IEEE Transactions on Biomedical Engineering BME-21, 257-264.

Carter, D.R., Spengler, D.M., 1978. Mechanical properties and composition of cortical bone. Clinical Orthopaedics and Related Research, 192-217.

Ceseracciu, E., Sawacha, Z., Cobelli, C., 2014. Comparison of markerless and marker-based motion capture technologies through simultaneous data collection during gait: Proof of concept. Plos One 9, e87640.

Chaber, R., Arthur, C.J., Depciuch, J., Łach, K., Raciborska, A., Michalak, E., Cebulski, J., 2018. Distinguishing ewing sarcoma and osteomyelitis using FTIR spectroscopy. Scientific Reports 8, 15081.

Chanda, S., Dickinson, A., Gupta, S., Browne, M., 2015. Full-field in vitro measurements and in silico predictions of strain shielding in the implanted femur after total hip arthroplasty. Proceedings of the Institution of Mechanical Engineers, Part H 229, 549-559.

Charras, G.T., Guldberg, R.E., 2000. Improving the local solution accuracy of large-scale digital image-based finite element analyses. Journal of Biomechanics 33, 255-259.

Choi, K., Goldstein, S.A., 1992. A comparison of the fatigue behavior of human trabecular and cortical bone tissue. Journal of Biomechanics 25, 1371-1381.

Ciarelli, M.J., Goldstein, S.A., Kuhn, J.L., Cody, D.D., Brown, M.B., 1991. Evaluation of orthogonal mechanical properties and density of human trabecular bone from the major metaphyseal regions with materials testing and computed tomography. Journal of Orthopaedic Research 9, 674-682.

Cilla, M., Borgiani, E., Martínez, J., Duda, G.N., Checa, S., 2017. Machine learning techniques for the optimization of joint replacements: Application to a short-stem hip implant. Plos One 12, e0183755.

Cleather, D.J., Bull, A.M., 2012. The development of lower limb musculoskeletal models with clinical relevance is dependent upon the fidelity of the mathematical description of the lower limb. Part 2: Patient-specific geometry. Proceedings of the Institution of Mechanical Engineers, Part H 226, 133-145.

Correa, T.A., Crossley, K.M., Kim, H.J., Pandy, M.G., 2010. Contributions of individual muscles to hip joint contact force in normal walking. Journal of Biomechanics 43, 1618-1622.

Cosmi, F., Hoglievina, M., Fancellu, G., Martinelli, B., 2006. A finite element method comparison of wear in two metal-on-metal total hip prostheses. Proceedings of the Institution of Mechanical Engineers, Part H: Journal of Engineering in Medicine 220, 871-879.

Cowin, S.C., 2001. Bone Mechanics Handbook, Second Edition.

Cristofolini, L., Juszczyk, M., Taddei, F., Viceconti, M., 2009. Strain distribution in the proximal human femoral metaphysis. Proceedings of the Institution of Mechanical Engineers, Part H 223, 273-288.

D'Lima, D.D., Fregly, B.J., Colwell, C.W., Jr., 2013. Implantable sensor technology: measuring bone and joint biomechanics of daily life in vivo. Arthritis Research & Therapy 15, 203.

Damsgaard, M., Rasmussen, J., Christensen, S.T., Surma, E., de Zee, M., 2006. Analysis of musculoskeletal systems in the AnyBody Modeling System. Simulation Modelling Practice and Theory 14, 1100-1111.

Davis, R.B., Ounpuu, S., Tyburski, D., Gage, J.R., 1991. A gait analysis data collection and reduction technique. Human Movement Science 10, 575-587.

Delp, S.L., Anderson, F.C., Arnold, A.S., Loan, P., Habib, A., John, C.T., Guendelman, E., Thelen, D.G., 2007. OpenSim: open-source software to create and analyze dynamic simulations of movement. IEEE Transactions on Biomedical Engineering 54, 1940-1950.

Deng, X., Tian, X., 2013. Nonlinear process fault pattern recognition using statistics kernel PCA similarity factor. Neurocomputing 121, 298-308.

Djuwari, D., Kant Kumar, D., Palaniswami, M., 2005. Limitations of ICA for Artefact Removal. IEEE Engineering in Medicine and Biology Society 5, 4685-4688.

Donaldson, F.E., Nyman, E., Jr., Coburn, J.C., 2015. Prediction of contact mechanics in metal-on-metal Total Hip Replacement for parametrically comprehensive designs and loads. Journal of Biomechanics 48, 1828-1835.

Dorn, T.W., Schache, A.G., Pandy, M.G., 2012. Muscular strategy shift in human running: dependence of running speed on hip and ankle muscle performance. The Journal of Experimental Biology 215, 1944-1956.

Duda, G.N., Heller, M., Albinger, J., Schulz, O., Schneider, E., Claes, L., 1998. Influence of muscle forces on femoral strain distribution. Journal of Biomechanics 31, 841-846.

Duda, G.N., Schneider, E., Chao, E.Y., 1997. Internal forces and moments in the femur during walking. Journal of Biomechanics 30, 933-941.

Durandau, G., Farina, D., Sartori, M., 2018. Robust Real-Time Musculoskeletal Modeling Driven by Electromyograms. IEEE Transactions on Biomedical Engineering 65, 556-564.

Durkin, J.L., Dowling, J.J., 2006. Body segment parameter estimation of the human lower leg using an elliptical model with validation from DEXA. Annals of Biomedical Engineering 34, 1483-1493.

English, T.A., Kilvington, M., 1979. In vivo records of hip loads using a femoral implant with telemetric output (a preliminary report). Journal of Biomedical Engineering 1, 111-115.

Eskinazi, I., Fregly, B.J., 2015. Surrogate modeling of deformable joint contact using artificial neural networks. Medical Engineering and Physics 37, 885-891.

Fabeck, L., Tolley, M., Rooze, M., Burny, F., 2002. Theoretical study of the decrease in the femoral neck anteversion during growth. Cells Tissues Organs 171, 269-275.

Favre, J., Hayoz, M., Erhart-Hledik, J.C., Andriacchi, T.P., 2012. A neural network model to predict knee adduction moment during walking based on ground reaction force and anthropometric measurements. Journal of Biomechanics 45, 692-698.

Field, D.A., 2000. Qualitative measures for initial meshes. International Journal for Numerical Methods in Engineering 47, 887-906.

Filardi, V., 2018. Healing of femoral fractures by the meaning of an innovative intramedullary nail. Journal of Orthopaedics 15, 73-77.

Fischer, M.C.M., Eschweiler, J., Schick, F., Asseln, M., Damm, P., Radermacher, K., 2018. Patient-specific musculoskeletal modeling of the hip joint for preoperative planning of total hip arthroplasty: A validation study based on in vivo measurements. Plos One 13, e0195376.

Fitzpatrick, C.K., Hemelaar, P., Taylor, M., 2014. Computationally efficient prediction of bone-implant interface micromotion of a cementless tibial tray during gait. Journal of Biomechanics 47, 1718-1726.

Fluit, R., Andersen, M.S., Kolk, S., Verdonschot, N., Koopman, H.F., 2014. Prediction of ground reaction forces and moments during various activities of daily living. Journal of Biomechanics 47, 2321-2329.

Forman, D.A., Forman, G.N., Robathan, J., Holmes, M.W.R., 2019. The influence of simultaneous handgrip and wrist force on forearm muscle activity. Journal of Electromyography and Kinesiology 45, 53-60.

Forrester, A.I.J., Keane, A.J., 2009. Recent advances in surrogate-based optimization. Progress in Aerospace Sciences 45, 50-79.

Friedman, J.H., Roosen, C.B., 1995. An introduction to multivariate adaptive regression splines. Statistical Methods in Medical Research 4, 197-217.

Frost, H.M., 1990. Skeletal structural adaptions to mechanical usage (SATMU): 2. Redefining Wolff's law: The remodeling problem. The Anatomical Record 226, 414-442.

Fuchs, R.K., Kersh, M.E., Carballido-Gamio, J., Thompson, W.R., Keyak, J.H., Warden, S.J., 2017. Physical Activity for Strengthening Fracture Prone Regions of the Proximal Femur. Current Osteoporosis Reports 15, 43-52.

Galloway, F., Kahnt, M., Ramm, H., Worsley, P., Zachow, S., Nair, P., Taylor, M., 2013. A large scale finite element study of a cementless osseointegrated tibial tray. Journal of Biomechanics 46, 1900-1906.

Gate, J., Schartz, M., Koop, S., Novacheck, T.F., 2009. The identification and treatment of gait problems in cerebral palsy. Mac Keith Press.

Georgios, G., Ilse, J., Mariska, W., Sam, V.R., Sabine, V., 2015. Loading of hip measured by hip contact forces at different speeds of walking and running. Journal of Bone and Mineral Research 30, 1431-1440.

Geraldes, D.M., Phillips, A.T., 2014. A comparative study of orthotropic and isotropic bone adaptation in the femur. International Journal for Numerical Methods in Biomedical Engineering 30, 873-889.

Ghorbani Menghari, H., Ziaeipoor, H., Farzin, M., Alves De Sousa, R.J., 2014. An approach to improve thickness distribution and corner filling of copper tubes during hydro-forming processes. Structural Engineering and Mechanics 50, 563–573.

Gibson, L.J., 1985. The mechanical behaviour of cancellous bone. Journal of Biomechanics 18, 317-328.

Gill, H.S., O'Connor, J.J., 1997. A new testing rig for force platform calibration and accuracy tests. Gait & Posture 5, 228-232.

Graichen, F., Bergmann, G., 1991. Four-channel telemetry system for in vivo measurement of hip joint forces. Journal of Biomedical Engineering 13, 370-374.

Grant, C.A., Wilson, L.J., Langton, C., Epari, D., 2014. Comparison of mechanical and ultrasound elastic modulus of ovine tibial cortical bone. Medical Engineering and Physics 36, 869-874.

Grassi, L., Schileo, E., Boichon, C., Viceconti, M., Taddei, F., 2014. Comprehensive evaluation of PCA-based finite element modelling of the human femur. Medical Engineering & Physics 36, 1246-1252.

Grassi, L., Vaananen, S.P., Ristinmaa, M., Jurvelin, J.S., Isaksson, H., 2017. Prediction of femoral strength using 3D finite element models reconstructed from DXA images: validation against experiments. Biomechanics and Modeling in Mechanobiology 16, 989-1000.

Grassi, L., Väänänen, S.P., Ristinmaa, M., Jurvelin, J.S., Isaksson, H., 2016. How accurately can subject-specific finite element models predict strains and strength of human femora? Investigation using full-field measurements. Journal of Biomechanics 49, 802-806.

Guidera, K.J., Ganey, T.M., Keneally, C.R., Ogden, J.A., 1994. The embryology of lower-extremity torsion. Clinical Orthopaedics and Related Research, 17-21.

Hall, M.G., Fleming, H.E., Dolan, M.J., Millbank, S.F., Paul, J.P., 1996. Static in situ calibration of force plates. Journal of Biomechanics 29, 659-665.

Halloran, J.P., Erdemir, A., van den Bogert, A.J., 2009. Adaptive surrogate modeling for efficient coupling of musculoskeletal control and tissue deformation models. Journal of Biomechanical Engineering 131, 011014.

Han, Z.H., Zhang, K.S., 2012. Surrogate-based optimization. Real-World Applications of Genetic Algorithms, Available at http://www.intechopen.com/books/real-world-applications-of-genetic-algorithms/surrogate-based-optimization.

Harper, M.C., Carson, W.L., 1987. Curvature of the femur and the proximal entry point for an intramedullary rod. Clinical Orthopaedics and Related Research, 155-161.

Hawkins, D.M., Basak, S.C., Mills, D., 2003. Assessing model fit by Cross-validation. Journal of Chemical Information and Computer Sciences 43, 579-586.

Heimann, T., Meinzer, H.-P., 2009. Statistical shape models for 3D medical image segmentation: A review. Medical Image Analysis 13, 543-563.

Heller, M.O., Bergmann, G., Kassi, J.P., Claes, L., Haas, N.P., Duda, G.N., 2005. Determination of muscle loading at the hip joint for use in pre-clinical testing. Journal of Biomechanics 38, 1155-1163.

Helwig, P., Faust, G., Hindenlang, U., Hirschmuller, A., Konstantinidis, L., Bahrs, C., Sudkamp, N., Schneider, R., 2009. Finite element analysis of four different implants inserted in different positions to stabilize an idealized trochanteric femoral fracture. Injury 40, 288-295.

Henkel, J., Woodruff, M.A., Epari, D.R., Steck, R., Glatt, V., Dickinson, I.C., Choong, P.F.M., Schuetz, M.A., Hutmacher, D.W., 2013. Bone regeneration based on tissue engineering conceptions — A 21st century perspective. Bone Research 1, 216.

Hildebrand, T., Laib, A., Muller, R., Dequeker, J., Ruegsegger, P., 1999. Direct three-dimensional morphometric analysis of human cancellous bone: microstructural data from spine, femur, iliac crest, and calcaneus. J Bone Miner Res 14, 1167-1174.

Holden, J.P., Selbie, W.S., Stanhope, S.J., 2003. A proposed test to support the clinical movement analysis laboratory accreditation process. Gait Posture 17, 205-213.

Holmes, M.W., Tat, J., Keir, P.J., 2015. Neuromechanical control of the forearm muscles during gripping with sudden flexion and extension wrist perturbations. Computer Methods in Biomechanics and Biomedical Engineering 18, 1826-1834.

Hoy, M.G., Zajac, F.E., Gordon, M.E., 1990. A musculoskeletal model of the human lower extremity: the effect of muscle, tendon, and moment arm on the moment-angle relationship of musculotendon actuators at the hip, knee, and ankle. Journal of Biomechanics 23, 157-169.

Hyvärinen, A., 2012. Independent component analysis: recent advances. Philosophical Transactions of the Royal Society A: Mathematical, Physical and Engineering Sciences 371, 20110534.

Iglesias, J.E., de Bruijne, M., 2007. Semiautomatic segmentation of vertebrae in lateral x-rays using a conditional shape model. Academic Radiology 14, 1156-1165.

Imai, K., Ohnishi, I., Bessho, M., Nakamura, K., 2006. Nonlinear finite element model predicts vertebral bone strength and fracture site. Spine (Phila Pa 1976) 31, 1789-1794.

Jin, R., Chen, W., Simpson, T.W., 2001. Comparative studies of metamodelling techniques under multiple modelling criteria. Structural and Multidisciplinary Optimization 23, 1-13.

Jin, Y., 2011. Surrogate-assisted evolutionary computation: Recent advances and future challenges. Swarm and Evolutionary Computation 1, 61-70.

Kadaba, M.P., Ramakrishnan, H.K., Wootten, M.E., 1990. Measurement of lower extremity kinematics during level walking. Journal of Orthopeadic Research 8, 383-392.

Kaneko, T.S., Bell, J.S., Pejcic, M.R., Tehranzadeh, J., Keyak, J.H., 2004. Mechanical properties, density and quantitative CT scan data of trabecular bone with and without metastases. Journal of Biomechanics 37, 523-530.

Karatsidis, A., Bellusci, G., Schepers, H.M., de Zee, M., Andersen, M.S., Veltink, P.H., 2016. Estimation of ground reaction forces and moments during gait using only inertial motion capture. Sensors (Basel, Switzerland) 17, 75.

Kazemi, M., Dabiri, Y., Li, L.P., 2013. Recent advances in computational mechanics of the human knee joint. Computational and Mathematical Methods in Medicine 2013, 27.

Keller, T.S., 1994. Predicting the compressive mechanical behavior of bone. Journal of Biomechanics 27, 1159-1168.

Kersh, M.E., Martelli, S., Zebaze, R., Seeman, E., Pandy, M.G., 2018. Mechanical loading of the femoral neck in human locomotion. Journal of Bone and Mineral Research 33, 1999-2006.

Keyak, J.H., 2001. Improved prediction of proximal femoral fracture load using nonlinear finite element models. Medical Engineering and Physics 23, 165-173.

Keyak, J.H., Rossi, S.A., 2000. Prediction of femoral fracture load using finite element models: an examination of stress- and strain-based failure theories. J Biomech 33, 209-214.

Keyak, J.H., Skinner, H.B., 1992. Three-dimensional finite element modelling of bone: effects of element size. Journal of Biomedical Engineering 14, 483-489.

Keyak, J.H., Skinner, H.B., Fleming, J.A., 2001. Effect of force direction on femoral fracture load for two types of loading conditions. Journal of Orthopaedic Research 19, 539-544.

Kheirollahi, H., Luo, Y., 2015. Assessment of Hip Fracture Risk Using Cross-Section Strain Energy Determined by QCT-Based Finite Element Modeling. Biomed Res Int 2015, 413839.

Kopperdahl, D.L., Keaveny, T.M., 1998. Yield strain behavior of trabecular bone. Journal of Biomechanics 31, 601-608.

Krčah, M., Székely, G., Blanc, R., Year Fully automatic and fast segmentation of the femur bone from 3D-CT images with no shape prior. In 2011 IEEE International Symposium on Biomedical Imaging: From Nano to Macro.

Krebs, D.E., Robbins, C.E., Lavine, L., Mann, R.W., 1998. Hip biomechanics during gait. Journal of Orthopaedic and Sports Physical Therapy 28, 51-59.

Kyra E. Stull, E.N.L.A.a.S.D.O., 2014. Using multivariate adaptive regression splines to estimate subadult age from diaphyseal dimensions. American Journal of Physical Anthropology 154, 376-386.

Laz, P.J., Browne, M., 2010. A review of probabilistic analysis in orthopaedic biomechanics. Proceedings of the Institution of Mechanical Engineers, Part H 224, 927-943.

Leardini, A., Cappozzo, A., Catani, F., Toksvig-Larsen, S., Petitto, A., Sforza, V., Cassanelli, G., Giannini, S., 1999. Validation of a functional method for the estimation of hip joint centre location. Journal of Biomechanic 32, 99-103.

Lenaerts, G., Bartels, W., Gelaude, F., Mulier, M., Spaepen, A., Van der Perre, G., Jonkers, I., 2009. Subject-specific hip geometry and hip joint centre location affects calculated contact forces at the hip during gait. Journal of Biomechanics 42, 1246-1251.

Lengsfeld, M., Burchard, R., Günther, D., Pressel, T., Schmitt, J., Leppek, R., Griss, P., 2005. Femoral strain changes after total hip arthroplasty — patient-specific finite element analyses 12 years after operation. Medical Engineering and Physics 27, 649-654.

Lewis, A., Stewart, C., Postans, N., Trevelyan, J., 2007. Development of an instrumented pole test for use as a gait laboratory quality check. Gait Posture 26, 317-322.

Li, C., Liao, G., Shen, Y., 2010. An improved method for independent component analysis with reference. Digital Signal Processing 20, 575-580.

Li, J., Redmond, A.C., Jin, Z., Fisher, J., Stone, M.H., Stewart, T.D., 2014. Hip contact forces in asymptomatic total hip replacement patients differ from normal healthy individuals: Implications for preclinical testing. Clinical Biomechanics 29, 747-751.

Liang, L., Liu, M., Martin, C., Sun, W., 2018. A deep learning approach to estimate stress distribution: a fast and accurate surrogate of finite-element analysis. Journal of the Royal Society Interface 15, pii: 20170844.

Lin, Y.C., Dorn, T.W., Schache, A.G., Pandy, M.G., 2012. Comparison of different methods for estimating muscle forces in human movement. Proceedings of the Institution of Mechanical Engineers, Part H 226, 103-112.

Lin, Y.C., Haftka, R.T., Queipo, N.V., Fregly, B.J., 2009. Two-dimensional surrogate contact modeling for computationally efficient dynamic simulation of total knee replacements. Journal of Biomechanical Engineering 131, 041010.

Lin, Y.C., Haftka, R.T., Queipo, N.V., Fregly, B.J., 2010a. Surrogate articular contact models for computationally efficient multibody dynamic simulations. Medical Engineering and Physics 32, 584-594.

Lin, Y.C., Walter, J.P., Banks, S.A., Pandy, M.G., Fregly, B.J., 2010b. Simultaneous prediction of muscle and contact forces in the knee during gait. Journal of Biomechanics 43, 945-952.

Linting, M., Meulman, J.J., Groenen, P.J., van der Koojj, A.J., 2007. Nonlinear principal components analysis: introduction and application. Psychological Methods 12, 336-358.

Lotz, J.C., Cheal, E.J., Hayes, W.C., 1991a. Fracture prediction for the proximal femur using finite element models: Part II--Nonlinear analysis. Journal of Biomechanical Engineering 113, 361-365.

Lotz, J.C., Gerhart, T.N., Hayes, W.C., 1990. Mechanical properties of trabecular bone from the proximal femur: a quantitative CT study. Journal of Computer Assisted Tomography 14, 107-114.

Lotz, J.C., Gerhart, T.N., Hayes, W.C., 1991b. Mechanical properties of metaphyseal bone in the proximal femur. Journal of Biomechanics 24, 317-329.

Low, F.H., Khoo, L.P., Chua, C.K., Lo, N.N., 2000. Determination of the major dimensions of femoral implants using morphometrical data and principal component analysis. Proceedings of the Institution of Mechanical Engineers, Part H 214, 301-309.

Lu, B.-W., Pandolfo, L., 2011. Quasi-objective nonlinear principal component analysis. Neural Networks 24, 159-170.

Lund, M.E., de Zee, M., Andersen, M.S., Rasmussen, J., 2012. On validation of multibody musculoskeletal models. Proceedings of the Institution of Mechanical Engineers, Part H 226, 82-94.

Mantoan, A., Pizzolato, C., Sartori, M., Sawacha, Z., Cobelli, C., Reggiani, M., 2015. MOtoNMS: A MATLAB toolbox to process motion data for neuromusculoskeletal modeling and simulation. Source Code for Biology and Medicine 10, 1-14.

Marieb, E.N., 2004. Human anatomy & physiology, New York, Pearson Education.

Marks, L.W., Gardner, T.N., 1993. The use of strain energy as a convergence criterion in the finite element modelling of bone and the effect of model geometry on stress convergence. Journal of Biomedical Engineering 15, 474-476.

Martelli, S., Calvetti, D., Somersalo, E., Viceconti, M., 2015a. Stochastic modelling of muscle recruitment during activity. Interface Focus 5.

Martelli, S., Kersh, M.E., Pandy, M.G., 2015b. Sensitivity of femoral strain calculations to anatomical scaling errors in musculoskeletal models of movement. Journal of Biomechanic 48, 3606-3615.

Martelli, S., Kersh, M.E., Schache, A.G., Pandy, M.G., 2014a. Strain energy in the femoral neck during exercise. Journal of Biomechanics 47, 1784-1791.

Martelli, S., Pivonka, P., Ebeling, P.R., 2014b. Femoral shaft strains during daily activities: Implications for atypical femoral fractures. Clinical Biomechanics 29, 869-876.

Martelli, S., Valente, G., Viceconti, M., Taddei, F., 2015c. Sensitivity of a subject-specific musculoskeletal model to the uncertainties on the joint axes location. Computer Methods in Biomechanics and Biomedical Engineering 18, 1555-1563.

Martens, M., Van Audekercke, R., Delport, P., De Meester, P., Mulier, J.C., 1983. The mechanical characteristics of cancellous bone at the upper femoral region. Journal of Biomechanics 16, 971-983.

Martin, R.B., 1991. Determinants of the mechanical properties of bones. Journal of Biomechanics 24, 79-88.

Martin, R.B., 1998. Bone as a ceramic composite material. Materials Science Forum 293, 5-16.

McKay, M.D., Beckman, R.J., Conover, W.J., 1979. A comparison of three methods for selecting values of input variables in the analysis of output from a computer code. Technometrics 21, 239-245.

Messmer, P., Matthews, F., Jacob, A.L., Kikinis, R., Regazzoni, P., Noser, H., 2007. A CT database for research, development and education: concept and potential. Journal of Digital Imaging 20, 17-22.

Modenese, L., Gopalakrishnan, A., Phillips, A.T., 2013. Application of a falsification strategy to a musculoskeletal model of the lower limb and accuracy of the predicted hip contact force vector. Journal of Biomechanics 46, 1193-1200.

Modenese, L., Phillips, A.T., Bull, A.M., 2011. An open source lower limb model: Hip joint validation. Journal of Biomechanics 44, 2185-2193.

Moltedo, M., Baček, T., Verstraten, T., Rodriguez-Guerrero, C., Vanderborght, B., Lefeber, D., 2018. Powered ankle-foot orthoses: the effects of the assistance on healthy and impaired users while walking. Journal of NeuroEngineering and Rehabilitation 15, 86.

Morgan, E.F., Bayraktar, H.H., Keaveny, T.M., 2003. Trabecular bone modulus-density relationships depend on anatomic site. Journal of Biomechanics 36, 897-904.

Morgan, E.F., Keaveny, T.M., 2001. Dependence of yield strain of human trabecular bone on anatomic site. Journal of Biomechanics 34, 569-577.

Mosekilde, L., Mosekilde, L., Danielsen, C.C., 1987. Biomechanical competence of vertebral trabecular bone in relation to ash density and age in normal individuals. Bone 8, 79-85.

Mouloodi, S., Rahmanpanah, H., Burvill, C., Davies, H.M.S., 2019a. Accuracy Quantification of the Reverse Engineering and High-Order Finite Element Analysis of Equine MC3 Forelimb. Journal of Equine Veterinary Science 78, 94-106.

Mouloodi, S., Rahmanpanah, H., Burvill, C., Davies, H.M.S., 2019b. Prediction of displacement in the equine third metacarpal bone using a neural network prediction algorithm. Biocybernetics and Biomedical Engineering.

Munckhof, S.V.D., Zadpoor, A.A., 2014. How accurately can we predict the fracture load of the proximal femur using finite element models? Clinical Biomechanics 29, 373-380.

Munih, M., Kralj, A., Bajd, T., 1992. Bending moments in lower extremity bones for two standing postures. Journal of Biomedical Engineering 14, 293-302.

Mysling, P., Petersen, K., Nielsen, M., Lillholm, M., 2013. A unifying framework for automatic and semi-automatic segmentation of vertebrae from radiographs using sample-driven active shape models. Machine Vision and Applications 24, 1421-1434.

Nakano, T., 2015. Bone tissue and biomaterial design based on the anisotropic microstructure, Advances in Metallic Biomaterials: Tissues, Materials and Biological Reactions. Springer Berlin Heidelberg, Berlin, Heidelberg, pp. 3-30.

Neumann, D.A., 2010. Kinesiology of the hip: a focus on muscular actions. Journal of Orthopaedic and Sports Physical Therapy 40, 82-94.

Nicolella, D.P., Bredbenner, T.L., 2012. Development of a parametric finite element model of the proximal femur using statistical shape and density modelling. Computer Methods in Biomechanics and Biomedical Engineering 15, 101-110.

Noda, M., Nakamura, Y., Adachi, K., Saegusa, Y., Takahashi, M., 2018. Dynamic finite element analysis of implants for femoral neck fractures simulating walking. Journal of Orthopaedic Surgery 26, 2309499018777899.

O'Donnell, J.M., Devitt, B.M., Arora, M., 2018. The role of the ligamentum teres in the adult hip: redundant or relevant? A review. Journal of Hip Preservation Surgery 5, 15-22.

O'Hagan, A., Kingman, J.F.C., 1978. Curve fitting and optimal design for prediction. Journal of the Royal Statistical Society. Series B (Methodological) 40, 1-42.

O'Rourke, D., Martelli, S., Bottema, M., Taylor, M., 2016. A computational efficient method to assess the sensitivity of finite-element models: An illustration with the hemipelvis. Journal of Biomechanical Engineering 138.

Oftadeh, R., Perez-Viloria, M., Villa-Camacho, J.C., Vaziri, A., Nazarian, A., 2015. Biomechanics and mechanobiology of trabecular bone: A review. Journal of Biomechanical Engineering 137.

Ota, T., Yamamoto, I., Morita, R., 1999. Fracture simulation of the femoral bone using the finite-element method: How a fracture initiates and proceeds. Journal of Bone and Mineral Metabolism 17, 108-112.

Pandy, M.G., 2001. Computer modeling and simulation of human movement. Annual Review of Biomedical Engineering 3, 245-273.

Pandy, M.G., Zajac, F.E., 1991. Optimal muscular coordination strategies for jumping. Journal of Biomechanics 24, 1-10.

Pauchard, Y., Fitze, T., Browarnik, D., Eskandari, A., Pauchard, I., Enns-Bray, W., Pálsson, H., Sigurdsson, S., Ferguson, S.J., Harris, T.B., Guðnason, V., Helgason, B., 2016. Interactive graph-cut segmentation for fast creation of finite eement models from clinical CT data for hip fracture prediction. Computer Methods in Biomechanics and Biomedical Engineering 19, 1693-1703.

Pawlak, Z., Urbaniak, W., Hagner-Derengowska, M., Hagner, W., 2015. The probable explanation for the low friction of natural joints. Cell Biochemistry and Biophysics 71, 1615-1621.

Peacock, M., Liu, G., Carey, M., Ambrosius, W., Turner, C.H., Hui, S., Johnston, C.C., Jr., 1998. Bone mass and structure at the hip in men and women over the age of 60 years. Osteoporosis International 8, 231-239.

Perillo-Marcone, A., Alonso-Vazquez, A., Taylor, M., 2003. Assessment of the effect of mesh density on the material property discretisation within QCT based FE models: a practical example using the implanted proximal tibia. Computer Methods in Biomechanics and Biomedical Engineering 6, 17-26.

Peter, M., Minoi, J.-L., Hipiny, I.H.M., 2019. 3D face recognition using Kernel-based PCA approach, in: Alfred, R., Lim, Y., Ibrahim, A.A.A., Anthony, P. (Eds.), Computational Science and Technology, Singapore, pp. 77-86.

Pizzolato, C., Lloyd, D.G., Barrett, R.S., Cook, J.L., Zheng, M.H., Besier, T.F., Saxby, D.J., 2017a. Bioinspired technologies to connect musculoskeletal mechanobiology to the person for training and rehabilitation. Frontiers in Computational Neuroscience 11, 96.

Pizzolato, C., Reggiani, M., Saxby, D.J., Ceseracciu, E., Modenese, L., Lloyd, D.G., 2017b. Biofeedback for gait retraining based on real-time estimation of tibiofemoral joint contact forces. IEEE Transactions on Neural Systems and Rehabilitation Engineering 25, 1612-1621.

Polgar, K., Gill, H.S., Viceconti, M., Murray, D.W., O'Connor, J.J., 2003. Strain distribution within the human femur due to physiological and simplified loading: finite element analysis using the muscle standardized femur model. Proceedings of the Institution of Mechanical Engineers, Part H 217, 173-189.

Prendergast, P.J., 1997. Finite element models in tissue mechanics and orthopaedic implant design. Clinical Biomechanics 12, 343-366.

Qasim, M., Farinella, G., Zhang, J., Li, X., Yang, L., Eastell, R., Viceconti, M., 2016. Patient-specific finite element estimated femur strength as a predictor of the risk of hip fracture: the effect of methodological determinants. Osteoporosis International 27, 2815-2822.

Rabuffetti, M., Ferrarin, M., Benvenuti, F., 2001. Spot check of the calibrated force platform location. Medical and Biological Engineering and Computing 39, 638-643.

Radcliffe, I.A.J., Taylor, M., 2007. Investigation into the affect of cementing techniques on load transfer in the resurfaced femoral head: A multi-femur finite element analysis. Clinical Biomechanics 22, 422-430.

Ranawat, A.S., McClincy, M., Sekiya, J.K., 2009. Anterior dislocation of the hip after arthroscopy in a patient with capsular laxity of the hip: A case report. The Journal of bone and joint surgery. American volume 91, 192-197.

Rao, C., Fitzpatrick, C.K., Rullkoetter, P.J., Maletsky, L.P., Kim, R.H., Laz, P.J., 2013. A statistical finite element model of the knee accounting for shape and alignment variability. Medical Engineering & Physics 35, 1450-1456.

Rasoulian, A., Rohling, R., Abolmaesumi, P., 2013. Lumbar spine segmentation using a statistical multi-vertebrae anatomical shape+pose model. IEEE Transactions on Medical Imaging 32, 1890-1900.

Rathnayaka, K., Sahama, T., Schuetz, M.A., Schmutz, B., 2011. Effects of CT image segmentation methods on the accuracy of long bone 3D reconstructions. Medical Engineering and Physics 33, 226-233.

Reilly, D.T., Burstein, A.H., 1974. Review article. The mechanical properties of cortical bone. Journal of Bone and Joint Surgery 56, 1001-1022.

Retchford, T.H., Crossley, K.M., Grimaldi, A., Kemp, J.L., Cowan, S.M., 2013. Can local muscles augment stability in the hip? A narrative literature review. The Journal of Musculoskeletal and Neuronal Interactions 13, 1-12.

Rho, J.-Y., Roy, M.E., Tsui, T.Y., Pharr, G.M., 1999. Elastic properties of microstructural components of human bone tissue as measured by nanoindentation. Journal of Biomedical Materials Research 45, 48-54.

Rho, J.Y., Ashman, R.B., Turner, C.H., 1993. Young's modulus of trabecular and cortical bone material: Ultrasonic and microtensile measurements. Journal of Biomechanics 26, 111-119.

Rho, J.Y., Hobatho, M.C., Ashman, R.B., 1995. Relations of mechanical properties to density and CT numbers in human bone. Medical Engineering and Physics 17, 347-355.

Rho, J.Y., Tsui, T.Y., Pharr, G.M., 1997. Elastic properties of human cortical and trabecular lamellar bone measured by nanoindentation. Biomaterials 18, 1325-1330.

Roberts, M.G., Cootes, T.F., Pacheco, E., Oh, T., Adams, J.E., 2009. Segmentation of lumbar vertebrae using part-based graphs and active appearance models, Medical Image Computing and Computer-Assisted Intervention-2009. Springer Berlin Heidelberg, Berlin, Heidelberg, pp. 1017-1024.

Roberts, M.G., Oh, T., Pacheco, E.M.B., Mohankumar, R., Cootes, T.F., Adams, J.E., 2012. Semi-automatic determination of detailed vertebral shape from lumbar radiographs using active appearance models. Osteoporosis International 23, 655-664.

Robertson, I., Sherwin, S., 1999. Free-surface flow simulation using hp/spectral elements. Journal of Computational Physics 155, 26-53.

Rohlmann, A., Mossner, U., Bergmann, G., Kolbel, R., 1983. Finite-element-analysis and experimental investigation in a femur with hip endoprosthesis. Journal of Biomechanics 16, 727-742.

Rydell, N.W., 1966. Forces acting on the femoral head-prosthesis. A study on strain gauge supplied prostheses in living persons. Acta Orthopaedica Scandinavica 37, 1-132.

Samy, V., Ayusawa, K., Yoshida, E., 2019. Real-time musculoskeletal visualization of muscle tension and joint reaction forces, IEEE/SICE International Symposium on System Integration (SII), pp. 396-400.

Sarkalkan, N., Waarsing, J.H., Bos, P.K., Weinans, H., Zadpoor, A.A., 2014a. Statistical shape and appearance models for fast and automated estimation of proximal femur fracture load using 2D finite element models. Journal of Biomechanics 47, 3107-3114.

Sarkalkan, N., Weinans, H., Zadpoor, A.A., 2014b. Statistical shape and appearance models of bones. Bone 60, 129–140.

Schache, A.G., Bennell, K.L., Blanch, P.D., Wrigley, T.V., 1999. The coordinated movement of the lumbo-pelvic-hip complex during running: a literature review. Gait Posture 10, 30-47.

Schaffler, M.B., Kennedy, O.D., 2012. Osteocyte signaling in bone. Current Osteoporosis Reports 10, 118-125.

Schellenberg, F., Oberhofer, K., Taylor, W.R., Lorenzetti, S., 2015. Review of modelling techniques for In vivo muscle force estimation in the lower extremities during strength training. Computational and Mathematical Methods in Medicine 2015, 483921.

Scheys, L., Loeckx, D., Spaepen, A., Suetens, P., Jonkers, I., 2009. Atlas-based non-rigid image registration to automatically define line-of-action muscle models: a validation study. Journal of Biomechanic 42, 565-572.

Schileo, E., Taddei, F., Cristofolini, L., Viceconti, M., 2008. Subject-specific finite element models implementing a maximum principal strain criterion are able to estimate failure risk and fracture location on human femurs tested in vitro. Journal of Biomechanics 41, 356-367.

Schileo, E., Taddei, F., Malandrino, A., Cristofolini, L., Viceconti, M., 2007. Subject-specific finite element models can accurately predict strain levels in long bones. Journal of Biomechanics 40, 2982-2989.

Seeger, M., 2004. Gaussian processes for machine learning. International Journal of Neural Systems 14, 69-106.

Seth, A., Pandy, M.G., 2007. A neuromusculoskeletal tracking method for estimating individual muscle forces in human movement. Journal of Biomechanics 40, 356-366.

Setha, A., Shermana, M., Reinboltb, J.A., Delp, S.L., 2011. OpenSim: a musculoskeletal modeling and simulation framework for in silico investigations and exchange. International Union of Theoretical and Applied Mechanics (IUTAM) 2 212–232.

Sherman, M.A., Seth, A., Delp, S.L., 2011. Simbody: multibody dynamics for biomedical research. International Union of Theoretical and Applied Mechanics (IUTAM) 2, 241-261.

Simoes, J., Vaz, M., Blatcher, S., Taylor, M., 2000. Influence of head constraint and muscle forces on the strain distribution within the intact femur. Medical Engineering & Physics 22, 453-459.

Small, S.R., Hensley, S.E., Cook, P.L., Stevens, R.A., Rogge, R.D., Meding, J.B., Berend, M.E., 2016. Characterization of Femoral Component Initial Stability and Cortical Strain in a Reduced Stem-Length Design. The Journal of Arthroplasty.

Stansfield, B.W., Nicol, A.C., Paul, J.P., Kelly, I.G., Graichen, F., Bergmann, G., 2003. Direct comparison of calculated hip joint contact forces with those measured using instrumented implants. An evaluation of a three-dimensional mathematical model of the lower limb. Journal of Biomechanics 36, 929-936.

Stolk, J., Verdonschot, N., Murphy, B.P., Prendergast, P.J., Huiskes, R., 2004. Finite element simulation of anisotropic damage accumulation and creep in acrylic bone cement. Engineering Fracture Mechanics 71, 513-528.

Taddei, F., Cristofolini, L., Martelli, S., Gill, H.S., Viceconti, M., 2006a. Subject-specific finite element models of long bones: An in vitro evaluation of the overall accuracy. Journal of Biomechanics 39, 2457-2467.

Taddei, F., Martelli, S., Reggiani, B., Cristofolini, L., Viceconti, M., 2006b. Finite-element modeling of bones from CT data: sensitivity to geometry and material uncertainties. IEEE Transactions on Biomedical Engineering 53, 2194-2200.

Taddei, F., Pancanti, A., Viceconti, M., 2004. An improved method for the automatic mapping of computed tomography numbers onto finite element models. Medical Engineering and Physics 26, 61-69.

Taghizadeh, E., Chandran, V., Reyes, M., Zysset, P., Buchler, P., 2017. Statistical analysis of the inter-individual variations of the bone shape, volume fraction and fabric and their correlations in the proximal femur. Bone 103, 252-261.

Taghizadeh, E., Kistler, M., Büchler, P., Reyes, M., 2015. Fast prediction of femoral biomechanics using supervised machine learning and statistical shape modeling. Computational Biomechanics for Medicine. Springer, Cham, 107-116.

Taylor, M., Barrett, D.S., Deffenbaugh, D., 2012. Influence of loading and activity on the primary stability of cementless tibial trays. Journal of Orthopaedic Research 30, 1362-1368.

Taylor, M., Perilli, E., Martelli, S., 2017. Development of a surrogate model based on patient weight, bone mass and geometry to predict femoral neck strains and fracture loads. Journal of Biomechanics 55, 121-127.

Taylor, M., Prendergast, P.J., 2015. Four decades of finite element analysis of orthopaedic devices: Where are we now and what are the opportunities? Journal of Biomechanics 48, 767-778.

Taylor, M., Tanner, K., Freeman, M., 1998. Finite element analysis of the implanted proximal tibia: A relationship between the initial cancellous bone stresses and implant migration. Journal of Biomechanics 31, 303-310.

Testi, D., Zannoni, C., Cappello, A., Viceconti, M., 2001. Border-tracing algorithm implementation for the femoral geometry reconstruction. Computer Methods and Programs in Biomedicine 65, 175-182.

Thelen, D.G., Anderson, F.C., Delp, S.L., 2003. Generating dynamic simulations of movement using computed muscle control. Journal of Biomechanics 36, 321-328.

Theobald, T.M., Cauley, J.A., Gluer, C.C., Bunker, C.H., Ukoli, F.A., Genant, H.K., 1998. Black-white differences in hip geometry. Study of Osteoporotic Fractures Research Group. Osteoporosis International 8, 61-67.

Tonnis, D., Heinecke, A., 1999. Acetabular and femoral anteversion: relationship with osteoarthritis of the hip. The Journal of Bone and Joint Surgery. American Volume 81, 1747-1770.

Tonnis, D., Skamel, H.J., 2003. Computerized tomography in evaluation of decreased acetabular and femoral anteversion. Radiologe 43, 735-739.

Tu, J.V., 1996. Advantages and disadvantages of using artificial neural networks versus logistic regression for predicting medical outcomes. Journal of Clinical Epidemiology 49, 1225-1231.

Tumer, N., Arbabi, V., Gielis, W.P., de Jong, P.A., Weinans, H., Tuijthof, G.J.M., Zadpoor, A.A., 2019. Three-dimensional analysis of shape variations and symmetry of the fibula, tibia, calcaneus and talus. Journal of Anatomy 234, 132-144.

Üzümcü, M., Frangi, A.F., Sonka, M., Reiber, J.H.C., Lelieveldt, B.P.F., 2003. ICA vs. PCA active appearance models: Application to cardiac MR segmentation, in: Ellis, R.E., Peters, T.M. (Eds.), Medical Image Computing and Computer-Assisted Intervention - MICCAI 2003, Berlin, Heidelberg, pp. 451-458.

Vaananen, S.P., Jurvelin, J.S., Isaksson, H., 2012. Estimation of 3D shape, internal density and mechanics of proximal femur by combining bone mineral density images with shape and density templates. Biomechanics and Modeling in Mechanobiology 11, 791-800.

Valente, G., Martelli, S., Taddei, F., Farinella, G., Viceconti, M., 2012. Muscle discretization affects the loading transferred to bones in lower-limb musculoskeletal models. Proceedings of the Institution of Mechanical Engineers, Part H 226, 161-169.

Valente, G., Pitto, L., Testi, D., Seth, A., Delp, S.L., Stagni, R., Viceconti, M., Taddei, F., 2014. Are subject-specific musculoskeletal models robust to the uncertainties in parameter identification? Plos One 9, e112625.

Van, D.P.B., Tarala, M., Homminga, J., Janssen, D., Buma, P., Verdonschot, N., 2011. Toward a more realistic prediction of peri-prosthetic micromotions. Journal of Orthopaedic Research 30, 1147-1154.

Vos, F.M., W. de Bruin, P., G. M. Aubel, J., Streekstra, G., Maas, M., Van Vliet, L., Vossepoel, A., 2004. A statistical shape model without using landmarks, Proceedings of the 17th International Conference on Pattern Recognition ICPR 2004.

Wagner, Kaan, D., Can, O., Grujicic, Pandurangan, Grujicic, 2010. Combined musculoskeletal dynamics/structural finite element analysis of femur physiological loads during walking. Multidiscipline Modeling in Materials and Structures 6, 417-437.

Walter, J.P., Pandy, M.G., 2017. Dynamic simulation of knee-joint loading during gait using force-feedback control and surrogate contact modelling. Medical Engineering and Physics 48, 196-205.

Wang, C., Duan, Q., Gong, W., Ye, A., Di, Z., Miao, C., 2014. An evaluation of adaptive surrogate modeling based optimization with two benchmark problems. Environmental Modelling & Software 60, 167-179.

Wang, G.G., Shan, S., 2006. Review of metamodeling techniques in support of engineering design optimization. Journal of Mechanical Design 129, 370-380.

Wang, L.I., Greenspan, M., Ellis, R., 2006a. Validation of bone segmentation and improved 3-D registration using contour coherency in CT data. IEEE Transactions on Medical Imaging 25, 324-334.

Wang, X.J., Chen, X.B., Hodgson, P.D., Wen, C.E., 2006b. Elastic modulus and hardness of cortical and trabecular bovine bone measured by nanoindentation. Transactions of Nonferrous Metals Society of China 16, 744-748.

Webster, T.J., Ahn, E.S., 2007. Nanostructured biomaterials for tissue engineering bone. Advances in Biochemical Engineering/Biotechnology 103, 275-308.

Weinans, H., Sumner, D.R., Igloria, R., Natarajan, R.N., 2000. Sensitivity of periprosthetic stress-shielding to load and the bone density-modulus relationship in subject-specific finite element models. Journal of Biomechanics 33, 809-817.

Weiner, S., Traub, W., Wagner, H.D., 1999. Lamellar bone: Structure – function relations. Journal of Structural Biology 126, 241-255.

Winder, J., Bibb, R., 2005. Medical rapid prototyping technologies: State of the art and current limitations for application in oral and maxillofacial surgery. Journal of Oral and Maxillofacial Surgery 63, 1006-1015.

Wu, G., Siegler, S., Allard, P., Kirtley, C., Leardini, A., Rosenbaum, D., Whittle, M., D'Lima, D.D., Cristofolini, L., Witte, H., Schmid, O., Stokes, I., 2002. ISB recommendation on definitions of joint coordinate system of various joints for the reporting of human joint motion--part I: ankle, hip, and spine. Journal of Biomechanics 35, 543-548.

Xia, W., Luo, B., Liao, X.-p., 2011. An enhanced optimization approach based on Gaussian process surrogate model for process control in injection molding. The International Journal of Advanced Manufacturing Technology 56, 929-942.

Xiao, M., Higginson, J., 2010. Sensitivity of estimated muscle force in forward simulation of normal walking. Journal of Applied Biomechanics 26, 142-149.

Yokota, F., Okada, T., Takao, M., Sugano, N., Tada, Y., Tomiyama, N., Sato, Y., Year Automated CT Segmentation of Diseased Hip Using Hierarchical and Conditional Statistical

Shape Models. In Medical image computing and computer-assisted intervention – MICCAI 2013. Berlin, Heidelberg.

Yosibash, Z., Trabelsi, N., Milgrom, C., 2007. Reliable simulations of the human proximal femur by high-order finite element analysis validated by experimental observations. Journal of Biomechanics 40, 3688-3699.

Yun, Y., Kim, H.C., Shin, S.Y., Lee, J., Deshpande, A.D., Kim, C., 2014. Statistical method for prediction of gait kinematics with Gaussian process regression. Journal of Biomechanics 47, 186-192.

Yunardi, R.T., Winarno, 2017. Marker-based motion capture for measuring joint kinematics in leg swing simulator, 5th International Conference on Instrumentation, Control, and Automation (ICA), pp. 13-17.

Zani, L., Erani, P., Grassi, L., Taddei, F., Cristofolini, L., 2015. Strain distribution in the proximal Human femur during in vitro simulated sideways fall. Journal of Biomechanics 48, 2130-2143.

Zhang, W., Goh, A.T.C., 2016. Multivariate adaptive regression splines and neural network models for prediction of pile drivability. Geoscience Frontiers 7, 45–52.

Zheng, G., Gollmer, S., Schumann, S., Dong, X., Feilkas, T., González Ballester, M.A., 2009. A 2D/3D correspondence building method for reconstruction of a patient-specific 3D bone surface model using point distribution models and calibrated X-ray images. Medical Image Analysis 13, 883-899.

Zhou, J.-J., Zhao, M., Liu, D., Liu, H.-Y., Du, C.-F., 2017. Biomechanical property of a newly designed assembly locking compression plate: Three-dimensional finite element analysis. Journal of Healthcare Engineering 2017, 8590251.

Ziaeipoor, H., Ghorbani Menghari, H., De Sousa, R.J.A., Moosavi, H., Parastarfeizabadi, M., Farzin, M., Sanei, H., 2014. A novel approach in manufacturing two-stepped tubes using a multi-stage die in tube hydroforming process. International Journal of Precision Engineering and Manufacturing 15, 2343-2350.

Ziaeipoor, H., Jamshidifard, S., Moosavi, H., Khademizadeh, H., 2010. Numerical analysis of wrinkling phenomenon in hydroforming deep drawing with hemispherical punch.

Ziaeipoor, H., Martelli, S., Pandy, M., Taylor, M., 2018. Efficacy and efficiency of multivariate linear regression for rapid prediction of femoral strain fields during activity. Medical Engineering and Physics 63, 88–92.

Ziaeipoor, H., Moosavi, H., 2013. An investigation of wrinkling and thinning in hydroforming deep drawing process with hemispherical punch. International Journal of Mechanic Systems Engineering Volume 3, , 89-96.

Ziaeipoor, H., Taylor, M., Pandy, M., Martelli, S., 2019. A novel training-free method for real-time prediction of femoral strain. Journal of Biomechanics 86, 110-116.

APPENDICES: PUBLICATIONS

Technical note

Efficacy and efficiency of multivariate linear regression for rapid prediction of femoral strain fields during activity

Hamed Ziaeipoor [a,*], Saulo Martelli [a,b], Marcus Pandy [c], Mark Taylor [a]

[a] Medical Device Research Institute, College of Science and Engineering, Flinders University, Clovelly Park, Tonsley, Adelaide, SA, Australia
[b] NorthWest Academic Centre, The University of Melbourne, St Albans, VIC, Australia
[c] Department of Mechanical Engineering, University of Melbourne, Parkville, VIC, Australia

ARTICLE INFO

ABSTRACT

Multivariate Linear Regression-based (MLR) surrogate models were explored to reduce the computational cost of predicting femoral strains during normal activity in comparison with finite element analysis. The musculoskeletal model of one individual, the finite-element model of the right femur, and experimental force and motion data for normal walking, fast walking, stair ascent, stair descent, and rising from a chair were obtained from a previous study. Equivalent Von Mises strain was calculated for 1000 frames uniformly distributed across activities. MLR surrogate models were generated using training sets of 50, 100, 200 and 300 samples. The finite-element and MLR analyses were compared using linear regression. The Root Mean Square Error (RMSE) and the 95th percentile of the strain error distribution were used as indicators of average and peak error. The MLR model trained using 200 samples (RMSE < 108 $\mu\varepsilon$; peak error < 228 $\mu\varepsilon$) was used as a reference. The finite-element method required 66 s per frame on a standard desktop computer. The MLR model required 0.1 s per frame plus 1848 s of training time. RMSE ranged from 1.2% to 1.3% while peak error ranged from 2.2% to 3.6% of the maximum micro-strain (5020 $\mu\varepsilon$). Performance within an activity was lower during early and late stance, with RMSE of 4.1% and peak error of 8.6% of the maximum computed micro-strain. These results show that MLR surrogate models may be used to rapidly and accurately estimate strain fields in long bones during daily physical activity.

A novel training-free method for real-time prediction of femoral strain

Hamed Ziaeipoor [a,*], Mark Taylor [a], Marcus Pandy [b], Saulo Martelli [a]

[a] Medical Device Research Institute, College of Science and Engineering, Flinders University, Clovelly Park, SA, Australia
[b] Department of Mechanical Engineering, University of Melbourne, Parkville, VIC, Australia

ABSTRACT

Surrogate methods for rapid calculation of femoral strain are limited by the scope of the training data. We compared a newly developed training-free method based on the superposition principle (Superposition Principle Method, SPM) and popular surrogate methods for calculating femoral strain during activity. Finite-element calculations of femoral strain, muscle, and joint forces for five different activity types were obtained previously. Multi-linear regression, multivariate adaptive regression splines, and Gaussian process were trained for 50, 100, 200, and 300 random samples generated using Latin Hypercube (LH) and Design of Experiment (DOE) sampling. The SPM method used weighted linear combinations of 173 activity-independent finite-element analyses accounting for each muscle and hip contact force. Across the surrogate methods, we found that 200 DOE samples consistently provided low error (RMSE < 100 $\mu\varepsilon$), with model construction time ranging from 3.8 to 63.3 h and prediction time ranging from 6 to 1236 s per activity. The SPM method provided the lowest error (RMSE = 40 $\mu\varepsilon$), the fastest model construction time (3.2 h) and the second fastest prediction time per activity (36 s) after Multi-linear Regression (6 s). The SPM method will enable large numerical studies of femoral strain and will narrow the gap between bone strain prediction and real-time clinical applications.

© 2019 Elsevier Ltd. All rights reserved.

182

AN EFFICIENT COMPUTATIONAL MODEL FOR PREDICTING THE STRAIN DISTRIBUTION DURING COMMON PHYSICAL ACTIVITIES: SURROGATE MODELING VS FE SIMULATIONS

Hamed Ziaei Poor, Saulo Martelli, Rami Al-Dirini, Dermot O'Rourke, Mark Taylor
Medical Device Research Institute, School of Computer Science, Engineering and Mathematics, Flinders University
Corresponding author email: hamed.ziaeipoor@yahoo.com, ziae0005@flinders.edu.au

INTRODUCTION

The ability to calculate femoral strain during a broad range of physical activities is essential to study the risk of fracture for the elderly population. Strain prediction using the current Finite Element-Musculoskeletal (FE-MS) models is computationally expensive [1]. Surrogate Modelling (SM) offers a unique alternative for predicting the strain field over the femur in a fraction of the time needed by FE-MS models. The objectives of this research were (i) to develop a surrogate model than can accurately and efficiently predict the strain distribution for five different activities, and (ii) to assess the effect of increasing the number of samples on the accuracy of the results.

MATERIALS AND METHODS

The VICON motion capture system were used for obtaining the marker trajectories and ground reaction force of a female subject (68 years, 53kg) during five different activities (walking (5 rep), fast-walking (5 rep), stairs up (5 rep), stairs down (4 rep) and rising from and lowering into a chair (1 rep)). Twenty four different muscle and joint reaction forces were calculated using a developed musculoskeletal model [2, 3]. The obtained forces were applied to an FE model of the subject's femur [2, 3].

Surrogate models of the strain distribution were developed using four different training samples (N = 50, 100, 200 and 300). For this purpose, muscle and joint reaction forces of the entire activity cycles were pooled into a single matrix, from which samples were generated using Latin hypercube sampling (LHS). Different levels of training were performed using a multi-linear regression model based on the generated data sets. Training the surrogate models returned the coefficients, which can be regarded as a link between the forces and the induced strain field. In other words, by showing the training data set to each element (as input variable) and the strain (as output), the response of each element was (the coefficients) obtained. The full field of microstrain for each element were predicted by multiplying the forces and the associated coefficients for different repetitions using the below equation (F_{Mi} = muscle force, F_{JR} = joint reaction force).

$$Microstrain = Constant + C_1F_{M1} + C_2F_{M2} + \ldots + C_{25}F_{JR}$$

To assess the accuracy of the technique, the SM prediction was compared to the FE prediction of strains using linear regression. This was repeated for each activity cycle. Furthermore, element-to-element comparisons were performed by finding the difference between FE and each SM.

RESULTS AND DISCUSSION

The study found that increasing the number of samples from 50 to 300, changed the peak RMSE from 200 µɛ to 150 µɛ. Out of the considered activities, and fast-walking had the greatest local error, with the peak and average value of 95% of the absolute error being less than 600 and 300 µɛ, respectively. It was noted that the accuracy is high within the stance phase of a gait ($R^2 > 0.8$), but it falls significantly in the swing phase of a gait ($R^2 = 0.29$). The worst prediction was for rising-from and lowering-into a chair when LHS50 was used (peak RMSE = 200 µɛ), followed by LH100-300, ranging from 175-165 µɛ, respectively. In terms of efficiency, the running time for FE simulations was 55min, compared with 13 seconds for the surrogate models.
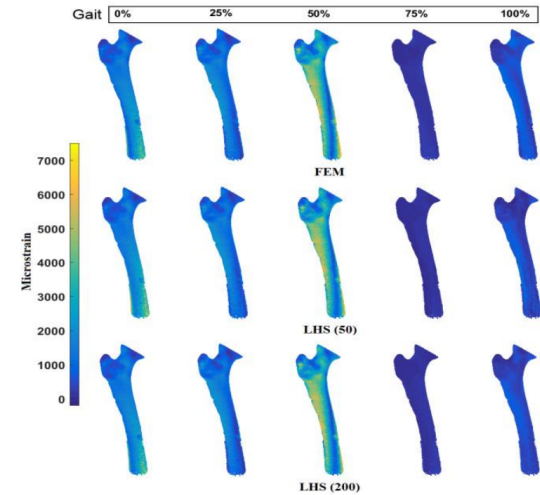

Figure 1: The strain prediction during a gait (in percent) using FE and SM (fast-walking, for LHS50 and 100)

CONCLUSIONS

This study demonstrated the development and validation of an efficient surrogate model of the femoral strain field based on data for five different physical activities. Also, while the accuracy improved by increasing the number of samples from 50-200, not that much difference observed by further increase in the number of samples.

REFERENCES

1. Fitzpatrick, C.K., et al. *Journal of Biomechanics,* **47**, 1718-26, 2014.
2. Martelli, S., et al. *Journal of Biomechanics,* **18**, 1555-63, 2015.
3. Martelli, S., et al. *Journal of Biomechanics,* **48,** 3606-15, 2015.

Comparison of computational methods for the calculation of femoral strain during normal activity

Hamed Ziaeipoor*, Saulo Martelli, Mark Taylor

Medical Devices Research Institute, College of Science and Engineering, Flinders University

*Corresponding author email: hamed.ziaeipoor@flinders.edu.au

Introduction

Fast calculation of femoral strain can promote large studies of the risk of bone fracture [1] and implant failure [2]. The aim of this research was to compare calculation of femoral strain during normal activity by different computational methods.

Method

Marker trajectories and ground reaction force for a healthy woman (68 years of age, 53kg weight) during normal walking, fast walking, stair ascent, stairs descent and chair sitting were taken from the previous work [3]. Each activity was sampled using 50 frames uniformly distributed resulting in 1000 frames across activities. The von Mises strain was calculated using earlier musculoskeletal and finite-element models [3]. Training sets of 50, 100, 200 and 300 samples were generated using using design of experiment and latin hypercube methods. Multi-linear regression, multivariate adaptive regression splines and gaussian surrogate models were trained. A novel method was developed based on the principle of superposition by calculating femoral strain for an arbitrary frame as a linear combination of a reduced set (173 simulations) of finite-element solutions. The training set and sampling method ensuring the best performance was identified for each surrogate method. The finite-element solution was used as reference for comparison. The different methods were compared in terms of strain error and time required.

Results

Design of experiment sampling and 200 samples provided the lowest error (RMSE < 170 µɛ) for each surrogate method. The peak error ranged from 167 µɛ for the principle of superposition to 455 µɛ for Multi-linear regression (Figure 1). Training time was lower for Multi-linear regression (0.15 h) compared with principle of superposition (3.2 h). The time for predicting strain in an entire activity (50 frames) ranged from 5 s for multi-linear regression to 3,300 s for the finite-element method. The total time (training and prediction) ranged from 0.18 h for multi-linear regression to 81.1 h for multivariate adaptive regression splines, compared with 18.3 h for FEM.

Conclusion

Multilinear regression and the principle of superposition can be used in large studies of the risk of bone fracture and implant failure as they combine the lowest error and prediction time among available computational methods.

References

[1] Chanda, S., et al. Proceedings of the Institution of Mechanical Engineers, part H 229, 549-559, (2015).

[2] Bessho, M., et al. Bone, 45, 226-231, (2009).

[3]. Martelli, S., et al. Journal of Biomechanics, 18, 1555-63, (2015).
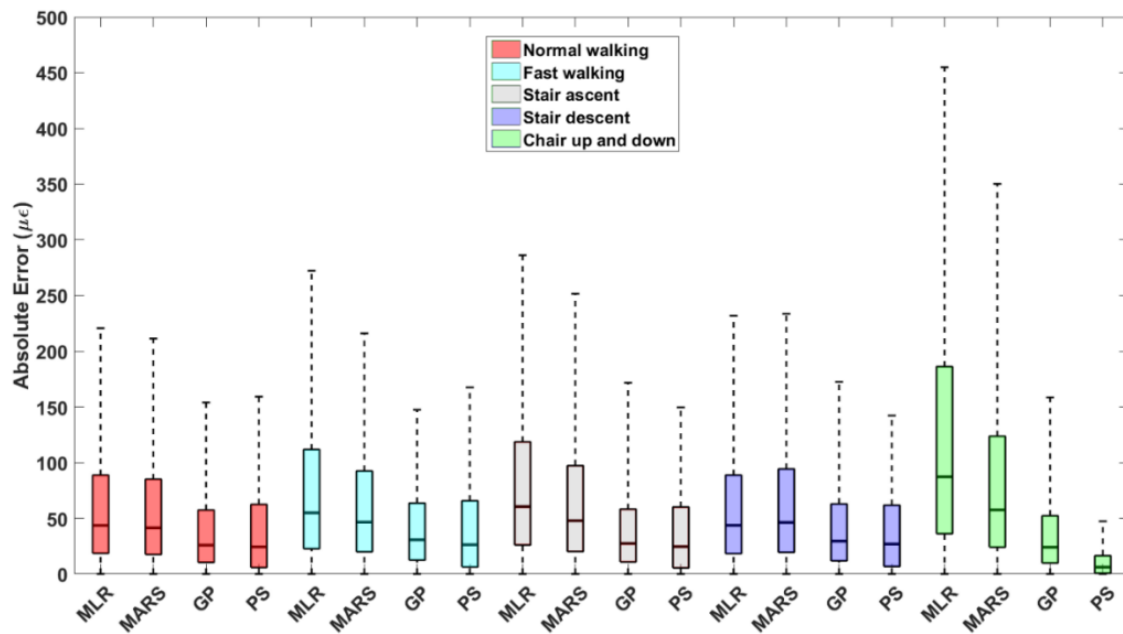
Figure 1. The error distribution. MLR: multi-linear regression; MARS: multivariate adaptive regression splines; GP: Gaussian process; PS: principle of superposition.

Rapid Prediction of Femoral Strain using a Novel Computational Model

Hamed Ziaeipoor*, Mark Taylor, Saulo Martelli

Medical Device Research Institute, College of Science and Engineering, Flinders University, Adelaide, SA
Email: hamed.ziaeipoor@flinders.edu.au

INTRODUCTION

Real-time prediction of femoral strain is important for different applications, such as bone fracture assessment [1], implant failure [2], and statistical studies of human motion [3]. The aim of this research was to compare the performance of a newly developed training-free method based on the principle of superposition (i.e., the Superposition Principle Method; SPM), and Multi-linear Regression (MLR), Multivariate Adaptive Regression Splines (MARS) and Gaussian Process (GP) as popular surrogate methods.

METHODS

Marker trajectories and ground reaction force for a healthy woman (68 years of age, 53kg weight) during repetitions of normal walking, fast walking, stair ascent, stairs descent and chair sitting were taken from the previous work [4]. Each activity was represented by 50 uniformly distributed frames of motion, resulting in 1000 frames in total. A coupled musculoskeletal and finite-element was used for calculating muscle and joint forces and femoral von Mises strain [4]. MLR, MARS and GP models were trained for each element in the mesh using training datasets with 50, 100, 200 and 300 samples determined using both Design of Experiment and Latin Hypercube sampling. Principle of superposition was constructed by computing femoral strain using a linear combination of 173 individual FE simulations with the below form:

$$\bar{\bar{\varepsilon}}_i = \sum_{j=1}^{24} \sum_{k=1}^{3} \frac{fm_{i,j,k}}{f_n} \times \bar{\bar{\varepsilon}}(fv_{j,k}) + \frac{fh_i}{f_n} \times \bar{\bar{\varepsilon}}(\overrightarrow{hf}v_{i,z})$$

Where $fm_{i,j,k}$ is the magnitude of the force for frame j, component k, muscle j,; $\bar{\bar{\varepsilon}}(fv_{j,k})$ is the strain tensor generated by a nominal force f_n applied at the muscle attachment site j along the coordinate axis k; fh_i is the magnitude of the hip contact force for frame i; and $\bar{\bar{\varepsilon}}(\overrightarrow{hf}v_{i,z})$ represents the strain tensor generated by a force vector $\overrightarrow{hf}v_z$ of magnitude fn applied to the node z at the femoral head surface.

A suitable sampling method and the best size of training datasets was idetified. The methods' performance was assesed by comparing femoral strain activity-by-activity and frame-by-frame and the required prediction time.

RESULTS AND DISCUSSION

Design of experiment sampling and 200 samples provided the lowest error (RMSE < 170 µε) for each surrogate method. The SPM method showed the lowest RMSE (40 µε) and peak (256 µε) errors across different activities. The RMSE was 99, 100, 53 µε for the MLR, MARS and GP methods, while the peak error was 521, 414, 316 µε, respectively. The frame-by-frame comparison showed a higher RMSE (135 µε) and peak (153 µε) errors for GP compared with SPM. The MLR provided the femoral strain for a full cycle (50 frames) within 6 sec, compared to 36 s for SPM.
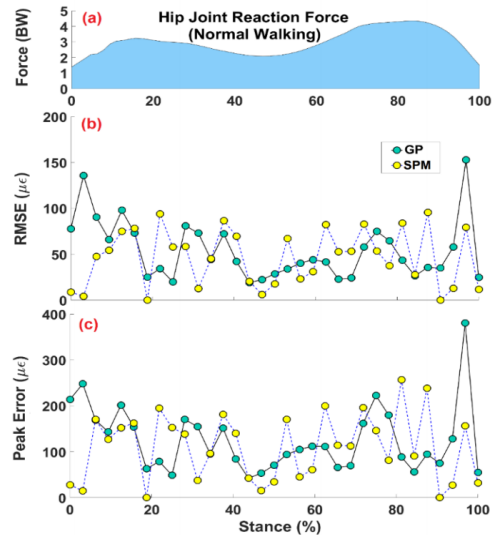

Figure 1: Comparison of the strain error in the SPM and GP methods during the stance phase of normal walking.

CONCLUSIONS

The principle of superposition presented the lowest strain error and the second lowest prediction time. Multilinear regression presented the fasted prediction time. SPM and MLR are best suited for large studies on femoral strain during physical activity.

REFERENCES

1. Chanda, S., et al. Proceedings of the Institution of Mechanical Engineers, part H **229**, 549-559, 2015.
2. Bessho, M., et al. Bone, **45**, 226-231, 2009.
3. Martelli, S., et al. Computer Methods in Biomechanics and Biomedical Engineering, **18**, 1555-63, 2015.
4. Martelli, S., et al. Journal of Biomechanics; **48**, 3606-3615 (2015).

186

TIME-EFFECTIVE POPULATION-BASED MODELLING OF FEMORAL MECHANICS DURING PHYSICAL ACTIVITY

Hamed Ziaeipoor (1), Mark Taylor (1), Saulo Martelli (1)

1. Medical Device Research Institute, College of Science and Eng., Flinders University, Tonsley SA, Australia

Introduction

Surrogate models of femoral mechanics are increasingly used for modelling anatomical and functional variations across individuals in large statistical studies of musculoskeletal function [1]. Here, we use Principal Component Analysis (PCA) and superposition principle for time-effectively predicting population-based solutions, not surrogates, of femoral strain during physical activity. We also compared the method's performance against common surrogate methods.

Methods

Motion and computed-tomography (CT) data were obtained earlier [2] from 21 healthy women (age range = 60 – 74). Activities included normal walking, fast walking, stair ascent, stairs descent and chair sitting. Muscle and joint forces were calculated using OpenSim [3]. The femur's von Mises strain map was calculated using locally-isotropic finite-element models based on the calibrated CT images. The PCA model of the femur was generated using 18 femurs by following an established procedure [4]. The strain tensor $\bar{\bar{\varepsilon}}_i$ for a generic frame of motion was calculated using linear combination of 173 independent strain maps generated by a nominal force ($fn = 100$ N) accounting for each muscle force and changes of the hip center of pressure during activity:

$$\bar{\bar{\varepsilon}}_i = \sum_{j=1}^{24} \sum_{k=1}^{3} \frac{fm_{i,j,k}}{f_n} \times \bar{\bar{\varepsilon}}(fv_{j,k}) + \frac{fh_i}{f_n} \times \bar{\bar{\varepsilon}}(\vec{hf}v_z) \quad \text{Eq. 1}$$

where $\bar{\bar{\varepsilon}}(fv_{j,k})$ is the nominal strain tensor generated by each muscle j directed along the coordinate axis k; $fm_{i,j,k}$ is the muscle force j, along axis k, motion frame i; $\bar{\bar{\varepsilon}}(\vec{hf}v_z)$ is the nominal strain tensor for the hip center of pressure z and fhi is the hip contact force at frame i. The superposition model (SPM) was assessed against finite-element (FE) solution, Multi-linear Regression (MLR), Multivariate Adaptive Regression Splines (MARS) and Gaussian Process (GP) methods. Surrogate models were trained using a training set of 200 samples determined using Design of Experiment. The SPM model was assessed for a single individual, 1000 frames of motion including all motor tasks, either in terms of strain error, using FE predictions as reference, and CPU time on a standard desktop PC. The strain tensor $\bar{\bar{\varepsilon}}$ was defined a function of the PCA modes of variation into a population-based model of physical activity (SPM2). The strain tensor generated by each force component was calculated using finite-element by varying each mode of variation by 0, $\pm$ 1 and $\pm$ 2 SD. A cubic polynomial curve was fitted to the strain tensor components and the PCA modes of variation. The error in the SPM2 model originating from the PCA and the polynomial fitting of strain components were assessed separately. The PCA error was calculated as the difference between femoral strain in CT-based models and corresponding best-fit PCA instances for three unseen femurs and 50 randomly selected frame of motion. For the same three femurs, the strain error generated by fitting PCA modes and strain components was quantified using FE solutions the best-fit PCA instances as reference.

Results

As opposed to all surrogate models, the model did not require motion data for training. The SPM model provided the lowest error (RMSE = 40 $\mu\varepsilon$), the fastest model construction time (3.2h) and prediction time for predicting 1000 frames of motion (Fig. 1A). The PCA error was below 951 $\mu\varepsilon$ (median error = 166 $\mu\varepsilon$) while the SPM2 error committed while linking SPM and PCA models was below 49 $\mu\varepsilon$ (median error = 4 $\mu\varepsilon$) (Fig. 1B).
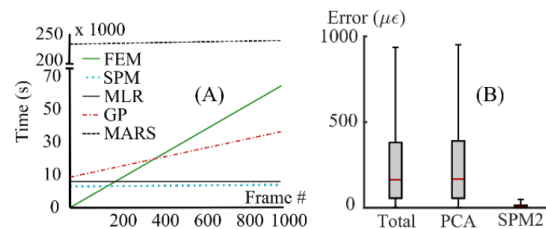

Fig. 1 – CPU time (A) and strain error ($\mu\varepsilon$) in the PCA and SPM2 models.

Discussion

The SPM2 method is a training-free method providing solutions of femoral strain during activity that outperform common surrogate models either in terms of error and computational time. The combination of superposition principle and PCA is an effective solution for running population-based simulation of femoral mechanics during activity.

References

1. Taddei et al, J. Biomech. 47:3433–40, 2014.
2. Martelli et al, J Biomech, 48:3606-15, 2015.
3. Ziaeipoor et al., Med. Eng. and Phys., 63: 88-92, 2018
4. Bryan et al, Med. Eng. and Phys., 32: 57-65, 2010

Acknowledgements

A Novel Computational Method for Rapid Prediction of Femoral Strain in the Population

Hamed Ziaeipoor*, Saulo Martelli, Mark Taylor
Medical Device Research Institute, College of Science and Engineering, Flinders University, Adelaide, SA
Email: hamed.ziaeipoor@flinders.edu.au

INTRODUCTION

Real-time prediction of femoral strain can promote large studies of the risk of bone fracture [1] and implant failure [2]. Superposition Principle Method (SPM) has been demonstrated to be a training-free method which can be used for rapid prediction of femoral strain during motion for a single subject study [3]. However, the capability of this technique needs to be explored for larger studies (e.g. population-based studies). So, the aim of this work was to develop a novel computational method called 'SPM2' by the integration of Superposition principle method and a statistical model for efficient calculation of femoral strain in a cohort of patients.

METHODS

A training set composed of 21 femurs for healthy women (65 ± 5 years; weight: 66 ± 12 kg; height: 160 ± 7 cm) was taken from a previous study [4]. A combined statistical shape and appearance model was then developed to capture the principle modes of variation in shape and modulus of population. Bone instances were generated by varying the PCA scores and then a set of nominal force vectors (100N) were applied in FE models and the resultant strain fields was determined. In the following, a second-order function was then fitted into the available strain fields across various standard deviations and modes, resulting in the calculation of coefficients and constants for each element. By leveraging the linearity of the problem, the Principle of superposition was used to calculate the strain field of each frame of motion as below:

$$\overline{\overline{\varepsilon_{ix}}} = \sum_{p=1}^{17} \sum_{j=1}^{24} \sum_{k=1}^{3} [\bar{\bar{\varepsilon}}(fv_{j,k,p}) - (d \times c)] \times \frac{fm_{i,j,k}}{f_n}$$

Where $fm_{i,k,p}$ is the magnitude of force computed by OpenSim for a given muscle or joint reaction force j, along the coordinate axis k, and mode of variation p; $\bar{\bar{\varepsilon}}(fv_{j,k,p})$ is the strain tensor computed by the nominal force vector of f_n with an arbitrary magnitude set to 100 N; c refers to the constants computed for each element through the second-order function; and $d = t - 1$, where t is the total number of modes in PCA.

The accuracy of SPM2 method was evaluated by comparing the predicted femoral strain against the corresponding FE results by investigating two sets of data: (i) 50 synthetic femurs produced randomly using the available PCA model, and (ii) three unseen femur which were not used for building PCA model. The performance of the method was also evaluated for 50 random frames of normal walking, fast walking, stair climbing, stair ascent, stair descent, and chair sitting.

RESULTS AND DISCUSSION

The SPM2 method showed a consistent prediction across the entire synthetic femurs by presenting a peak error ranging from 124 − 725 με. However, when the error associated with the reconstruction of unseen femurs using PCA model was accounted, less accurate predictions was noticed (Fig. 1). From the total SPM2 error, the PCA model was presented to be the major source of error by yielding RMSE and peak error of 488 με and 945 με, respectively, compared with the interpolation error (RMSE = 24 με, peak error = 49 με) which was occurred while performing the interpolation via the second-order function. Furthermore, the SPM2 provided the femoral strain for a full cycle (40 frames) within 3 minutes, compared to 44 minutes for FEM.
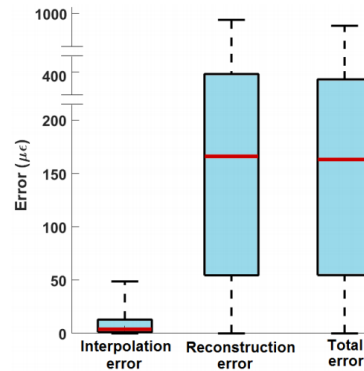

Figure 1: The accuracy of SPM2 method for femoral strain calculation for three unseen femurs and 50 random frames of motion.

CONCLUSIONS

The SPM2 was used as a novel computational method for calculation of femoral strain during physical activities. Therefore, SPM2 is a training-free method which would faciliate running large scale studies, such as assessing the risk of fracture in a cohort of patients.

REFERENCES

1. Chanda, S., et al. Proceedings of the Institution of Mechanical Engineers, part H **229**, 549-559, 2015.
2. Bessho, M., et al. Bone, **45**, 226-231, 2009.
3. Ziaeipoor, H., et al. Journal of Biomechanics, 86, 110-11, 2019.
4. Martelli, S., et al. Journal of Biomechanics; **48**, 3606-3615, 2015.